Signature inversion of ^{124}La and ^{126}La

Takehito HAYAKAWA

Signature inversion of ^{124}La and ^{128}La

Takehito HAYAKAWA

A dissertation submitted to the Doctoral Program in Physics, the University of Tsukuba in partial fulfillment of the requirements for the degree of Doctor of Philosophy (Physics)

January, 1995

Abstract

In order to study the signature inversion of odd-odd La isotopes, two experimental investigations have been carried out. The first experiment was an in-beam γ ray spectroscopy of ^{124}La for the purpose of the extension of systematics in high-spin band structures for light odd-odd La isotopes. The second experiment was made on the β decays of ^{128}La and ^{128}Ce for the experimental determination of spins of the high-spin bands in ^{128}La.

From the study of ^{124}La, three band structures having rotational character have been observed. The configurations of these bands has been discussed in comparison with neighboring odd-A nuclei and other odd-odd La isotopes. The signature inversion is clearly observed in ^{124}La.

From the study of β decay, it has turned out that there are two β unstable isomeric states in ^{128}La. An upper limit of the half life of newly found state is 2 minute. A probable spin would be 1^+ or 2^+. The half life of another isomeric state is 5.2$\pm$0.3 minute. This is in agreement with the value measured in a previous investigation. The spin of this isomer has been assigned to be 5^+. The spin of the rotational band of ^{128}La is assigned.

The experimental signature splitting has been compared with a calculation by the particle-rotor model including a triaxial core and residual proton-neutron interaction.

Contents

Chapter 1

Introduction

High spin states of nuclei in the mass number $A \sim 130$ region have been studied extensively by In-beam γ ray spectroscopic method. The nuclei with the proton number $Z > 50$ and the neutron number $N < 82$ are located in the neutron deficient side, and exhibit gradual increase in collectivity as the neutron number decreases. The energies of the first 2^+ state in even-even nuclei become low, and higher states built on the 2^+ state show typical rotation like spectra near the neutron number $N \simeq 70$. This rotation like band is named as the ground-state band. The property of the ground-state band can be interpreted by collective rotation of a deformed nucleus around the axis perpendicular to the symmetry axis of quadrupole deformation. The geometrical shape of this nucleus is approximated by an axially symmetric spheroid in a prolate shape with deformation parameters in the range of $\varepsilon_2 = 0.2 \sim 0.25$. Since the Fermi surface lies in the vicinity of the $h_{11/2}$ deformed shell model orbital in this mass region, an interplay between the collective rotation or vibration and single particles sitting in the above high-j intruder orbital produces rich structures of excited states as the rotation alignment in even-even nuclei, decoupled bands in odd-A and band structures in odd-odd nuclei. Therefore, the nucleus in this mass region provides an excellent testing ground for various kinds of current nuclear structure theories.

The structure of excited states in odd-odd nuclei is much more complex than even-even or odd-A nuclei. Usually, an odd-odd nucleus can be treated by an approximation that it consists of an even-even core, of which spin and parity are 0^+,

a proton and a neutron. The number of the proton-neutron configuration becomes large, and thus the level density becomes high. There is a large number of decay paths accompanied by γ transitions. It is often difficult to resolve doublet peaks in γ ray spectra, even if we use a detector with very high resolution. Some of the transitions are difficult to observe because of their low energies due to small energy spacings between excited states. Sometimes, there are isomeric states. These facts are the reasons for the experimental difficulty for the complex structure in odd-odd nuclei especially at lower excitation energies.

In spite of the above difficulties, one can observe clear band structures at higher excitation energies in cases where excited states are populated *via* heavy-ion fusion-evaporation reactions. A large angular momentum is carried into a compound nucleus. The subsequent evaporation of a small number of light particles as protons or neutrons does not carry away a large amount of angular momenta, and thus a state for γ ray emission remains in a high angular-momentum state. Since the angular momenta of γ rays are substantially 1 or $2\hbar$, relatively selective γ transitions occur in cascades along high-spin yrast states. In addition to this physical reason, a γ ray spectrometer of new generation, which is called as "crystal-ball", has made it possible to identify a lot of band structures even in odd-odd nuclei. Recent standard crystal-ball spectrometers comprise 20-50 Compton-suppressed HPGe detectors for γ ray detection and some additional detectors which are a γ-ray multiplicity filter and a particle multiplicity filter for channel selection.

One of the remarkable properties in the band structures in the odd-odd nuclei in the mass A$\sim$130 region is the low-spin signature inversion in the yrast band. Contrary to the prediction of a simple cranking model, excited states with "favored" signature are higher in energy than states with "unfavored" signature. We give the name of "signature inversion" in this sense(see Appendix B).

At first, this phenomenon was observed in the band members located higher than the first backbend of odd-A nuclei in the mass number $A \sim 160$ [1]. Hot discussions were made on the effect of non axially symmetric deformation, the

contribution of γ vibration, and so on [2][3]. Hereafter, we use a word of "triaxial deformation" instead of non axially symmetric deformation. For odd-odd nuclei, Pinston and his coworkers reported that similar inversion occurred in the yrast bands of ^{152}Eu, ^{154}Tb and some other odd-odd nuclei in the mass number $A \sim 160$ [4][5]. Later on, such an inversion was also observed in odd-odd nuclei in the mass number $A \sim 130$ [6][7]. *It should be noted, however, that the inversion in odd-odd nuclei is mentioned for low spin states at lower excitation energies.*

From the theoretical point of view, Hamamoto reported that a particle-rotor model with a core of axial symmetry could explain the signature inversion [8]. Matsuzaki investigated in terms of the cranked shell model(CSM) including γ deformation [9]. Yoshida *et.al.* have reported the calculation by IBFM model in which a proton and a neutron are coupled to the core of SU(3) or O(6) in the IBM2 model [10]. Hara developed the theory of angular momentum projection to reproduce experimental signature inversion [11]. Recently, Semmes *et al.* have investigated the effects of residual interaction between a valence proton and neutron coupled to a triaxially deformed core by means of their particle-rotor model. They concluded that the residual interaction was very effective and that the triaxial deformation was not necessary for the explanation of the signature inversion [12]. Tajima expected that the triaxial deformation might contribute to the signature inversion from the existence of low-energy γ bands in neighboring even-even nuclei. He calculated the signature dependence of excitation energies and the ratios of $B(\mathrm{M1})/B(\mathrm{E2})$ for ^{124}Cs and some other nuclei [13]. The calculations are in agreement with the experimental signature splittings in Ce isotopes. A gross feature of calculated signature splittings of La and Cs are similar to each other.

The signature inversion of odd-odd nuclei, however, is not still fully understood. There is a common feature in the two mass regions of $A \sim 160$ and $A \sim 130$. The valence proton and neutron occupy the $\pi h_{11/2}$ with high Ω and $\nu i_{13/2}$ with low Ω orbitals in the $A \sim 160$ region. The proton in the $\pi h_{11/2}$ with low Ω orbital and the neutron sitting in the $\nu h_{11/2}$ with high Ω orbital play the principal

role on the yrast band in the $A \sim 130$ region. In other words, one nucleon can easily align its angular momentum along the axis of collective rotation, while the other nucleon tends to remain its angular momentum along the axis of deformation symmetry. These nucleons are defined as "rotation aligned" and "deformation aligned" nucleons, respectively. The behavior of the signature inversion seems to be dependent on the proton number in the $A \sim 160$ region, and on the neutron number in the $A \sim 130$ region. This suggests that the coupling of the valence nucleons should be investigated more carefully with attention to the shell filling of the deformation aligned nucleon.

The most important point in the investigation of the signature inversion is firm experimental spin assignments of the band members. In this sense, the present experimental data are very inadequate. In the mass number $A \sim 130$, experimental spin assignments are made only for the two nuclei of ^{124}Cs and ^{126}Cs [7]. The signature inversions are reported in other Cs isotopes [14][15]. In odd-odd La isotopes, the signature inversion is observed in ^{126}La, and might be in ^{128}La [16][17][18]. The signature inversion is not so clear in ^{130}La [18]. In these Cs and La isotopes, it cannot be discussed whether the inversion occurs at low spins or not, because the spin assignments are ambiguous. The calculations by Tajima indicate not only that the agreement between the theoretical signature splittings and experimental data is not sufficient, but also that the sign of the calculated signature splittings are opposite to the experimental data on La isotopes. One of the reason for this discrepancy would be due to the spins of the bands in La isotopes. The spins are given by theoretical discussions as routhians or aligned angular momenta, and thus are not assigned experimentally. In lighter La isotopes, even rotational bands are not reported in ^{124}La or ^{122}La for instance. Some more experimental data are clearly required for the more deeper understanding of the signature inversion in odd-odd nuclei.

The present work has been initiated by the above motivations. It consists of two investigations. The first investigation is the observation of rotational bands

of ^{124}La aiming at the extension of the systematics of lighter odd-odd La isotopes. The second study is the spin assignment of the rotational bands of ^{128}La. This has been performed in order to determine whether the signature inversion appears at low spins or high spins.

In the following chapter, the experimental procedures of the in-beam spectroscopy of ^{124}La, the β decay and the in-beam spectroscopy of ^{128}La for the spin assignment will be described in chapter 2. chapter 3 will be given to the report on the experimental results. The configurations of the bands in ^{124}La, the spin assignment of ^{128}La and the systematics of the signature inversion will be discussed in chapter 4. In the final chapter, we will summarize the conclusions derived from the present investigation.

Chapter 2

Experimental procedure

2.1 In-beam spectroscopy of ^{124}La

Several well developed band structures are observed in ^{126}La [16], ^{128}La and ^{130}La [17][18]. From a qualitative theoretical discussion and experimental systematics, it is proposed that the bands populated with high intensity have $\pi h_{11/2} \otimes \nu h_{11/2}$ and $\pi h_{11/2} \otimes \nu g_{7/2}$ configuration. On the excited states of ^{124}La, however, detailed experimental data have not been reported so far, although a γ ray spectrum recorded in conjunction with the Daresbury recoil mass separator and a few of γ ray energies have been reported [19]. In order to study the high-spin band structures in ^{124}La, an in-beam spectroscopy was undertaken.

The excited states of ^{124}La were populated through the ^{35}Cl+^{92}Mo reaction at beam energies of 150 and 135 MeV. The target was a self-supporting metallic foil 960 μg/cm^2 thick. A γ-γ coincidence experiment was performed at 150 MeV using the NORDBALL spectrometer and the tandem-booster system at the Niels Bohr Institute in Denmark. The calibration of the energy scale and the photo-peak efficiency of the γ ray detectors were carried out by ^{152}Eu and ^{133}Ba sources. The coincidence data were recorded on magnetic tapes event by event when at least two of the BaF_2 detectors and two of the Ge detectors fired. In this experiment, 4×10^8 γ-γ coincidence events were collected.

The cross section of the production of ^{124}La is dominant in the ^{35}Cl+^{92}Mo reactions. The compound nucleus ^{127}Pr for this reaction is located far from the line

of β-stability and many channels of particle evaporation are open at 150 MeV. In such a case, the mass assignment of residual nuclei, in general, becomes difficult. Since the measurement of γ-ray yield at different beam energies is helpful for the mass assignment of reaction products, we changed the beam energy to 135 MeV. The experiment at this lower beam energy was performed by the tandem-booster system at the University of Tsukuba. Moreover, a charged-particle multiplicity filter and a neutron detector were used. Particle-γ coincidence measurements were powerful to the selection of exit channels.

2.1.1 NORDBALL

The NORDBALL spectrometer consisted of 18 Compton-suppressed HPGe detectors, one LEPS for the detection of low-energy γ rays and the inner ball of 52 BaF_2 scintillation detectors for γ multiplicity measurement. The frame of the NORDBALL is a truncated icosahedron having 20 hexagonal surfaces and 12 pentagonal surfaces. Compton suppressed γ ray detectors can be mounted on the hexagonal surfaces arranged in such a way that the first five surfaces with a polar angle of 37° surround the beam axis at azimuthal angles every 72°, and the second five surfaces with a polar angle of 79° surround the beam axis in every 72°. This yields 2 rings with 5 detectors equidistantly placed. Ten γ ray detectors can be placed in the forward hemisphere in this way. Another 10 γ ray detectors are arranged symmetrically at the backward hemisphere. The polar angles of each ring are θ=37°, 79°, 101° and 143° with respect to beam direction. The surfaces of the pentagonal shape are usually occupied by the photo multiplier tubes of BaF_2 scintillation counters for γ multiplicity filter. In our experiment, the LEPS was mounted on a hexagonal surface located at the θ=101° ring. The energy resolutions of γ ray detectors were 2.2–2.6 keV for 1.3 MeV γ ray of ^{60}Co source.

2.1.2 Multi detector array of the University of Tsukuba

The spectrometer system consisted of 6 HPGe detectors with BGO anti-Compton shield, one liquid scintillation detector and a charged particle multiplicity filter. The efficiencies of Ge detectors were in the range of 30~40 % relative to a $3^{in} \times 3^{in}$ NaI detector. The ratio of the geometrical solid angle of one detector to 4π was limited to 6.16×10^{-3} by lead collimator. The sum of two photo peak areas for ^{60}Co source was typically 47 % of total area of the spectrum($P/T \sim 0.47$). The Ge detectors and neutron detector were mounted on a dodecahedral frame. Five Ge detectors were placed in axial symmetry with respect to the beam. The polar angle θ was 116.5° (backward direction), whereas azimuthal angles φ's were at every 72°. One Ge detector was placed at $\theta = 0°$. The energy resolutions of HPGe detectors were 1.9−2.2 keV for 1.3 MeV γ ray of ^{60}Co source.

The neutron detector was placed at $\theta = 63.5°$. It was a liquid scintillator made by Bicron BC-501A with a volume of about 5 liter. The detection efficiency was measured by neutrons from an Am-Be source placed at the target position. A standard module of 2160A supplied by CANBERRA was used for $n - \gamma$ discrimination. The detection efficiency was about 40 % for neutrons from the Am-Be source.

The charged particle multiplicity filter was designed in a similar manner to the Si ball developed at Kyushu University. It comprised 17 Si detectors 200 μm thick. The shape of the detector array was chosen to be a pentagonal box in order to minimize the attenuation of γ rays to the Ge detectors arranged in pentagonal symmetry. Faces of the beam entrance and exit were five-segmented pentagonal detectors. The length of the side was 17 mm and a 6 mm hole was prepared at the center to pass the beam. These detectors were developed at Kyushu University [20]. Each of the pentagonal sides was covered by three rectangular detectors 10 mm wide and 24 mm long. The detectors are the model S2662 made by Hamamatsu Photonics Co. Three rectangular detectors were placed along the beam direction

over the length of about 30 mm. The total number of segments was 25, and the total solid angle of active area was 74 % of 4π around the target. From the limitation of electronics in actual operation, number of segments was reduced to 16 by connecting five segments of the entrance face and five rectangular detectors together at backward angles. The discrimination of protons from alpha particles was achieved by measuring pulse heights. Larger pulses correspond to alpha particles, if the chance of hits by two protons in one segment is sufficiently small. The particle discrimination was successful at emission angles smaller than 104°, although it becomes inadequate a little at angles larger than 104°. The channel selectivity was satisfactory for the separation of $3p$ channel from $1p$ and $2p$ channels.

2.2 Spectroscopic investigation of low-lying states in ^{128}La

As described earlier, the spin of the band members is crucial to the occurrence of signature inversion in odd-odd nuclei. For the spin assignment for rotation like bands built at higher excitation energies, the spin and parity of the ground state must be known as well as the multipolarities of linking transitions between the higher excited states and the ground state. The detailed data of the low-lying states are required.

There have been a little data on low-lying states of odd-odd La isotopes in the mass number of A$\sim$130. In ^{132}La, the spin and parity of the ground state is reported to be 2^-. The ground state decays *via* β^+/EC decay with a half life of 4.8 h. An isomeric state with $I^\pi = 6^-$ and $T_{1/2} = 24.3$ min is located at 188.5 keV. This isomeric state decays *via* β^+/EC decay and γ decays of E4 and M3 transitions [21]. Idrissi *et al.* have recently reported the existence of two β-unstable isomers in ^{124}La, though the γ transitions between the isomers were not mentioned[22]. There is no such experimental data on ^{126}La, ^{128}La and ^{130}La. Only one β- unstable state is reported in these odd-odd isotopes.

Odd-A nuclei in this mass region have systematically high-spin isomers caused

by the $h_{11/2}$ high-j intruder orbital or the $g_{7/2}$ orbital. All of the ground-state spins are $1/2^+$ in ^{127}Ba, ^{129}Ba, and ^{131}Ba [23][24][25]. The spins of the ground states in ^{129}La and ^{131}La are $(3/2^+)$ and $3/2^+$ [26][27]. From these systematics of odd-A nuclei and two example of odd-odd La nuclei mentioned above, it is expected that ^{128}La might have two β unstable isomers also. One of them would be of high-spin and the other would be a low spin isomer.

On the basis of such an argument, two kinds of experiments were undertaken. The first experiment was made on the β-decay chain of ^{128}Ce$\rightarrow$^{128}La $\rightarrow$^{128}Ba. The second experiment was the search for the β^+/EC and γ decays from a high-spin isomer from ^{128}La. If the low-spin isomer has spins of 1^+ or 2^+ originated from the coupling of the proton $3/2^+$ state and the neutorn $1/2^+$ state, strong feeding should be observed *via* the β decay from ^{128}Ce.

The half life of the β decay of ^{128}Ce is described as $T_{1/2} = 5.5^{+1.0}_{-2.0}$ minute in reference [28]. This value, however, is not adopted in reference [29]. There is no data of γ rays after the β decay of ^{128}Ce. Neither the low-lying states nor the existence of two β-unstable isomers are reported on ^{128}La.

Godfrey *et al.* and Nolan *et al.* observed the high spin states of ^{128}La [17][18]. However, the γ rays located below the rotational bands are not reported at all. If ^{128}La would have a high-spin isomeric state, the flow of γ ray intensity would be terminated at the isomer. The experimental results by Godfrey and Nolan suggests that linking transitions are very week, and thus the isomer would be a β unstable state. If we could observe linking γ transitions, the half life of them should agree with that of the β decay of high-spin isomer of ^{128}La.

The β decay of ^{128}La were investigated by previous authors [30][31]. The low-lying excited states of ^{128}Ba, the end-point energy of β rays and log ft values are presented in reference [31] in detail.

In order to measure the γ rays and decay curves, we used a tape transport system. Two reactions of ^{103}Rh(^{28}Si, 1p2n)^{128}Ce and ^{115}In(^{16}O, 3n)^{128}La were employed for cross bombardments. The former reaction produces both of ^{128}La

and ^{128}Ce, while the latter reaction never produces ^{128}Ce.

2.2.1 Tape transport system

The tape transport system is a mechanical system to move radioactive products from the production target to an appropriate detection system for β and/or γ rays. A loop made of an old magnetic tape for computers is mounted on a drive pulley at one end and an idler pulley at the other end. To prevent from the breaking of the tape due to the radiation damage by beam irradiation, a lead layer is pasted on the magnetic tape. The lead layer is sufficiently thick to stop the beam as well as reaction products recoiled out from the target. The drive and idling pulley are of course installed in vacuum. The drive pulley is set about 40 cm above the target position. Detectors are placed below the target by 30 cm. The idler pulley is put further down by about 60 cm.

The tape transport system was used in the following sequence. At first, recoiled reaction products were captured in the lead layer during the beam irradiation time. After the irradiation, the tape was moved by the stepping motor to the detector position within a transport time of 0.7 sec. Then measurements of radiation was started. The total length around the loop is approximately 3 m. The length of movement from the target to the detector position should be changed in each cycle of the beam irradiation and subsequent measurements to avoid observations of unwanted activities with long lifetime. After a long time, however, a loop has to be replaced by new one. The fluctuation in positioning of the recoil products at the detector position after transport was negligible in the present experiments.

In some cases, the background from in-beam reaction was low enough, so that a continuous sequence was used to increase counting statistics. During the measurements, the beam irradiated the target and recoil products were collected for the next measurement.

At the detector position, a thin mylar window 50 μm thick is prepared for

penetration of low energy γ and/or β rays. Heavy shields are made to reduce backgrounds. In the measurement of decay curves, the timing of each event was measured by multi-stop TDC with the resolution of 1 s. The multi-stop TDC is our original cammac module. It counts the number of pulses which are generated by a pulse generator. When the data taking system is triggered by the Ge detectors, the number of the multi-stop TDC is accepted as time records.

The stepping motor, a beam chopper and the data taking system were controlled by a personal computer PC-9801E. The data taking system and the multi-stop TDC received a start and reset pulse from the personal computer.

A simple but not minor problem was electrical noise from the personal computer. In our case, the noise was minimized by cutting off the power to the display monitor of the personal computer in periods of the measurements.

2.2.2 The β decay of ^{128}Ce

In this experiment, measurements were performed on γ-γ coincidence and decay curves of γ rays after the β decay of ^{128}Ce. The nucleus ^{128}Ce was produced in the ^{103}Rh(^{28}Si, 1p2n)^{128}Ce reaction at 105 MeV. The Si beam was supplied by the tandem accelerator of University of Tsukuba. The target was a self-supporting foil consisted of natural Rh 1.24 mg/cm^2 thick. The natural abundance of ^{103}Rh is 100 %. From an in-beam spectroscopic measurement, it was known that ^{128}Ce was a dominant reaction product. Off-line measurements were undertaken using the tape transport system described in the preceding subsection. Both of the times of beam irradiation and measurement were 6 min. The γ rays were measured by two HPGe detectors, each of which had a thin Be-window to allow the penetration of low energy photons. The energy resolutions were 2.0-2.2 keV for the 1.333 MeV γ ray of ^{60}Co source. The distance from the source to the surface of detectors was 30 mm. A total of 9×10^7 γ-γ coincidence events were collected.

2.2.3 The β decay of ^{128}La

The nucleus ^{128}La has been produced through the ^{115}In(^{16}O, 3n)^{128}La reaction. The target was a self-supporting foil consisted of natural In 2.7 mg/cm^2 thick. The natural abundance of ^{115}In is 95.7 %. The nucleus of ^{128}La was a dominant reaction product. The excitation function, decay curves of γ rays and the γ-γ coincidences were measured off line using the tape transport system. The excitation function was measured at bombarding energies of 61, 65, 69 and 73 MeV. The decay curve and γ-γ coincidence were measured at 65 and 73 MeV.

The times of irradiation and measurement were 5 min in the excitation function and γ-γ coincidence measurements. The times were 15 min in the decay curve measurements. The γ rays were measured by three HPGe detectors in the γ-γ coincidence. Two of them had thin Be-windows. The energy resolutions were 2.1-2.2 keV. Another detector with a normal Al-window had an energy resolution of 2.0 keV for the 1.333 MeV γ ray of ^{60}Co source. The distance from the source to the surface of detectors were 42-45 mm. The three detectors were placed in a horizontal plane within an angle less than 180°. The angle of one detector was arbitrary and defined as 0°. The other two detectors were positioned at 80° and 160° with respect to the first detector. Angular correlation of $W(0°, 20°)$ and $W(0°, 80°)$ could be measured in this arrangement. In the analysis of the data, the ratios of these two yields were employed. The number of accumulated γ-γ coincidence events were 2×10^8 at 65 MeV and 8×10^8 at 73 MeV.

2.2.4 In-beam spectroscopy of ^{128}La

There is a discrepancy between the level scheme of high-spin band structures in ^{128}La proposed by Nolan *et al.* [17] and that by Godfrey *et al.* [18]. Nolan *et al.* reported a cascade of 138, 104 and 85 keV γ rays below the rotational band, for which the, $\pi h_{11/2}\otimes\nu h_{11/2}$ configuration was assumed. The ordering of these γ rays, however, remains uncertain. The excited states of ^{128}La were produced by the ^{98}Mo(^{37}Cl,α3n)^{128}La reaction at a beam energy of E=145 MeV and the

^{115}In(^{16}O,3n)^{128}La reaction at $E_{\rm lab}$ = 68 MeV. The latter reaction was used to measure an angular distribution only.

According to Godfrey *et al.*, on the other hand, they observed a 66 keV γ ray in the rotational band, whereas the 85 keV γ ray was not observed. They used the ^{95}Mo(^{36}S,p2n)^{128}La reaction at bombarding energies of E=135, 145 MeV.

In order to remove this discrepancy and to determine the spin of the band head of the rotation-like high-spin band, in-beam spectroscopic studies were carried out on ^{128}La through the ^{115}In(^{16}O,3n)^{128}La reaction at $E_{\rm lab}$=66 MeV and the ^{103}Rh(^{28}Si,2pn)^{128}La reaction at $E_{\rm lab}$=105 MeV. These two reactions produce two different compound nuclei of ^{131}La and ^{131}Pr, so that our new experiment would be a part of wide varieties of cross bombardments by combining with previous experiments.

The ^{16}O and ^{28}Si beam were supplied by the tandem accelerator of University of Tsukuba. The ^{128}La was the dominant product in the ^{115}In(^{16}O,3n)^{128}La reaction, but not in the ^{103}Rh(^{28}Si,2pn)^{128}La reaction. The In and Rh targets were both self-supporting metric foils. The thicknesses were 1 mg/cm^2 for In, and 6.8 mg/cm^2 for Rh. The materials were in the natural abundance.

The spectrometer system consisted of 6 HPGe detectors with BGO anti-Compton shield. A neutron detector and a charged particle multiplicity filter were used in the ^{115}In(^{16}O,3n)^{128}La reaction. The details of these detectors were described in section 2.1.2. Two fold γ-γ coincidence events were accumulated to obtain total counts of 1.6×10^6 for the ^{115}In(^{16}O,3n)^{128}La reaction and 3×10^7 in the ^{103}Rh(^{28}Si,2pn)^{128}La reaction.

Chapter 3

Experimental result

3.1 The nucleus ^{124}La

The experimental data was analyzed off line by VAX computer system at the Tandem Accelerator Center in University of Tsukuba. Fig. 1 shows typical γ ray spectra observed in coincidence with protons and neutrons. In the spectrum sorted by placing the gate on the $3p0n$ channel, γ rays from ^{124}Ba are enhanced. According to the calculation in terms of the statistical model, the cross section leading to the $1p1n$ channel is much smaller than that to the $2p1n$ channel. In practice, the spectrum obtained from the $1p1n$ gate did not include any γ rays with strong intensity. The spectrum displayed in the lowest panel of Fig. 1 was observed by summing the spectra gated by $1p1n$ and $2p1n$ channels. Tight correspondence to the spectrum reported in reference [19] can be seen in the pattern of the spectrum in Fig. 1. Besides, the change in the intensities of γ rays from ^{124}La observed at two beam energies was in agreement with that from the statistical-model calculation. The majority of photo peaks, therefore, can be reasonably attributed to the γ rays from ^{124}La. The number of neutron evaporation channels was small, so that even one neutron detector was effective to assign to the $2p1n$ channel. Other γ rays belonging to ^{124}La were identified by coincidence relationships between these γ rays. Of course we rejected known gamma rays from ^{124}Ba [32][33][34], ^{123}Ba [35] and several other nuclei during the analysis. Fig. 2 shows sample gated spectra.

The relative intensities of γ rays were estimated from gated spectra. As seen

in Fig. 1, it is impossible to determine the intensities for γ rays of interest from the singles spectrum. At first the relative intensities were derived for only prominent γ rays in each structure from a total projection spectrum, which included many γ rays from other nuclei. The final value of relative intensities including weak γ rays were obtained from gated spectra by normalizing to those of prominent γ rays.

The energies and relative intensities of γ rays identified in the present work are given in Table 1, 2 and 3. Since the ground state is unknown as well as linking transitions between the ground state and the band head, the excitation energies are tentatively measured from the lowest level of each band. Only the statistical error is taken into account in the uncertainty of the relative intensity.

A proposed partial level scheme drawn in Fig. 3 was constructed from the coincidence relationships. Three band structures are identified as band 1, 2 and 3. The bands 1 and 3 consist of two sequences of crossover transitions, which are connected by interband cascade transitions. The transitions in the band 2 are cascade. Several interband transitions are observed at lower energies between the band 2 and 3.

The pattern of the excited states in the band 1 is similar to those observed in ^{126}La, ^{128}La and ^{130}La. The configuration is proposed to be of $\pi h_{11/2} \otimes \nu h_{11/2}$ by previous authors [16][18]. The band 3 is also similar in the level pattern to the bands, in which the $\pi h_{11/2} \otimes \nu g_{7/2}$ configuration is proposed. A band similar to the band 2 is reported only in ^{126}La [16]. The feeding of the band 2 in ^{124}La seems to be stronger than in ^{126}La. The band members are identified up to the levels near the highest level of the $\pi h_{11/2} \otimes \nu g_{7/2}$ band in ^{126}La. In contrast to this structure, the band 2 in ^{124}La is identified up to much higher energies than those of the levels in the band 3. Several interband transitions are observed between low-lying states of the band 2 and 3 in both of ^{124}La and ^{126}La.

In order to estimate the multipolarities of the above transitions, we used the intensity ratio of $I(37°)/I(79°)$, because the Ge detectors of the NORDBALL can be grouped into two parts depending on polar angles. The intensity of $I(37°)$ for

a certain γ ray, for instance, was obtained by summing gated spectra for all other detectors. This procedure corresponds to the integration of angular correlation function for one γ ray in a γ-γ cascade over the whole solid angle. Thus it gives an approximate angular distribution in large detector arrays.

Theoretical values of $I(37°)/I(79°)$ are nearly equal to 1.6 for stretched ΔI=2 cascade transitions, and 0.8 for stretched ΔI=1 transitions with an assumption of complete alignment in the initial state. These values depend on initial spins. The effect on the ratio, however, is small at high spins.

The experimental ratios of $I(37°)/I(79°)$ are given in Table 1, 2 and 3 as angular distribution ratios. In spite of several assumptions, the cascade transitions in the bands 1 and 3 could be assigned as dipole transitions. Similarly, crossover transitions in the bands 1 and 3, and transitions in the band 2, would be quadrupole transitions. The ratios of $I(37°)/I(79°)$ for 68.8, 122.1, 132.7 keV transitions in the band 1 indicate sizable mixture of E2 component in these cascade transitions. The sudden decrease in the intensity from 422.5 to 297.4 keV transition in the band 2 suggests that the 382.1 keV level might be the band head.

The branching ratios of dipole to quadrupole transitions for several lower states in the band 1 and 3 were derived from the spectra gated by the γ ray located just above the state for ratio estimate. Branching ratios were deduced to $B(M1)/B(E2)$ ratios using the following relation;

$$\frac{B(M1 : I \rightarrow I-1)}{B(E2 : I \rightarrow I-2)} = 0.697 \times \frac{E_\gamma^5(E2)}{E_\gamma^3(M1)} \times \frac{I_\gamma(M1)}{I_\gamma(E2)}.$$

In the present analysis, it was assumed that $\Delta I = 1$ transitions were pure dipole. The results are listed in Table 1 and 3.

3.2 The nucleus ^{128}La

3.2.1 Low-lying states of ^{128}La

First of all, the γ rays of ^{128}La were searched by the β decay of ^{128}Ce. Fig. 4 shows a typical singles spectrum of photons. Strong photo peaks in the spectrum are La-X rays and γ rays from ^{128}Ba, which is the daughter nucleus of ^{128}La. The 104, 147, 68 keV γ rays are in coincidence with La-X rays. La-X rays are emitted by electron capture (EC) of the parent nucleus ^{128}Ce and internal conversions of γ decays in ^{128}La.

Fig. 5 shows the decay curves of La-X rays and two γ rays. The half life of the La-X ray, the 104 and 68 keV γ rays are almost in agreement each other within the uncertainty of 0.1 min. The experimental half life has been determined to be 4.1 $\pm$ 0.3 min. The error includes the statistical and systematic error. The γ rays and the half life of β decay chains of neighboring nuclei are known; ^{125}Ce, 11 s; ^{126}Ce, 50 s; ^{127}Ce, 32 s; ^{129}Ce, 3.5 min [28]. The 105 and 68 keV γ rays of ^{129}La are known. These energies are very close to the 104 and 68 keV γ rays of ^{128}La. However, the 105 and 68 keV γ rays of ^{129}La are in coincidence with each other, while the 104 and 68 keV γ rays are not in coincidence with each other. Other γ rays observed off line in the ^{28}Si+^{103}Rh are listed in Table 4.

A level scheme constructed from the γ-γ coincidence relationships after the β decay of ^{128}Ce is displayed in Fig. 6. The energies and relative intensities are summarized in Table 5. No γ ray in this level scheme, however, was observed in the experiment by the ^{16}O+^{115}In reaction, which never produces the ^{128}Ce. This fact implies that the γ rays in this level scheme are emitted from excited states in ^{128}La populated through the β decay of ^{128}Ce. The spin and parity could not be determined because angular correlations of γ rays and log ft values were not measured. However, the spins are expected to be low from the selection rule of the β decay from the even-even nucleus ^{128}Ce. Thus, spins and parities would be 1^+ or 0^+ in most of the excited states in Fig. 6.

A new finding is clearly observed in the 284 keV γ ray (see Fig. 4). This is the γ ray of 2_g^+ to the 0^+ ground state of ^{128}Ba. This suggests strongly that the spin and parity of the ground state of ^{128}La might be 1^+ or 2^+, instead of the (5^-) assignment by previous authors [31]. A careful inspection of the decay curves of γ rays supports this anticipation. In Fig. 7, decay curves are displayed for γ rays from ^{128}Ba measured with the ^{28}Si+^{103}Rh reaction. Both of the nuclei ^{128}La and ^{128}Ce are produced in this reaction. The half life of 284 keV γ rays from the 2_g^+ to 0^+ ground state is shorter than those of 479 keV ($4_g^+ \rightarrow 2_g^+$) and 643 keV ($6_g^+ \rightarrow 4_g^+$) γ rays. During this analysis, it turned out that the relative intensity of the 284 keV transition is larger than those of 479 and 643 keV transitions by about 40 %. This additional intensity could be ascribed to the side feeding from a low-spin isomeric state of ^{128}La. It is quite reasonable to suppose that the 4_g^+ and 6_g^+ states in ^{128}Ba are fed by the β decay of the high-spin isomeric state in ^{128}La as reported in reference [31]. In regard to the 2_g^+ state in ^{128}Ba, however, the following two routes of decay are possible(see also Fig. 23);

$$^{128}\mathrm{La(high\ spin)} \xrightarrow{\beta} {}^{128}\mathrm{Ba(high\ spin)} \xrightarrow{\gamma} {}^{128}\mathrm{Ba}(2_g^+)$$

and

$$^{128}\mathrm{Ce}(0^+) \xrightarrow{\beta} {}^{128}\mathrm{La}(1^+ \text{ or } 2^+) \xrightarrow{\beta} {}^{128}\mathrm{Ba}(2_g^+).$$

Thus an analysis has been made on the decay curve of the 284 keV γ ray by taking into account the above two decay routes. Denoting the numbers of radioactive nuclei for high- and low-spin isomer of ^{128}La and ^{128}Ce by $N(h.s.)$, $N(l.s.)$ and N_{C}, the counting rate of the 284 keV γ ray can be expressed by

$$\frac{dN}{dt} = \frac{dN(h.s.)}{dt} + \frac{dN(l.s.)}{dt}. \tag{3.1}$$

The second term can be written as

$$\frac{dN(l.s.)}{dt} = N_{\mathrm{C}}(0)\left[-\frac{\tau_{\mathrm{B}}}{\tau_{\mathrm{A}}}\frac{1}{\tau_{\mathrm{A}}-\tau_{\mathrm{B}}}\exp\left(-\frac{t}{\tau_{\mathrm{A}}}\right) + \frac{1}{\tau_{\mathrm{A}}-\tau_{\mathrm{B}}}\exp\left(-\frac{t}{\tau_{\mathrm{B}}}\right)\right] \tag{3.2}$$

by solving the decay rate equation. Here, The symbols τ_{A} and τ_{B} are the mean lifetimes of ^{128}Ce and ^{128}La(l.s.), respectively. With the mean lifetime of τ_{I} for

^{128}La(h.s.), the eq. (3.1) is expressed in the following form;

$$\frac{dN}{dt} = -\frac{1}{\tau_1} N_L(0) \exp\left(-\frac{t}{\tau_1}\right) + N_C(0) \left[-\frac{\tau_B}{\tau_A} \cdot \frac{1}{\tau_A - \tau_B} \exp\left(-\frac{t}{\tau_A}\right) + \frac{1}{\tau_A - \tau_B} \exp\left(-\frac{t}{\tau_B}\right) \right]. \tag{3.3}$$

The quantities of $N_C(0)$ and $N_L(0)$ are the numbers of radioactive nuclei of ^{128}Ce and ^{128}La in the high-spin isomeric state at the time $t = 0$. The ratio of these numbers were estimated from the feeding intensity ratio. The mean lifetimes are known to be $\tau_1 = 7.5$ min for the high-spin isomer in ^{128}La from the decay curves of $6^+ \rightarrow 4^+$ 644 keV and $4^+ \rightarrow 2^+$ 479 keV γ rays in ^{128}Ba, and $\tau_A = 5.9$ min for the ground state of ^{128}Ce from the present work. Thus we can search for the unknown mean lifetime τ_B by fitting the decay curve of the 284 keV γ ray to eq.(3.3). In the present case, two mean lifetimes have approximately same values; namely we can put them to $\tau = \tau_A \simeq \tau_1$. It is easily seen in eq.(3.3) that the slope of the decay curve is mainly determined by τ, if a condition $\tau_B \ll \tau$ is fulfilled. The experimental decay curves shown in Fig. 7 are indicative for this situation. The above analysis resulted in the half life of $T_{1/2} \leq 2$ minute for the low-spin isomeric state of ^{128}La. There is a similar case of the ^{124}La [22]

3.2.2 The half life of the β decay of ^{128}Ce

From the analysis of the decay curves shown in Fig. 5, we report a new data of 4.1±0.3 min as the half life of the β^+ decay from the ground state in ^{128}Ce.

3.2.3 Level scheme of ^{128}Ba

The level scheme of ^{128}Ba was reexamined based on the γ-γ coincidence measurement after the β decay of the ^{128}La. Prior to our work, the low-lying excited states, feeding intensities and an end point energy of β rays were reported [30][31].

The results of our new measurement are summarized in Table 6 on the energies, relative intensities of γ rays and multipolarities. Fig. 8 shows a new level scheme of ^{128}Ba, which was constructed from the $\gamma - \gamma$ coincidence relations

and intensity balance. The relative intensities of γ rays were estimated from a singles spectrum. Although γ rays from nuclei other than ^{128}Ba were observed in the spectrum, the nucleus ^{128}La is a dominant product in the ^{16}O+^{115}In reaction, and thus the γ rays of ^{128}Ba were observed with stronger intensities than those of other nuclei. Higher energies of γ rays from an even-even nucleus compared to odd-A or odd-odd nuclei made it easy to distinguish the γ rays of ^{128}Ba. The feeding intensities to the excited states of ^{128}Ba from ^{128}La were estimated from the γ ray intensities. The values of log ft were evaluated with the aid of these intensities and Q_β quoted in reference [30][31]. The results are given in Table 7. Our new level scheme and log ft values are in good agreement with the previous data by Zolnowski and Sugihara [31], except for several new spin assignments and small discrepancies in γ ray energies within 1 keV.

The ground state band, γ band and several negative parity bands are established on the excitation energies, spins and parities by in-beam spectroscopies [36][37]. In Fig. 8, the ground state band is observed up to the 6^+ 1406.7 keV level. The levels in quasi-γ band are 2^+ 884.5, 3^+ 1324.2, 4^+ 1372.0, 5^+ 1931.0 and 6^+ 1939.0 keV levels. The 2395.5, 2412.4 and 2038.7 keV levels are assigned as negative parity levels by in-beam spectroscopy. The energies of 5^- 2038.7 and 3^+ 2038.3 keV levels can not be resolved by the observation of a singles γ ray spectrum. The difference, however, is clearly significant in coincidence spectra and coincidence relations. The placement of these two levels is reliable in the level scheme in Fig. 8.

The results on angular correlations are as follows.

1) Calibration In Fig. 9(a), the measured ratios of

$$\mathrm{DCR} = W(\gamma_1; 0°, 20°)/W(284; 0°, 80°)$$

are plotted for $J_i \xrightarrow{\gamma_1(\delta)} 2^+ \xrightarrow{284} 0^+$ cascades. The 284 keV γ ray is emitted in the $2^+_g \rightarrow 0^+_{\mathrm{gnd}}$ transition with pure E2 character. The γ_1 = 479 and 1088 keV γ rays are known to be E2, while the 600 and 1040 keV γ rays are known to be

M1 dominant. The experimental DCR's are in agreement with calculated DCR's. Similar results are obtained for $J_i \xrightarrow{\gamma_1(\delta)} 4_g^+ \xrightarrow{479} 2_g^+$ cascades. It is consistent that the 644 keV γ ray is E2, and that the 561 and 609 keV γ rays are M1 dominant. With these calibrations, the assignments of M1/E2 was given to the γ ray of 1053 keV(see Fig. 9(c) and (d)). And the assignment of ΔI=1 transition (M1 or E1) were given to the γ rays of 1036 and 1070 keV(see Fig. 9(b)) and two γ rays of 1549 and 1754 keV(see Fig. 9(a). The assignment for the last two γ rays are less certain due to large experimental errors.

2) 1799.3 keV level Since this level decays into 4^+ level in the ground state band, the possible spins are 3, 4 or $5\hbar$ from angular momentum conservation. The assignment of $I^\pi = 5^\pm$ is unlikely from the observed intensity of the transitions to 2_g^+ and 2_γ^+ states. We can not determine the parity of this level immediately at this stage. However, an overall consistency of the transition intensities connected to this level leads to an assignment of $I^\pi = (3^+)$ or (4^+) (see discussions on the 2424.9 keV level).

3) 1832.9 keV level This level decays into the 4^+ and 2^+ levels in the ground state band. As seen in the level scheme in Fig. 8, the transition energies are 1070 and 1549 keV. These transitions are likely to be $\Delta I = 1$ from the angular correlation described above, though the experimental uncertainties are rather large for 1549 keV γ ray. Possible spins of this level are 3, 4, and $5\hbar$ from the angular momentum coupling of $4\hbar$; and 1, 2, and $3\hbar$ from the coupling to the 2^+ level. Thus, the most probable spin is $3\hbar$, and the parity would be positive from intensity considerations.

4) 2424.9 keV level The transition with the energy of 1053 keV is crucial to the determination of the spin and parity of this level. The experimental data of the angular correlation indicate that this transition composes mixed multipoles of $L = 1$ and 2. In our measurement, a $L = 1$ transition with *small* mixture of $L = 2$ can not be discriminated from a pure $L = 1$ transition, because the observation of coincidence yields are performed at only two angles. However, the experimental DCR can be reproduced by a calculation involving significantly large mixture. This

is illustrated in Fig. 10. A large mixture of E1 and M2 is not probable in usual γ transitions. Consequently we have assigned the 1053 keV transition to be M1/E2. Possible spins are 3, 4, and $5\hbar$ from the coupling to the 4^+_γ level. The parity is positive. The assignments of $I^\pi = 3^+$ and $I^\pi = 4^+$ can be rejected, because possible transitions to the 2^+ levels is not observed. From these results, the assignment of $I^\pi = 5^+$ is almost uniquely given to this level.

The negative parity for the 1832.9 keV level is not consistent with the experimental intensity of 592 keV γ ray. The transition from 5^+ 2424.9 keV level to the 3^- 1832.9 keV level must be M2. Similarly, the negative parity of the 1799.3 keV level is outside for the choice. The 4^- assignment makes it difficult to give sufficient intensity to the 1515 keV transition into 2^+ level; the 3^- assignment is not compatible with the 626 keV transition from the 2424.9 keV 5^+ level.

The spins and parities of other levels were tentatively assigned from the coincidence relations and intensity balance. The 2201.9 keV level is suggested to be a (4^+) or (3^+) state, since this level decays to 2^+_g, 2^+_γ, 4^+_g and 4^+_γ levels, and since any decay to negative parity level is not observed. Similar arguments was made on the assignment of $I^\pi = (5^+)$ or (4^+) for the 2976.6 keV level, and $I^\pi = (5^-)$ or (6^+) for the 2877.1 keV level.

The smallest value of log ft is 5.6 for the 5^+ 2429.5 keV level. The 2877.1 keV (5^- or 6^+) level has a log ft value of 5.8. The log ft value of to the 2976.6 keV (5^+ or 4^+) level is determined to be 6.1. The log ft values of other states are lager than 6.5. These experimental results strongly suggest that the γ rays in the level scheme in Fig. 8 are fed by the β decay of a high-spin isomer in ^{128}La with the spin and parity of $I^\pi = 5^+$.

3.2.4 High spin states of ^{128}La

Figs. 11 to 13 show typical γ ray spectra observed in the γ-γ coincidence measurements of ^{128}La. The level scheme shown in Fig. 14 was established from the γ-γ coincidence relationships and intensity balance. These band structures are

in good agreement with those report by Godfrey and Nolan *et al.* [17][18], except for the lower part of the bands.

The spectra gated by 66, 85, 104, 138 keV γ rays confirm the level structures in the band 1 (see Fig. 11 and 12). These γ rays have strong intensities and belong to a decay cascade. In the spectra obtained by placing gates on the 104 and 138 keV γ rays, two weak photo peaks are clearly observed at energies of 114 and 48 keV in spite of a small number of counts. The spectrum gated by the 66 keV γ ray gives a weak peak at 48 keV as well as at 85 keV, but not at 114 keV(see Fig. 15). On the other hand, neither the 48 keV peak nor the 114 keV peak appear in the spectrum gated by the 85 keV γ ray. Thus the 114 keV γ ray should be placed in parallel to the 66 keV γ ray, and the 48 and 85 keV γ rays should be placed under the 66 keV γ ray in parallel. In this construction of the level scheme, a γ ray is assumed. It is the 37 keV γ ray, and was not verified directly in the coincidence spectra. The energies of La-X ray are 33 and 37 keV, and this obscured the direct verification of 37 keV transition. La-X ray is in coincidence with many γ rays in the band members of ^{128}La. Nevertheless, efforts to estimate the intensity of this transition did not yield any reliable result. Another γ ray of 168 keV in energy could not be combined in the present. It is in coincidence only with 85 keV γ ray. A transition between a very small gap of 5 keV in the band 2 is missing, and thus the placement is tentative. Since no other γ ray was observed in prompt coincidence, we have assumed that *the lowest level of the band 1 is the high-spin isomer of* $I^{\pi} = 5^{+}$.

The low energy part of the band 1 of ^{128}La obtained from the present study is compared with level schemes reported by previous authors in Fig. 16. The level scheme (a) given by Nolan *et al.* includes a cascade of the 138, 104 and 84 keV γ rays. The 66 keV γ ray is not observed. Godfrey *et al.* reported the 138, 104 and 66 keV γ rays in the level scheme (b). They mentioned that the 85 keV γ ray could not be observed. In our study, the 66 and 85 keV γ rays are clearly observed and the placement in the level scheme is established.

The energies and relative intensities of the γ rays for high-spin bands are

summarized in Table 8. The error includes statistical error and uncertainty of efficiency calibration for detectors. The 65 and 66 keV γ rays could not be resolved, so that the intensities were estimated from intensity ratios of gated spectra. The correction for internal conversion coefficients was performed by using theoretical coefficients.

In order to determine the multipolarities of γ rays, DCO ratios are estimated from the γ-γ coincidence matrix. There are two DCO ratios of

$$R_{3,2} = \frac{W(117°, 117°, \Delta\varphi = 144°)}{W(117°, 117°, \Delta\varphi = 72°)}$$

and

$$R_1 = \frac{W(117°, 0°)}{W(0°, 177°)},$$

(see Appendix A). The DCO ratio of R_1 is more sensitive to the multipolarity than $R_{3,2}$. Unfortunately, however, the attenuation of low energy photons to 0° detector in our crystal ball was high due to the absorption in a beam stopper. Although the sensitivity for the determination of multipolarities is not so high, there is a merit in the ratio $R_{3,2}$ that the number of combinations of detectors are larger (20 sets) than that for R_1 (5 sets). The counting statistics is large in $R_{3,2}$. In the analysis of DCO ratios, $R_{3,2}$ was evaluated from the coincidence data taken with five detectors at a backward angle of θ=117°. It is assumed that $\Delta I = 1$ transitions are pure dipole transitions and $\Delta I = 2$ transitions are of quadrupole. Theoretical values are $R_{3,2} = 0.93$ for stretched $\Delta I = 2$ transitions, and $R_{3,2} = 1.06$ for stretched $\Delta I = 1$ transitions.

The experimental DCO ratios for the band 1 and 2 in ^{128}La are given in Table 8. Fig. 17 shows the experimental DCO ratios $R_{3,2}$. Two groups of dipole and quadrupole transitions are separated clearly. The determination is much reliable for dipole transitions than quadrupole transitions. This is due to the fact that the intensities of dipole transitions are higher than those in quadrupole transitions. The assignment of $\Delta I = 2$ for the 85 and 114 keV γ rays are very consistent in our new level scheme.

Chapter 4

Discussion

4.1 The band structure of ^{124}La

In the present experiment, the absolute values of excitation energies, spins and parities of each level are not determined. Nevertheless, a brief discussion can be made on the structure of the bands in comparison with experimental data on heavier La isotopes. In the following analysis, we assumed that the band 1 and 3 consisted of E2 cascades connected by M1 transitions, and that the band members in the band 2 were connected by E2 transitions.

The experimental routhians for the band 1 indicate an appreciable signature splitting as shown in Fig. 18. Two routhians cross each other at $\hbar\omega \sim 0.1$ and $\hbar\omega \sim 0.44$ MeV. On the contrary, the splitting is very small in the band 3. The values of e' in the band 2 are close to those of the band 3 at low rotational frequencies, and then gradually come down to the values of the band 1 at higher frequencies. The experimental alignment of the band 1 increases sharply at $\hbar\omega \sim 0.5$ MeV. The alignment of the band 3 increases monotonically up to $\hbar\omega \sim 0.4$ MeV. The alignment of the band 2 indicates weak increases at $\hbar\omega \sim 0.44$ and at $\hbar\omega \sim 0.6$ MeV (see Fig. 19).

The nucleus ^{124}La can be approximated by a model in which a neutron and a proton coupled to an even-even core of ^{122}Ba. In the ground-state band of ^{122}Ba, a large spin alignment is observed at $\hbar\omega = 0.35$ MeV [38]. This alignment is attributed to the $h_{11/2}$ proton by blocking argument, because the spin alignment

of the $h_{11/2}$ band in ^{123}Ba increases sharply at $\hbar\omega = 0.35$ MeV [35]. On the other hand, no sharp spin alignment is observed in the π $h_{11/2}$ band in ^{123}La [40]. This could also be understand from the blocking of alignment for the $h_{11/2}$ proton. Weak alignments at $\hbar\omega \sim 0.4$ and at $\hbar\omega \sim 0.6$ MeV are due to the $h_{11/2}$ neutron.

From these facts, the delay of the alignment in the band 1 in ^{124}La could be interpreted by the blocking of alignments in both of $h_{11/2}$ proton and $h_{11/2}$ neutron. The weak increase in alignment of the band 3 at $\hbar\omega \sim 0.4$ MeV might be caused by the $h_{11/2}$ neutron as compared to the $\nu h_{11/2}$ band in ^{123}La. The slow increases in the alignment of the band 2 could be attributed to the alignment of $h_{11/2}$ neutron in comparison with the $\pi h_{11/2}$ proton band in ^{123}La.

The experimental data described above can be compared to some theoretical calculations. Figs. 20 and 21 show calculated quasiparticle energies e' in the rotating frame for protons and neutrons as a function of rotational frequency $\hbar\omega$ for ^{124}La. Before this calculation, we have estimated deformation parameters β and γ by a calculation of the total routhian surface (TRS) [41]. The parameters are listed in Table 4 for several configurations. The values of $\beta = 0.27$ and $\gamma = 0°$ were adopted in the calculation of e'.

In Fig. 20, the orbital "a" originated from the $h_{11/2}$ [550]1/2 Nilsson state is the lowest in energy. The signature splitting between "a" and "b" is very large. The first crossing of the $h_{11/2}$ proton occurs at $\hbar\omega$=0.35 MeV(ab crossing). Likewise, the $h_{11/2}$ [523]7/2 Nilsson state has the lowest energy for neutron orbitals shown by A and B in Fig. 21. The signature splitting, however, is not large. The first crossing is predicted at $\hbar\omega = 0.44$ MeV. These results imply that the $\pi h_{11/2} \otimes \nu h_{11/2}$ band becomes the yrast band, and are consistent with experimental data. Thus one could reasonably propose that the configuration of the band 1 would be π $h_{11/2}$ $\otimes$ ν $h_{11/2}$ with positive parity.

In Fig. 21, the signature splitting is very small in a $g_{7/2}$[413]5/2 orbital, which makes it possible to observe both signature partner. The $g_{7/2}$ orbital is rather isolated from other orbitals, and the $g_{7/2}$ neutron does not block the alignment of

the $h_{11/2}$ neutron. Therefore, the $\pi\ h_{11/2} \otimes \nu\ g_{7/2}$ configuration with negative parity could be proposed for the band 3 in ^{124}La.

On the configuration of the band 2, the following discussion could be made. As seen in Fig. 19, a weak alignment occurs at $\hbar\omega \sim 0.4$ MeV followed by somewhat stronger alignment at $\hbar\omega \sim 0.6$ MeV. The alignments in the $\pi h_{11/2}$ band of ^{123}La take place at almost the same rotational frequencies as ^{124}La. In ^{123}La, the alignments are considered to be due to the first and second $h_{11/2}$ neutron crossings. Since the backbend of the $h_{11/2}$ proton would be blocked, it is expected that the configuration of this band would be $\pi h_{11/2} \otimes \nu s_{1/2}$. The $\nu s_{1/2}$ orbital (E and F) lies between the $\nu h_{11/2}$ (A and B) and $\nu g_{7/2}$ (C and D) orbitals, and its signature splitting is large as seen in Fig. 21. The observation of signature partner would be difficult for the sake of this splitting. This is consistent with experimental facts that the band 2 is a single E2 cascades without the observation of the signature partner, and that the alignment behavior is analogous to ^{123}La. With regard to the interband transitions between the band 2 and 3, they are observed between only a few low lying levels in ^{124}La, whereas the interband transitions in ^{126}La take place up to higher levels. In the neutron quasiparticle diagram in Fig. 21 for ^{124}La, the energy of $\nu s_{1/2}$ state (E) is much lower than that of $g_{7/2}$ (C and D). In ^{126}La, the energy of $\nu s_{1/2}$ (E) orbital is only slightly higher than the energy of $d_{5/2}$ (C and D) orbital around $\hbar\omega \sim 0.2$ MeV. The level crossing between D and F in Fig. 22 brings about the mixture of the wave functions at around $\hbar\omega \sim 0.3$ MeV. This would be a reason for the difference in the interband transitions of ^{124}La from ^{126}La. The configuration of the band 2, therefore, could be proposed to be $\pi h_{11/2} \otimes \nu s_{1/2}$.

In the calculation of experimental routhians and alignments plotted in Fig. 18 and 19, the spins of the band members and K-value of the band head must be input to the program. We used the same method as in references [16][18], which was applied to ^{126,128,130}La. The configuration of the band 1 and 3 were assumed to be $\pi h_{11/2} \otimes \nu h_{11/2}$ and $\pi h_{11/2} \otimes \nu g_{7/2}$, respectively. The K-value of the band 1 is 4 from the Gallagher-Moskowski coupling rule for the assumed configuration. The

values of $I^{\pi} = 4^{+}$ and $K = 4$ were tentatively given to the head of the band 1. In the band 2, $I^{\pi} = 3^{-}$ and $K = 0$ were assumed. The band 3 was assumed to be built on the band head with $I^{\pi} = 2^{-}$ and $K = 2$.

However, it should be noted that the spin of the band head would not be so small. According to experimental studies on β decay of ^{124}La, there are two β-unstable isomers. The spin of the high-spin isomer is proposed to be 6, 7 or 8 $\hbar$ [32][39][22]. Although the detail of transitions at low-lying levels involved two β-unstable states is uncertain, it could not be rejected out that the bands are built on a high-spin isomer.

4.2 Low-lying states in ^{128}La

The spin assignment of high-spin states of ^{128}La has been performed mainly by the β decay of ^{128}La and ^{128}Ce. From the experimental results described in the preceeding section, it turned out that ^{128}La has two β unstable isomeric states. The mode of decay is illustrated in a simplified decay scheme in Fig. 23. The β unstable ground state of ^{128}La is assumed to have the spin and parity of (1^{+}) or (2^{+}). It is considered that there is a decay to the ground state of ^{128}Ba from the β unstable ground state of ^{128}La by . It is considered that the β unstable ground state can decay to the ground state of ^{128}Ba directly. However, the β ray and the intensity by this decay pass were not measured.

Heavy ion reactions populate, in general, high spin states, which decay into low-lying states in turn though yrast line. If there is a high-spin isomeric state in the course of the decay cascade, considerable intensity of γ rays would branch into this isomer. It is possible in some cases that high spin states decay to the ground state though a bypass which do not include the high-spin isomer. At first, we measured the γ rays emitted from low-lying states in ^{128}La by the β decay of ^{128}Ce. Secondly, a bypassing transition was searched through the in-beam spectroscopy. If a bypassing transition exists, γ rays of low-lying states should be observed in coincidence with the γ rays of high-spin state. However, such a γ ray was not observed in both in a

previous report and in our present study.

The next experiment was the search for a γ transition between the high-spin isomer and the low-lying states in ^{128}La. We have searched for γ rays other than those from ^{128}Ba with the half life of 5.2 min, which is $T_{1/2}$ of the high-spin isomer. Since we have already gotten the data on γ rays of low-lying states of ^{128}La, a $\gamma - \gamma$ coincidence could enhance such γ rays. This trial did not any positive result, although we analyzed lifetimes of peaks with relative intensities as low as 0.5% of 284 keV γ ray of ^{128}Ba. From these results, it is concluded that the branching ratio of γ ray emission (not mean the decay to the ground state)is smaller than about 1% of the β decay.

At present, the extremely weak γ emission from the high-spin isomer of ^{128}La can be discussed in the following manner. The decay to the ground state are highly converted; or the high-spin isomer is the ground state.

If we assume the spin of 1^+ for the ground state, and if the energy gap between the high-spin isomer and the ground state is 100 keV, the type of transition type is E4; the internal conversion coefficient is about ICC= 2×10^2; and the partial half life is about 10^5 s. If we assume, however, an E3 transition, ICC is 30 and partial half life is of the order of 1 second. The γ transition between the isomer and the ground state is still open, and thus measurements of conversion electron are highly required to determine the decay scheme more rigorously.

As described earlier, it is assumed that the high spin states almost decay into the β-unstable high-spin isomeric state with $I^\pi = 5^+$. The sudden change of the intensity of a $\Delta I = 2$ transition suggests that the spin and parity of 7^+ could be given to the band head of the $\pi h_{11/2} \otimes \nu h_{11/2}$ configuration.

4.3 Isomeric states in ^{128}La

The isomeric states in ^{128}La can be discussed by a simple principle. An odd-odd nucleus consists of an even-even core with $K = 0$, a proton and a neutron.

The data of neighboring odd-A nuclei are as follows. The nucleus ^{131}Ba has an isomer of $I^\pi = 9/2^-$ with $\nu h_{11/2}$ configuration; I^π of the ground state is known to be $1/2^+$. Nearly degenerated two states of $\nu s_{1/2}$ and $\nu d_{3/2}$ are main component of the ground state [25]. In ^{129}Ba, a $\nu g_{7/2}$ $I^\pi = 7/2^+$ isomer and the $I^\pi = 1/2^+$ ground state are reported. Moreover, the $\nu h_{11/2}$ $I^\pi = 11/2^-$ state exist above the ground state [24]. Similarly, the nucleus ^{127}Ba has a $\nu h_{11/2}$ $I^\pi = 7/2^-$ isomer and the $I^\pi = 1/2^+$ ground state [23][42]. The $\nu h_{11/2}$ and $\nu g_{7/2}$ states are 80 keV above the ground state, and these excitation energies are nearly equal.

The Nilssn orbitals are slightly different in odd-Z isotopes. In ^{129}La and ^{131}La, a $\pi h_{11/2}$ $I^\pi = 11/2^-$ isomer and the $\pi g_{7/2}$ $I^\pi = 3/2^+$ ground state are known. The two orbitals of $\pi g_{7/2}$ and $\pi d_{5/2}$ are nearly degenerated in energy [26][27].

An $h_{11/2}$ rotational band is reported on ^{127}La. However, an isomer is not reported and the ground state is unknown [43]. It is predicted that the energy gap between the $h_{11/2}$ and $g_{7/2}$ states is small for the systematics of the odd-A La isotopes. The $\pi h_{11/2}$ state might be the ground state. The feeding intensity is stronger in the $\pi h_{11/2}$ band.

It is well known for the rotation of deformed nuclei that the projection of angular momentum of a single particle on the symmetry axis Ω is responsible for the spin of nuclei. If the K-value of a nucleon (j, Ω) is large, this nucleon strongly coupled to the core. The spin of the ground state is given by $I = \Omega$ $(K = \Omega)$. On the contrary, if K-value is small, the nucleon aligns its angular momentum toward the axis of rotation. The spin of the ground state would be $I = j$. In fact, the ground states of odd-A La isotopes have $I^\pi = 11/2$ with the $\pi h_{11/2}$ (Ω=1/2) configuration. The odd-A Ce isotopes have lower spin than 11/2 in their ground states in the $\nu h_{11/2}$ ($\Omega \leq 7/2$) configuration [44][45]. The K-values for odd-odd nuclei are given by

$$K = |\Omega_\pi \pm \Omega_\nu| \qquad \text{with} \qquad I \geq K \tag{4.1}$$

The parity must fulfil the relation

$$\pi = \pi_\pi \times \pi_\nu \tag{4.2}$$

The Nilsson orbitals relevant to the low-lying states in ^{127}Ba are $h_{11/2}(\Omega_\nu = 7/2)$, $g_{7/2}(\Omega_\nu = 5/2)$ and $d_{3/2}(\Omega_\nu = 1/2)$. For ^{127}La, those are $h_{11/2}(\Omega_\pi = 1/2)$ and may be $g_{7/2}$ which and $d_{5/2}$ state ($\Omega_\pi = 3/2$) are degenerated. The coupling of the proton and neutron combined to ^{128}La are listed in Table 10.

Table 10. Proton-neutron configuration of ^{128}La

Configuration	K^π		Lower state
$\pi[550]1/2\uparrow \otimes \nu[411]1/2\downarrow$	0^-	1^-	0^-
$\pi[550]1/2\uparrow \otimes \nu[523]7/2\uparrow$	3^+	4^+	4^+
$\pi[550]1/2\uparrow \otimes \nu[402]5/2\uparrow$	2^-	3^-	3^-
$\pi[422]3/2\downarrow \otimes \nu[411]1/2\downarrow$	1^+	2^+	2^+
$\pi[422]3/2\downarrow \otimes \nu[523]7/2\uparrow$	2^-	5^-	2^-
$\pi[422]3/2\downarrow \otimes \nu[402]5/2\uparrow$	1^+	4^+	1^+

From the present experiment, I^π of the low-spin state is very probable to be 1^+ or 2^+. The high-spin isomer is assigned to be $I^\pi = 5^+$. Gallaer-Moscowsky rule suggests the spin of the ground state.

$$I = \Omega_p + \Omega_n \qquad \text{if} \quad \Omega_p = \Lambda_p \pm \frac{1}{2} \quad \text{and} \quad \Omega_n = \Lambda_n \pm \frac{1}{2} \tag{4.3a}$$

$$I = |\Omega_p - \Omega_n| \qquad \text{if} \quad \Omega_p = \Lambda_p \pm \frac{1}{2} \quad \text{and} \quad \Omega_n = \Lambda_n \mp \frac{1}{2} \tag{4.3b}$$

The $\pi h_{11/2} \otimes \nu d_{3/2}$ configuration can produce the low spin of 0^-. However, this configuration is in negative parity and the $\pi h_{11/2}$ orbit generates an aligned angular momentum with large spin.

If the spin of the ground state is $1\hbar$, a possible configuration for the ground state would be $\pi g_{7/2} \otimes \nu g_{7/2}$. Only this configuration can make the low spin of 1^+.

If the spin of the ground state is $2\hbar$, possible configurations would be of $\pi h_{11/2} \otimes \nu g_{7/2}$ and $\pi g_{7/2} \otimes \nu d_{3/2}$. The former configuration has the negative parity. If the ground state is 2^-, an E3 transition between 2^- and 5^+ states should be observed.

The high spin isomer may have the $\pi h_{11/2} \otimes \nu h_{11/2}$ configuration. The K-values of other configurations are too small.

4.4 Systematics of signature inversion of odd-odd La isotopes

Fig. 24 shows the signature splitting $E(I) - E(I-1)$ of the $\pi h_{11/2} \otimes \nu h_{11/2}$ bands of odd-odd La and Cs isotopes. The data of ^{126,128,130}La were taken from references [16][18]. The signature splitting of ^{130}La is rather uniform with increase of spins. The splitting in ^{124}La, ^{126}La and ^{128}La are clearly different from ^{130}La. The splitting grows up from a small value at low spin; gradually decreases with spin; and a crossing occurs between two sequences having opposite signatures. This feature implies signature inversion. The signature inversion in this sense is clearly observed in ^{124}La. The signature splitting depends on the neutron number. The crossing point of two signature partner becomes lowest in ^{124}La.

The spin assignment of the ^{128}La performed in the present study has proved that the signature inversion occur in the low spin region. The sign of the signature splitting defined by $E_{\rm unfavored}(I) - E_{\rm favored}(I)$ has been determined from the spin of the rotational band. It is opposite to the other odd-odd La isotopes. However, the same tendency as Cs isotopes has been found. The signature inversion in ^{130}La and ^{128}Cs is not so clear at present. The normal signature dependence is reported in ^{132}La [46]. It is anticipated, therefore, that a dramatic change might appear at around a neutron number of 73.

In Fig. 25, the experimental signature splitting is compared with the calculation in terms of the particle rotor model by Tajima [13]. The sign of the signature splitting was opposite to the calculation in all the La isotopes so far. Fig. 25 indicates that the calculation is not in agreement with the present data, although it was successful in the case of Cs isotopes. Since the signature inversion depends on the effect of shell filling, new calculations would be necessary by extending the

model space outside the $h_{11/2}$ orbital.

Chapter 5

Conclusion

In order to study the signature inversion of odd-odd La isotopes, two experimental investigations have been carried out. The first experiment was an in-beam γ ray spectroscopy of ^{124}La for the purpose of the extension of systematics in high-spin band structures for light odd-odd La isotopes. The second experiment was made on the β decays of ^{128}La and ^{128}Ce for the experimental determination of spins of the high-spin bands in ^{128}La. An in-beam spectroscopic study was also performed to remove a discrepancy in previous works for the lower part of the $\pi h_{11/2} \otimes \nu h_{11/2}$ band in ^{128}La.

The conclusions of the first investigation are as follows.

1) Three band structures having rotational character have been observed. The absolute values of excitation energies of the levels in these bands were not determined because of the lack of knowledge on low-lying states and the ground state in ^{124}La. The spins of these band members was also not determined in an experimental manner from the same reason as for energy.

2) In comparison with experimental data on heavier odd-odd La isotopes and neighboring odd-A nuclei, a qualitative discussion has been made on the experimental routhians and alignments of these bands. As a result, dominant configurations of the valence proton and the neutron can be proposed to be $\pi h_{11/2} \otimes \nu h_{11/2}$ in the band 1, $\pi h_{11/2} \otimes \nu s_{1/2}$ in the band 2 and $\pi h_{11/2} \otimes \nu d_{5/2}$ in the band 3. These configurations are reasonably consistent with quasiparticle energies in the rotating frame calculated by the cranking shell model.

3) A signature splitting larger than those of heavier La isotopes was observed in the $\pi h_{11/2} \otimes \nu h_{11/2}$ band. The sign of signature splitting $E(I) - E(I-1)$ changes clearly at rotational frequency around $\hbar\omega \sim 0.45$ MeV. This frequency is lower than that in heavier isotopes. Thus, the signature inversion occurs in the $\pi h_{11/2} \otimes \nu h_{11/2}$ band in ^{124}La. Since the spin is not determined, however, it is still open question whether the inversion takes place at low spin region or it is manifested in high spin region.

The conclusions of the second investigation are as follows.

A) The half life of the β^+ decay of ^{128}Ce has been determined with higher accuracy than the previous value. It is 4.1 ± 0.3 min.

B) It has been found that there are two β unstable states in ^{128}La. The half life of 5.2 ± 0.3 min is in good agreement with the value reported by previous authors. An upper limit of the half life of newly found state is 2 min. A probable spin would be 1^+ or 2^+ from the fact that this new state is populated *via* β decay of the 0^+ ground state in ^{128}Ce. The extremely weak intensity of γ rays with the half life of 5.2 min suggests that γ transitions between two isomeric states might be highly converted due to the high multipolarity and small transition energies. There might be some hindrance caused by nuclear structure.

C) The low-lying state of ^{128}Ba have been re-examined by the β decay of ^{128}La. Measurements of angular correlation resulted in a new spin assignment of 2424.9 keV level to be 5^+, instead of the previous assignment of (4^-). The value of log ft for this level leads to a spin assignment of $I^\pi = 5^+$ for the state with the half life of 5.2 min. The proton-neutron configuration of these two β unstable states have been proposed to be $\pi h_{11/2} \otimes \nu h_{11/2}$ for the state of $I^\pi = 5^+$ and $T_{1/2} = 5.2$ min., and $\pi g_{7/2} \otimes \nu g_{7/2}$ or $\pi g_{7/2} \otimes \nu d_{5/2}$ for the state with $T_{1/2} < 2$ min.

D) The spin of the band 1 with a proposed configuration of $\pi h_{11/2} \otimes \nu h_{11/2}$ has been determined. This spin assignment confirmed the occurrence of the signature inversion at low spins in ^{128}La. The sign of the signature splittings agrees

qualitatively with calculations by particle-rotor model including a triaxial core and proton-neutron interaction. A quantitative agreement, however, is inadequate.

Acknowledgments

The author wishes to express his gratitude for the guidance and encouragement recieved from Prof. K. Furuno. He also whishes to express his thanks to Dr. T. Komatsubara, Dr. J. Lu, Dr. J. Niiya and the other members of his group. The experiment of ^{124}La was supported by the NORDBALL collaboration. The other expriments were suported by the Tandem Accelerator Center of the University of Tsukuba.

Appendix A

A.1 Gamma-gamma directional correlation and DCO ratios

In experiments with detector arrays of the crystal-ball type, the measurements of singles spectra are in general difficult partly because the data taking system cannot process tremendously large number of counts and partly because the detectors are placed in fixed angles. The number of independent detection angles is not so large.

On the contrary, good measurements of angular correlation is feasible by virtue of the large number of detectors. Thus, the angular momentum of a certain γ ray is determined by DCO ratios derived from two dimensional γ-γ coincidence matrix. DCO is an abbreviation of Directional Correlation from Oriented nuclei. The theory of angular correlation in γ transitions is well established [47].

Let I_0, I_1 and I_2 be the angular momenta of three states connected by cascade γ rays of γ_1 and γ_2. If the initial state I_0 is prepared by a nuclear reaction, it is in general aligned with respect to its magnetic substates. This alignment is characterized by the following orientation parameter;

$$B_{\lambda_0}(I_0) = \sqrt{2I_0+1} \cdot \frac{\sum_{m_0=-I_0}^{I_0} (I_0 \; -m_0 \; I_0 \; m_0 | \lambda_0 \; 0) \exp\left(-\frac{m_0^2}{\sigma^2}\right)}{\sum_{m_0=-I_0}^{I_0} \exp\left(-\frac{m_0^2}{\sigma^2}\right)} \qquad (A1.1)$$

Here, the quantity σ represents the distribution of substate population $P(m_0)$ approximated by Gaussian distribution. The axis of quantization is taken to the beam direction. If one observe the first radiation γ_1 in a direction of polar angles (θ_1, φ_1), and the second radiation γ_2 in a direction (θ_1, φ_1) with respect to the beam

direction, the probability for observation of γ_2 in coincidence with γ_1 is expressed by

$$W_{\gamma-\gamma}(\theta_1,\theta_2,\varphi)=\frac{d\Omega_1 d\Omega_2}{4\pi}\sum_{\lambda_0,\lambda_1,\Lambda}B_{\lambda_0}(I_0)A_\Lambda^{\lambda_1\,\lambda_0}(\gamma_1)A_{\lambda_1}(\gamma_2)H_{\lambda_0\,\lambda_1\,\Lambda}(\theta_1,\theta_2,\varphi) \quad (A1.2)$$

where $\lambda_0,\lambda_1 and \Lambda$ are limited to only even numbers. This limitation is derived from an oblate alignment($P(m)=P(-m)$), parity and angular momentum conservation and rotational invariance of nuclear Hamiltonian. The solid angles of detectors are written by $d\Omega_1$ and $d\Omega_2$. The azimuthal angle φ is defined to be $\varphi=\varphi_2-\varphi_1$.

The parameters $A_\Lambda^{\lambda_1\lambda_0}(\gamma_1)$ and $A_{\lambda_1}(\gamma_2)$ are relevant to the first and second radiation, respectively.

$$A_\Lambda^{\lambda_1\,\lambda_0}(\gamma_1)=\frac{1}{1+\delta_1^2(\gamma_1)}\Big[F_\Lambda^{\lambda_1\,\lambda_0}(L\,L\,I_1\,I_0) +2\delta_1(\gamma_1)F_\Lambda^{\lambda_1\,\lambda_0}(L\,L+1\,I_1\,I_0)+\delta_1^2(\gamma_1)F_\Lambda^{\lambda_1\,\lambda_0}(L+1\,L+1\,I_1\,I_0)\Big] \quad (A1.3a)$$

and

$$A_{\lambda_1}(\gamma_2)=\frac{1}{1+\delta_2^2(\gamma_2)}[F_{\lambda_1}(L\,L\,I_1\,I_0) +2\delta_2(\gamma_2)F_{\lambda_1}(L\,L+1\,I_1\,I_0)+\delta_2^2(\gamma_2)F_{\lambda_1}(L+1\,L+1\,I_1\,I_0)] \quad (A1.3b)$$

In these expressions, $F_\Lambda^{\lambda_1\,\lambda_0}$ is generalized F-coefficients; F_{λ_1} stands for so called angular distribution coefficients or simply named as F-coefficients. These coefficients includes the coupling of angular momenta given by Clebsch-Gordan, Racah coefficients and $9j$ symbols. The quantity δ is a mixing ratio, and defined as

$$\delta\equiv\frac{\gamma(\pi',L+1)}{\gamma(\pi,L)}. \quad (A1.4)$$

The final term $H_{\lambda_0\,\lambda_1\,\Lambda}(\theta_1,\theta_2,\varphi)$ in eq.(A1.2) is a function of angles, and takes the following form;

$$H_{\lambda_0\,\lambda_1\,\Lambda}(\theta_1,\theta_2,\varphi) = \sum_{q_1\geq 0}(2-\delta_{q_1,0})\sqrt{\frac{2\Lambda+1}{2\lambda_1+1}\cdot\frac{(\Lambda-|q_1|)!(\lambda_1-|q_1|)!}{(\Lambda+|q_1|)!(\lambda_1+|q_1|)!}} \times(\lambda_0\,0\,\Lambda\,q_1|\lambda_1\,q_1)P_\Lambda^{|q_1|}(\cos\theta_1)P_{\lambda_1}^{|q_1|}(\cos\theta_2)\cos(q_1\varphi) \quad (A1.5)$$

It should be noted that the correlation function (A1.2) satisfies the symmetry relations, namely

$$W(\theta_1,\theta_2,\varphi)=W(180^\circ-\theta_1,180^\circ-\theta_2,\varphi), \quad (A1.6)$$

$$W(\theta_1, \theta_2, \varphi) = W(\theta_1, 180^\circ - \theta_2, \varphi + 180^\circ) = W(180^\circ - \theta_1, \theta_2, \varphi + 180^\circ), \quad (A1.7)$$

and

$$W(\theta_1, \theta_2, \varphi) = W(\theta_1, 180^\circ - \theta_2, 180^\circ - \varphi) = W(180^\circ - \theta_1, \theta_2, 180^\circ - \varphi). \quad (A1.8)$$

The relation (A1.6) is based on the fact that the excited states populated by nuclear reactions are in a substate population of $P(m) = P(-m)$, unless evaporated particles is observed in a specific direction with respect to the beam. In other words, there is no difference in γ ray yields observed at the forward and backward angles. The relations (A1.7) and (A1.8) can be derived from the following formula;

$$\cos(q_1\varphi) = (-1)^{q_1} \cos q_1(\varphi + 180^\circ) = (-1)^{q_1} \cos q_1(180^\circ - \varphi) \quad (A1.9)$$

and

$$P_\Lambda^{q_1}(\cos\theta) = (-1)^{q_1} P_\Lambda^{q_1}(\cos(180^\circ - \theta)). \quad (A1.10)$$

The actual values of correlation function (A1.2) can be calculated for various cases by a computer program "GCORREL". For comparison with experimental data, careful attention must be payed to the correction of solid angles, detection efficiencies of detectors, and the calibration of orientation parameters in eq(A1.2). One finds the details of these corrections in the recent work by Ekström and A. Nordlund [48].

The angles of detectors in the multi detector array at the University of Tsukauba are listed in the Table A1.1.

Table A1.1 Detector angles in the multi detector array at the University of Tsukuba

No.	θ(deg)	φ(deg)
1	116.6	0
2	116.6	72
3	116.6	144
4	116.6	216
5	116.6	188
6	0	—

With this array, we can deduce three independent correlation function listed in the table below. In this table, the function $W(0^\circ\ 117^\circ)$ is proportional to the events in which the first radiation γ_1 $W(117^\circ\ 0^\circ)$. The ratio of these two correlation functions

is one of the DCO, and can be deduced from the 2-fold coincidence matrix specified as "I" in the Table A1.2.

Table A1.2 Correlation functions

	$W(\theta_1, \theta_2, \Delta\varphi)$	combination	number of combinations
I	$W(117°, 0°, -)$	$1-6,\ 2-6,\ 3-6$	5 sets
		$4-6,\ 5-6$	
II	$W(117°, 117°, 72°)$	$1-2,\ 2-3,\ 3-4$	5 sets
		$4-5,\ 5-1$	
III	$W(117°, 117°, 144°)$	$1-3,\ 2-4,\ 3-5$	5 sets
		$4-1,\ 5-2$	

As an example, DCO ratios defined in the following manner are displayed in Table A1.3. In this calculation, the E2/M1 mixing was ignored.

$$R_1 \equiv \frac{W(117°, 0°)}{W(0°, 117°)} \qquad R_{3,2} \equiv \frac{W(117°, 117°, \Delta\varphi = 144°)}{W(117°, 117°, \Delta\varphi = 72°)} \tag{A1.11}$$

Table A1.3 DCO ratios for two successive γ rays in cascade without mixing

I_0, I_1, I_2	L	DCO ratios	
		R_1	$R_{3,2}$
$12 \to 10 \to 8$	$2 : 2$	1.00	1.06
$12 \to 10 \to 9$	$2 : 1$	0.58	0.96
$12 \to 10 \to 9$	$2 : 2$	0.90	1.03
$12 \to 10 \to 10$	$2 : 1$	1.14	1.10
$12 \to 10 \to 10$	$2 : 2$	0.35	0.90
$11 \to 10 \to 8$	$1 : 2$	1.73	0.95
$11 \to 10 \to 9$	$1 : 1$	1.00	1.04
$11 \to 10 \to 9$	$1 : 2$	1.56	0.99
$11 \to 10 \to 10$	$1 : 1$	1.99	0.94
$11 \to 10 \to 10$	$1 : 2$	0.60	1.07

Appendix B

B.1 Signature and signature quantum number

An odd-A nucleus in a uniform rotation around a fixed axis is described in terms of the following Hamiltonian;

$$H = \frac{\hbar^2}{2\mathrm{M}}(\mathrm{I} - \mathrm{j}_p)^2 + H_{int}, \qquad (A2.1)$$

where I denotes the total angular momentum, M denotes moment , H_{int} stands for nucleonic motion with spin jp within the body fixed coordinate system. This description is based on the assumption that a nucleon is coupled to a core with axially symmetric quadrupole deformation, and that the speed of rotation is slow compared to that of the nucleon. We further assume that there is no coupling between rotation and other degree of freedom. Then, the intrinsic structure given by H_{int}, which is the particle degree of freedom, is decoupled from the rotation. This state of rotation can be represented by

$$\Psi_{IKM} = \Phi_K \phi_{IKM}, \qquad (A2.2)$$

where Φ_K is the intrinsic motion of a nucleon in the body fixed coordinate system and ϕ_{IKM} describes the rotation of the nucleus as a whole in the laboratory frame. The orientation of the nucleus is specified by three Euler angles. It is well known that rotation matrices D^I_{MK} can be used for the rotational wave function ϕ_{IKM}, since they are eigenfunctions of the total angular momentum I, its projection M and the projection K of I to the symmetry axis of the deformed core. The wave function (A2.2) is expressed as

$$\Psi_{IKM} = \sqrt{\frac{2I+1}{8\pi^2}} D^I_{MK}. \qquad (A2.3)$$

The projection K is not only a constant of motion but the projection of jp on the symmetry axis of the core. This implies that the value of K is determined by the intrinsic motion. It should remain constant in a series of levels for a rotational band; the function Φ_K should not change also. This feature is valid only at low spin region. At higher spins, the coupling of the single particle motion to the collective rotation through Corioli's force can not be ignored, and thus the deviation from the above simple picture occurs.

If there is a symmetry of the intrinsic Hamiltonian for the rotation around the axis perpendicular to the symmetry axis by 180° in addition to the axial symmetry, a constraint is introduced into the property of the rotational band. Let z' be the axis of symmetry for deformation. The rotation by 180° around x' is written as

$$\mathcal{R}_{x'} = \exp^{-i\pi I_{x'}} . \qquad (A2.4)$$

The operator $\mathcal{R}^2_{x'}$ is equivalent to the rotation of the nucleus through the 2π, and it does not influence the wave function of an even-even nucleus. On the contrary, an odd-A nucleus transforms under the operation of $\mathcal{R}^2_{x'}$ like spinors, and consequently the corresponding total wave function changes sign. Namely, it is expressed as

$$\mathcal{R}^2_{x'} = (-1)^A. \qquad (A2.5)$$

Now, the symmetry of the intrinsic Hamiltonian for the rotation around the axis perpendicular to the symmetry axis by 180° demands

$$\mathcal{R} = \mathcal{R}_{ext} = \mathcal{R}_{int} \qquad \text{around } x' \text{ axis.} \qquad (A2.6)$$

Here, $\mathcal{R}_{ext}$ and $\mathcal{R}_{int}$ refer to rotations acting on intrinsic and external variables, respectively. One obtains, therefore,

$$\mathcal{R}^{-1}_{int}\, \mathcal{R}_{ext} \Psi_{IKM} = \Psi_{IKM} \qquad (A2.7)$$

If $\mathcal{R}_{int}$ is applied to the intrinsic wave function, the value of K changes sign to give the function $\Phi_{\overline{K}}$. The application of $\mathcal{R}_{ext}$ on the rotational wave function gives

$$\mathcal{R}_{ext} D^I_{MK} = \exp^{i\pi I_{x'}} D^I_{MK} = (-1)^{I+K} D^I_{M-K} \qquad (A2.8)$$

In order to satisfy eq(A2.6), the wave function must be written as follows:

$$\Psi_{IKM} = \frac{1}{\sqrt{2}}(1 + \mathcal{R}_{int}^{-1}\,\mathcal{R}_{ext})\sqrt{\frac{2I+1}{8\pi^2}}\Phi_K D^I_{MK}.$$

Using the relation (A2.8), one obtains the wave function

$$\Psi_{IKM} = \sqrt{\frac{2I+1}{16\pi^2}}\left[\Phi_K D^I_{MK} + (-1)^{I+K}\Phi_{\overline{K}} D^I_{M-K}\right]. \qquad (A2.9)$$

As a consequence of the invariance under the rotation $\mathcal{R}$, two intrinsic states of Φ_K and $\Phi_{\overline{K}}$ with eigenvalues K and $-K$, respectively, degenerate. If we adopt $K > 0$, only one series of rotational states appears with spins I;

$$I = K, K+1, K+2, K+3, \cdots\cdots \qquad (A2.19)$$

The phase factor in eq(A2.9)

$$\sigma = (-1)^{I+K} \qquad (A2.11)$$

is referred to the "signature" in the text book by Bohr and Mottelson [49]. It changes sign within a band and rotational bands, in general, can be classified into two groups of states with spins $I = K, K+2, K+4, \cdots$ and $I = K+1, K+3, K+5, \cdots$ with opposite signature. For the special case of $K = 0$, the function D^I_{MK} reduces simply spherical harmonics. One obtains easily

$$\mathcal{R}_{ext} Y_{IM} = (-1)^I Y_{IM} \qquad (A2.12)$$

The eigenvalue of $\mathcal{R}_{ext} = \mathcal{R}_{int}$ is

$$r = (-1)^I \qquad (A2.13)$$

The rotational band with $K = 0$ are then

$$I = 0, 2, 4, \cdots\cdots \qquad r = +1 \qquad (A2.14a)$$

and

$$I = 1, 3, 5, \cdots\cdots \qquad r = -1 \qquad (A2.14b)$$

Bengtsson and Frauendorf defined "signature quantum number" in somewhat different form [49]. By their definition, the signature quantum number α is related to r in the form of

$$r = \exp^{-i\pi\alpha} \qquad (A2.15)$$

With this definition, $r = +1$ is equivalent to $\alpha = 0$ and $r = -1$ to $\alpha = 1$. It is easily shown that

$$I = \alpha + 2n \qquad n = 0, 1, 2, 3 \cdots \qquad (A2.16)$$

This is valid for nuclei with even mass number. For odd-A nuclei, the relation

$$2\alpha = (-1)^{I-\frac{1}{2}} \qquad (A2.17)$$

must be used. From the definition (A2.15) and the relation given just above, one finds that rotational states in odd-A nuclei can be classified into two groups in the following way;

$$I = \frac{1}{2}, \frac{5}{2}, \frac{9}{2}, \frac{13}{2}, \cdots \qquad \alpha = +\frac{1}{2}, \qquad r = -i \qquad (A2.18)$$

and

$$I = \frac{3}{2}, \frac{7}{2}, \frac{11}{2}, \frac{15}{2}, \cdots \qquad \alpha = -\frac{1}{2}, \qquad r = +i \qquad (A2.19)$$

B.2 Signature splitting

In a particle-rotor model for axially symmetric nuclei, the Hamiltonian (A2.1) is explicitly written in the following form;

$$H_{rot} = \frac{\hbar^2}{2\mathrm{M}} \left[(I_{x'} - j_{x'})^2 + (I_{y'} - j_{y'})^2 \right] + H_{int}, with$$

$$\mathrm{M} = \mathrm{M}_{x'} = \mathrm{M}_{y'}.$$

This is the moment of inertia around x', and y' axis. Using the relations

$$j_{x'} \pm j_{y'} = j_{\pm} \qquad and \qquad I_x \pm I_y = I_{\pm},$$

the rotational part of the Hamiltonian can be written as follows;

$$H_{rot} = \frac{\hbar}{2\mathrm{M}}(I^2 - I_z^2) - \frac{\hbar}{2\mathrm{M}}(I_+ j_- + I_- j_+) + \frac{\hbar}{4\mathrm{M}}(j_+ j_- + j_- j_+) \qquad (A2.20)$$

The second term is referred to Corioli's term, and the third term is named as recoil term. The Corioli's term influence the single particle motion of a nucleon. In particular, nucleon in a high-j orbital is strongly perturbed by this term and thus the phenomenon of backbend is caused. It is well known that diagonal element for the Coriori's term calculated with the wave function (A2.9) is non zero only for $K = 1/2$. The energy is given by

$$E_{IK} = \frac{\hbar}{2\mathrm{M}}\left[I(I+1) - K^2 - (-1)^{I-j}\left(I+\frac{1}{2}\right)\left(j+\frac{1}{2}\right)|c_{\Omega=\frac{1}{2}}|^2\delta_{K,\frac{1}{2}}\right] \qquad (A2.21)$$

From this expression, one can see that the energy depends on the phase factor $(-1)^{I-j}$. Since both of I and j are half integer in odd-A nuclei, the following signature quantum number α_I is given to the states with spin I in accordance with eqs (A2.18) and (A2.19), namely,

$$\alpha_I = \frac{1}{2}(-1)^{I-\frac{1}{2}}. \qquad (A2.22)$$

In the rotational band having an odd nucleon in a high-j intruder orbital as intrinsic configuration, states with $I = j + even$ is lower in energy than the states with $I = j + odd$. The states with $I = j + even$ are called as "favored" and the states with $I = j + odd$ are referred to "unfavored" states. The corresponding signature quantum numbers are

$$\text{favored signature} \qquad \alpha_f = \frac{1}{2}(-1)^{j-\frac{1}{2}} \qquad \text{(for high } j \text{ orbital)} \quad (A2.23)$$

and

$$\text{unfavored signature} \qquad \alpha_f = \frac{1}{2}(-1)^{j+\frac{1}{2}} \qquad \text{(for high } j \text{ orbital)} \quad (A2.24)$$

The signature dependence in rotational energies E_{IK} splits the band members into two groups according to the signatures α_f and α_f. The differences between $E_{IK}(favored)$ and $E_{IK}(unfavored)$ is a measure of "signature splitting", and varies with spins or the intrinsic configuration.

The operator of the magnetic dipole transition is resemble to the Corioli's interaction, and then the values of B(M1) has also signature dependence. According

to the cranking model, the relation is as follows;

$$B(\mathrm{M1} : favored \rightarrow unfavored, \Delta I = -1) > B(\mathrm{M1} : unfavored \rightarrow favored, \Delta I = -1) \tag{A2.25}$$

This relation is found in many experimental data on odd-A nuclei at above the first backbend as well as the behavior of $E(unfavored) > E(favored)$ in the energy spectrum. We could define these characters as *normal signature dependence*. The properties of the bands studied in the present work violate this rule, thus we have given to them the terminology of *signature inversion*.

Bibliography

[1] G.B.Hagemann, J.D.Garett, B.Herskind, J.Kownacki, B.M.Nyakó, P.L.Nolan and J.F.Sharpey-Shafer, Nucl. Phys. **A242**(1984)365

[2] R.Bengtsson, H.Frisk, F.R.May and J.A.Piston, Nucl. Phys. **A415**(1984)189

[3] A.Ikeda and T.Shimano, Phys.Rev.Letters, **63**, No.2(1989)139

[4] J.A.Pinston, R.Bengtsson, E.Monnand, F.Schussler and D.Barneoud, Nucl. Phys. **A361**(1981)464

[5] R.Bengtsson, J.A.Pinston, D.Barneoud, E.Monnand and F.Schussler, Nucl. Phys. **A389**(1982)158

[6] T.Komatsubara, K.Furuno, T.Hosoda, J.Espino, J.Gascon, G.B.Hagemann, Y.Iwata, D.Jerrestam, N.Kato, T.Morikawa, J.Nyberg, G.Sletten and P.O.Tjøm, Zeit. Phys. **A335**(1990)113

[7] T.Komatsubara, K.Furuno, T.Hosoda, J.Mukai, T.Hayakawa, T.morikawa, Y.Iwata, N.Kato, J.espino, J.Gascon, N.Gjørup, G.B.Hagemann, H.J.Jensen, D.Jerrestam, J.Nyberg, G.Sletten, B.Cederwall and P.O.Tjøm, Nucl. Phys. **A557**(1993)419c

[8] I.Hamamoto, Phys.Lett. **B235**(1990)221

[9] M.Matsuzaki, Nucl. Phys. **A504**(1989)456

[10] N.Yoshida, H.Sagawa, T.Otsuka, Nucl. Phys. **A567**(1994)17

[11] K.Hara and Y.Sun, Nucl. Phys. **A531**(1991)221

[12] Paul B.Semmes, Ingemar Ragnarsson, Proceedings of the International Conference on High Spin Physics and Gamma-Soft Nuclei, 17-21 September 1990 Pittsburg, PA USA, P.500

[13] N.Tajima, Nucl. Phys. **A572**(1994)365

[14] B.Cederwall, F.Lidén, A.Johnson, L.Hildingsson, R.Wyss, B.Fant, S.Juutinen, P.Ahonen, S.Mitarai, J.Mukai, J.Nyberg, I.Ragnarsson and P.B.Semmes, Nucl. Phys. **A542**(1992)454

[15] N.Xu, Y.Liang, R.Ma, E.S.Paul and D.B.Fossan, Phys.Rev. **C41**(1990)2681

[16] B.M.Nyakó, J.Gizon, D.Barneoud, A.Gizon, M.Jozsa, W.Klamra, F.A.Beek and J.C.Merdinger, Zite. Phys. **A332**(1989)235

[17] P.J.Nolan, R.Aryaeinejad, P.J.Bishop, M.J.Godfrey, A.Kirwan, D.J.G.Love, A.H.Nelson, D.J.Thornley and D.J.Unwin, J. Phys. **G13**(1987)1555

[18] M.J.Godfrey, Y.Het, I.Jenkins, A.Kirwan, P.J.Nolan, D.J.Thornley, S.M.Mullins and R.Wadsworth, J. Phys. **G15**(1989)487

[19] K.L.Ying, P.J.Bishop, A.N.James, A.J.Kirwan, D.J.G.Love, T.P.Morrison, P.J.Nolan, D.C.B.Watson, K.A.Connell, A.H.Nelson and J.Simpson, J. Phys. **G12**(1986)L211

[20] S.Mitarai, K.Setoguchi, T.Maeda, Y.Haruta, H.Tomura, B.J.Min, K.Heiguchi, S.Suematsu, Y.Ishikawa and T.Kuroyanagi, Nucl. Instrum. Methods **A227**(1989)491

[21] B.Harmatz and T.H.Handley, Nucl. Phys. **A191**(1972)497

[22] N.Idrissi, A.Gizon, J.Genevey, P.Paris, V.Barci, D.Barnéoud, J.Blachot, D.Bucurescu, R.Duffait, J.Gizon, C.F.Liang and B.Weiss Zite. Phys. **A341**(1992)427

[23] D.Ward, H.R.Andrews, V.P.Janzen, D.C.Radford, J.K.Johansson, D.Prévost, J.C.Waddington, A.Galindo-Uribarri and T.E.Drake, Nucl. Phys. **A539**(1992)547

[24] A.P.Byrne, K.Schiffer, G.D.Dracoulis, B.Fabricius, T.Kibeédi, A.E.Stuchbery and K.P.Lieb, Nucl. Phys. **A548**(1992)131

[25] R.Ma, Y.Ling, E.S.Paul, N.Xu and D.B.Fossan Phys.Rev. **C41**(199)717

[26] Y.He, M.J.Godfrey, I.Jenkins, A.J.Kirwan, S.M.Mullins, P.J.Nolan, E.S.Paul and R.Wadsworth, J. Phys. **G18**(1992)99

[27] E.S.Paul, C.W.Beausang, D.B.Fossan, R.Ma, W.F.Piel,Jr., and N.Xu, L.Hildingsson and G.A.Leander, Phys.Rev. **C58**(1987)984

[28] C.M. Lederer and V.S. Shirley, Table of isotpopes(7th ed.), A Wiley-Interscience Publication, John-Wiley & Sons, New York, 1978, and E. Browne and R.B. Firestone, Table of radioactive isotopes, A Wiley-Interscience Publication, John-Wiley & Sons, New York, 1986

[29] K.Kitao, M.Kanbe, Z.Matumoto Nuclear Data Sheets, Volume 38, Number 2, February 1983, P.191

[30] A.C.Li, I.L.Preiss, P.M.Strdler, and D.A.Bromley, Phys.Rev. **141**(1966)1089

[31] D.R.Zolnowski and T.T.Sugihara, Phys, Rev. **C16**(1977)408

[32] T.Komatsubara, T.Hosoda, H.Sakamoto, T.Aoki and K.Furuno, Nucl. Phys. **A496**(1989)605

[33] J.P.Martin, V.Barci, H.El-Samman, A.Gizon, J.Gizon, W. Klamra and B.M. Nyakó, Nucl. Phys. **A489**(1988)169

[34] S.P.Pilotte, S.Flibotte, S.Monado, N.Nadon, D.Prévost, P.Taras, H.R.Andrews, D.Horn, V.P.Janzen, D.C.Radford, D. Ward, J.K. Johansson,

J.C. Waddington, T.E. Drake, A. Galindo-Urribarri and R. Wyss, Nucl. Phys. **A514**(1990)545

[35] R.Wyss, F.Lidén, J.Nyberg, A.Jonhnson, D.J.G.Love A.H.Nelson, D.W.Banes, J.Simpson, A.Kirwan, and R.Bengtsson, Zite. Phys. **A330**(1988)123

[36] K.Schiffer, A.Dewald, A.Gelberg, R.Reinhardt, K.O.Zell, Sun Xiangfu and P.von Brentano, Nucl. Phys. **A548**(1986)337

[37] U.Neuneyer. H.Wolters, A.Dewald, W.Lieberg, A.Gelberg, E.Ott, J.Theuerkauf, R.Wirowski, P.von BRentano, K.Schiffer, D.Alber and K.H.Maier, Zite. Phys. **A336**(1990)245

[38] R.Wyss, A.Johnson, F.Lidén, J.Nyberg, Proc.XXV Int.Winter Meeting Nucl. Phys., Bormio (1989)542

[39] T.Sekine, H.Iimura, S.Ichikawa, M.Oshima, K.Hata, Y.Nagame, N.Takahashi and A.Yokoyama, JAERI Annual Report (1987) P.121

[40] R.Wyss ,F.Lidén, J.Nyberg, A.Johnson, D.J.G.Love, A.H.Nelson, D.W.Banes, J.Simpson, A.Kirwan and R.Bengtsson Nucl. Phys. **A503**(1989)244

[41] R.Wyss, J.Nyberg, A.Johnson, R.Bengtsson and W.Nazarewicz, Phys.Lett. **B215**(1988)211

[42] A.Gizon and J.Gizon, Recent advances in nulcear structure, Predeal, Romania 28 Aug - 8 Sept 1990, P.61

[43] P.J.Smith, D.J.Unwin, A.Kirwan, D.J.G.Love, A.H.Nelson, P.J.Nolan, D.M.Todd and P.J.Twin, J. Phys. **G11**(1985)1271

[44] B.M.Nyakó, J.Gizon, V.Barci, A.Gizon, S.André, D.Barnéoud, D.Curien, J.Genevey, and J.C.Merdinger, Zite. Phys. **A334**(1989)513

[45] R.Aryaeinejad, D.J.G.Love, A.H.Nelson, P.J.Nolan, P.J.Smith, D.M.Todd and P.J.Twin, J. Phys. **G10**(1984)955

[46] J.R.B.Oliveira, L.G.R.Emediato, M.A.Rizzutto, R.V.Ribas, W.A.Seale, M.N.Rao, N.H.Medina, S.Botelho and E.W.Cybulska, Phys. Rev. **C39**(1989)2250

[47] K.S. Krane, R.M. Steffen and R.M. Wheeler, Nucl. Data Tables,**11**(1973)351

[48] L.P.Ekstrom, Cosmic and Subatomic Physics report, December 1991, P.1

[49] A. Bohr and B.R.Mottelson, Nuclear Structure, 1969.

Tables

Table 1. Excitation energies, γ-ray energies, angular distribution ratios, γ-ray relative intensities, branching ratios and B(M1)/B(E2) ratios for the band 1 of ^{124}La. The uncertainties of γ ray energies are in the range from 0.2 keV for strong transitions to 1.2 keV for weak high-energy transitions. Doublets are marked by asterisks.

E_X (keV)	$E_\gamma^\dagger$ (keV)	Angular distribution ratio	Relative intensity	Branching ratio	$B(M1)/B(E2)$ (μ_n^2/e^2b^2)
68.5	68.5	1.71(9)	35.2(4)		
191.1	122.1	1.47(2)	100	95.3(11)	1.98(14)
	191.0	1.47(26)	3.2(1)	4.7(3)	
323.9	132.7	1.25(17)	88.9(10)	83.6(7)	1.64(4)
	255.0	1.52(5)	17.2(5)	16.4(4)	
548.7	224.6	0.92(14)	86.3(10)	80.8(7)	1.52(3)
	357.6	1.52(5)	19.5(6)	19.2(4)	
749.3	200.5	0.93(14)	60.1(8)	50.0(8)	1.20(3)
	425.3	1.48(4)	54.7(10)	50.0(9)	
1068.9	319.6	0.80(2)	43.0(9)	60.2(11)	1.23(4)
	520.4	1.96(6)	29.3(9)	39.8(10)	
1343.0	273.7	0.84(2)	21.8(6)	27.4(9)	0.94(4)
	593.6	1.70(4)	57.7(1)	72.6(17)	
1738.9	396.2	0.76(2)	24.7(8)	39.7(22)	1.00(7)
	669.9	1.76(6)	23.2(9)	60.3(30)	
2093.1	353.8	0.78(4)	7.2(4)	13.7(8)	0.59(4)
	749.5	1.80(5)	43.6(11)	86.3(22)	
2542.3	449.4	0.79(4)	8.4(4)	25.6(24)	0.88(10)
	803.3	1.80(7)	21.7(8)	74.4(48)	
2985.4	892.3	1.49(6)	22.7(9)		
3461.2	918.9	1.98(13)	15.2(8)		
3998	1013	*			
4472	1011	*			
5095	1097	2.07(35)	7.3(3)		
5550	1078	1.61(14)	2.4(2)		
6235	1140	*			
6688	1138	*			

Table 2. Excitation energies, γ-ray energies, angular distribution ratios and γ-ray relative intensities for band 2 of ^{124}La. See also the captions of Table 1.

E_X (keV)	E_γ (keV)	Angular distribution ratio	Relative intensity
84.7	84.7	1.46(7)	28.8(2)
382.7	170.3	1.07(17)	32.5(5)
	297.4	1.14(32)	6.7(3)
805.5	206.3	0.92(16)	5.2(2)
	401.1	1.40(10)	9.7(3)
	422.5	1.55(5)	23.6(5)
1346.9	541.1	1.65(6)	30.3(5)
1997.9	650.6	1.71(5)	*
2746.8	748.5	1.80(8)	*
3584.3	837.1	1.73(11)	16.8(5)
4498.7	914.0	1.78(16)	11.9(5)
5474.2	975.2	1.69(21)	4.8(4)
6535	1062	1.52(32)	2.8(5)
7676	1141		
8864	1190		
10110	1246		

Table 3. Excitation energies, γ-ray energies, angular distribution ratios, γ-ray relative intensities, branching ratios and B(M1)/B(E2) ratios for band 3 of ^{124}La. See also the captions of Table 1.

E_X (keV)	E_γ (keV)	Angular distribution ratio	Relative intensity	Branching ratio	$B(M1)/B(E2)$ (μ_n^2/e^2b^2)
211.9	126.9	1.45(5)	42.2(5)		
403.9	192.0	*	19.2(4)		
598.4	194.0	*	6.1(3)	30.2(13)	0.77(5)
	386.4	1.40(9)	10.4(3)	32.2(13)	
	215.5	0.92(15)	10.4(3)	37.6(11)	
859.0	261.5	0.89(4)	10.8(3)	63.1(21)	1.61(10)
	455.5	1.73(19)	6.9(3)	30.0(16)	
	477.1	1.64(19)	3.2(2)	6.9(9)	
1129.0	268.7	0.97(5)	7.5(3)	40.5(16)	1.03(6)
	531.0	1.70(8)	13.5(4)	59.5(24)	
1452.8	324.6	*			
	593.8	1.78(20)	8.5(4)		
1780.6	326.5	*			
	651.6	*			
2153.1	373.9	*			
	700.3	1.78(16)	6.2(3)		
2529.0	748.4	*			
2933.1	780.0	1.55(20)	9.2(5)		

Table 4. The energies, relative intensities and half-lives of the γ rays observed off-line for the ^{28}Si+^{103}Rh reaction. They are classfied according to the half-lives.

^{128}Ba				
$E_\gamma(keV)$	Intensity	Error	$T1/2(sec)$	Error
284.5	1042.0	51.0	300	1
440.6	44.22	2.6	388	50
479.9	520.6	16.0	323	4
488.5	88.58	3.6	321	21
561.4	50.93	3.8	315	36
601.3	129.0	4.7	345	17
607.6	42.94	3.2	423	72
609.9	81.33	3.8	380	36
627.0	31.39	2.8	579	212
633.6	56.00	2.9	340	33
644.6	128.6	4.2	323	20
659.4	49.19	3.3	334	47
796.4	50.14	5.1	308	46
885.7	82.08	4.2	333	32
916.4	22.09	3.4	273	81
1037.0	34.36	3.3	274	53
1041.0	101.2	4.1	424	39
1054.0	78.61	3.8	341	39
1089.0	74.22	4.3	320	31
1071.0	38.70	3.5	367	81
1102.0	32.52	4.2	409	109
^{128}Cs				
$E_\gamma(keV)$	Intensity	Error	$T1/2(sec)$	Error
273.8	251.3	12.0	-11125	6374
^{128}Xe				
$E_\gamma(keV)$	Intensity	Error	$T1/2(sec)$	Error
527.1	180.5	5.9	6567	3708
970.0	21.22	3.4	1731	1954
1141.0	23.70	3.9	1412	1830
^{127}Ba				
$E_\gamma(keV)$	Intensity	Error	$T1/2(sec)$	Error
26.43	14.03	1.6	304	15
56.41	50.11	4.7	319	10
^{127}Cs				
$E_\gamma(keV)$	Intensity	Error	$T1/2(sec)$	Error
115.3	52.56	4.1	838	68
181.9	59.01	4.0	804	81

Table 4. continued.

^{127}Xe				
$E_\gamma(keV)$	Intensity	Error	$T1/2(sec)$	Error
125.0	11.94	1.3	116358	5707617
412.3	203.9	8.3	22321	37532

^{125}Cs				
$E_\gamma(keV)$	Intensity	Error	$T1/2(sec)$	Error
141.1	36.10	2.3	339	26

210sec				
$E_\gamma(keV)$	Intensity	Error	$T1/2(sec)$	Error
324.4	25.32	2.6	210	28
338.5	79.54	4.7	218	18

240sec				
$E_\gamma(keV)$	Intensity	Error	$T1/2(sec)$	Error
23.55	34.01	3.6	244	7
26.43	14.03	1.6	304	15
33.47	1291.0	131	254	0
37.88	297.1	29.0	246	1
66.76	48.66	4.4	248	7
68.27	65.88	5.8	253	6
104.2	150.9	10.0	243	2
121.0	18.72	1.6	234	28
137.5	19.70	1.5	243	26
176.9	67.13	4.0	240	20
178.6	73.79	4.3	229	15
219.7	124.9	6.9	237	7
267.7	58.01	3.4	246	15
545.8	121.7	5.2	257	16
827.0	28.18	3.5	238	36

280sec				
$E_\gamma(keV)$	Intensity	Error	$T1/2(sec)$	Error
25.34	7	1.1	276.845	24
118.0	24.20	2.1	273	31
134.5	76.29	4.8	278	8
171.7	116.0	6.6	272	9
579.1	44.56	3.6	280	53
927.8	42.65	3.8	277	53
1037.0	34.36	3.3	274	53

Table 4. continued.

300sec

$E_\gamma(keV)$	Intensity	Error	$T1/2(sec)$	Error
22.35	29.73	3.2	311	12
26.43	14.03	1.6	304	15
56.41	50.11	4.7	319	10
65.69	23.93	2.4	337	26
77.34	42.00	3.5	312	10
141.1	36.10	2.3	339	26
180.6	117.6	6.9	289	14
191.7	31.65	2.2	334	47
221.8	49.57	3.1	313	26
520.7	25.15	2.9	314	73
543.5	41.64	3.6	323	60
1107.0	18.34	3.6	299	56

350sec

$E_\gamma(keV)$	Intensity	Error	$T1/2(sec)$	Error
79.64	38.74	3.2	349	17
587.3	80.81	4.6	361	44
887.6	38.33	3.8	330	61
953.9	28.02	3.7	355	85
1165.0	43.22	4.0	340	64

390sec

$E_\gamma(keV)$	Intensity	Error	$T1/2(sec)$	Error
32.24	832.6	84.0	380	2
36.46	193.9	19.0	399	4
202.1	26.27	2.1	386	66
340.9	33.18	10.0	388	50
440.6	44.22	2.6	388	50
567.9	58.41	4.1	401	67.020
764.5	46.47	3.8	398	69

400sec

$E_\gamma(keV)$	Intensity	Error	$T1/2(sec)$	Error
15.06	23.71	3.2	580	38
90.59	6	1.0	533.987	131
146.7	523.1	31.0	520	5
168.8	21.07	1.6	446	76
234.4	50.02	3.0	513	57
271.6	46.03	2.9	502	71
316.6	41.00	2.9	413	63
319.0	57.56	3.6	548	92
330.8	17.26	2.5	467	162
596.8	29.00	2.8	491	143
940.1	18.92	3.5	472	140
991.3	24.14	4.1	433	137

Table 4. continued.

600sec				
$E_\gamma(keV)$	Intensity	Error	$T1/2(sec)$	Error
31.00	522.0	53.0	743	7
142.9	25.51	1.8	667	141
354.3	11.17	2.5	637	112
399.7	47.10	3.4	593	90
454.7	52.16	2.8	637	112
503.5	57.47	3.6	706	96
571.0	34.22	3.6	678	227
584.5	56.74	4.1	710	262
627.1	48.84	5.0	579	212
1084.0	70.75	20.	705	114
1146.0	174.4	5.8	672	81
800sec				
$E_\gamma(keV)$	Intensity	Error	$T1/2(sec)$	Error
115.3	52.56	4.1	838	68
181.9	59.01	4.0	804	81
208.5	12.12	1.5	736	252
253.8	104.0	5.6	873	102
335.9	34.51	2.9	892	529
349.2	12.91	1.9	891	197
449.1	58.82	3.1	891	197
794.7	44.60	5.1	792	271
1000sec				
$E_\gamma(keV)$	Intensity	Error	$T1/2(sec)$	Error
20.12	30.77	3.3	1658	232
55.29	12.74	1.4	958	223
110.7	138.7	9.5	1425	104
278.8	258.8	13.0	1239	81
307.3	54.75	3.4	1076	280
357.4	16.10	2.6	1086	167
372.5	137.6	6.3	2450	561
457.5	92.12	4.2	1086	167
556.6	38.40	3.8	1195	542
672.2	59.85	3.5	1002	274
1141.0	23.70	3.9	1412	1830
1177.0	71.86	5.0	1545	691
other				
$E_\gamma(keV)$	Intensity	Error	$T1/2(sec)$	Error
112.0	66.09	4.6	7466	5136
188.7	223.1	12.0	39333	75127
214.3	22.95	1.9	3302	4377

Table 5. Excitation energies, γ-ray energies and relative intensities observed in the β decay of ^{128}Ce. The intensities are normalized to the intensity of the 147 keV γ ray (I_{147keV}=100). Doublet are marked by asterisks.

$E_X(keV)$	$E_\gamma(keV)$	Intensity	$E_X(keV)$	$E_\gamma(keV)$	Intensity
23.4	23.4	30.0(8)	938.8	476.3	1.6(3)*
127.5	104.1	60.5(7)		578.5	8.6(8)
170.0	146.6	100.0(8)		632.9	12.3(9)
242.8	72	*		812.3	4.5(19)*
	115.4	7.4(4)	950.0	707.2	10.5(28)*
	219.4	37.0(7)	1079.9	708.7	3.7(10)
245.0	117.9	8.9(3)		717.2	3.6(9)
	221.6	12.4(5)		774.5	6.2(9)
305.9	178.4	14.4(5)		910.2	4.8(11)
329.6	87	*		952.4	6.7(11)
	159.2	1.1(3)	1129.1	666.2	1.4(7)
	202.0	7.7(6)		885.2	29.1(14)
	306.2	4.1(6)		959.1	10.5(11)
346.9	102.0	3.2(3)	1187.3	816.0	1.6(3)*
	176.9	12.0(4)		825.8	9.5(10)
361.5	191.5	6.2(4)		1159.0	1.6(4)*
	234.2	14.8(5)	1394.6	1149.6	5.6(12)
	338.1	16.4(7)	91.5	68.1	35.4(7)
370.8	243.3	18.2(5)	263.0	171.5	24.0(5)
463.1	293.1	4.6(5)	271.8	180.3	22.7(5)
	335.5	4.8(6)	422.0	330.1	3.7(5)
631.1	388.3	4.4(6)	463.7	372.1	8.5(6)
	459.8	1.9(3)*	469.8	378.3	5.0(5)
			487.6	395.8	4.3(6)

Table 6. Excitation energies, γ-ray energies, relative intensities($I_{284} = 100$) and multiporalities of the transitions in ^{128}Ba.

$E_X(keV)$	$E_\gamma(keV)$	Intensity	Multipolarity
284.1	284.1	100.00(40)	E2
763.1	479.3	58.30(20)	E2
884.5	600.4	10.91(8)	M1/E2
	884.3	8.11(8)	E2
1324.2	440.0	2.17(4)	M1/E2
	561.2	0.99(3)	M1/E2
	1040.1	10.31(10)	M1/E2
1372.0	487.8	10.94(7)	E2
	609.0	8.61(7)	M1/E2
	1087.9	8.75(9)	E2
1406.7	643.6	15.15(11)	E2
1799.3	427.2	0.80(4)	
	475.1	1.08(5)	
	914.8	3.14(5)	
	1036.0	1.69(5)	M1 or E1
	1514.6	0.68(4)	
1832.9	1070.1	4.77(7)	M1 or E1
	1548.8	1.57(4)	M1 or E1
1931.0	606.8	2.21(4)	
	1167.5	1.62(5)	
1939.0	531.3	0.40(5)*	
	567.0	4.08(6)	
	1175.7	1.21(4)	
2009.0	1724.9	0.61(5)	
2038.3	715.5	0.50(5)	
	1154.3	0.40(4)	
	1754.2	1.12(5)	M1 or E1
2038.7	632.5	6.23(6)	
	1275.6	4.76(7)	
2174.7	1411.6	3.75(7)	
2201.9	1318.0	0.69(5)	
	1439.1	1.58(5)	
	1917.8	1.16(5)	
2244.8	1481.7	0.57(5)	
2395.5	988.8	1.71(6)	
2412.4	1005.7	1.16(5)	

Table 6. continued.

$E_X(keV)$	$E_\gamma(keV)$	Intensity	Multipolarity
2424.9	249.8	0.38(4)	
	386.0	1.81(4)	
	494.1	1.24(3)	
	591.8	1.00(4)	
	626.0	3.86(5)	
	1052.9	10.01(10)	M1/E2
	1100.7	4.76(7)	
	1660.9	0.98(5)	
2450.3	412.0	1.06(4)	
	1078.8	1.78(5)	
	1687.2	0.51(4)	
2530.5	491.7	0.57(3)	
	1123.8	1.17(6)	
2570.0	531.3	0.40(5)*	
	1163.5	0.75(4)	
2625.7	451.2	0.29(6)	
	587.0	0.87(5)	
2626.7	793.8	1.83(15)	
	1302.1	1.35(4)	
2669.3	1906.2	0.57(4)	
2720.7	682.0	0.62(5)	
2848.3	673.1	0.35(4)	
	1049.0	0.19(8)	
2877.1	482.5	0.77(3)	
	838.7	1.06(6)	
	938.8	2.66(5)	
	1505.1	3.67(7)	
	1505.1	3.67(8)	
2929.0	1096.1	0.64(4)	
2976.6	774.7	1.32(4)	
	1046.4	0.22(6)	
	1143.8	1.45(5)	
	1604.7	1.43(6)	
	1652.6	0.45(4)	
3116.7	1710.0	0.31(4)	

Table 7. Energy levels, spins, parities, $I(\mathrm{EC}+\beta^+)$ and log ft for the β decay of $^{128}\mathrm{La}\rightarrow{}^{128}\mathrm{Ba}$.

	our work			previous work		
$E_X(keV)$	I^π	$I(\mathrm{EC}+\beta)\%$	log ft	I^π	$I(\mathrm{EC}+\beta)\%$	log ft
1406.7	6^+	3.35	7.1	6^+	7.0	6.6
1799.3	$(4^+,3^+)$	3.09	7.0	$3^\pm,4^+$	3.7	6.6
1832.9	3^+	1.91	7.1	$3^\pm,4^+$	4.0	6.6
1931.0	5^+	1.55	7.2	5^+	2.0	7.2
1939.0	6^+	2.62	7.0	(6^+)	2.3	6.8
2038.7	5^-	4.00	6.8	(5^+)	7.8	6.3
2174.7		2.68	6.8	(4^-)	2.2	6.7
2201.9	(4^+)	2.29	7.0	$3^\pm,4^\pm$	2.9	6.6
2395.5	(7^-)	1.26	7.0	(7^-)		
2424.9	5^+	22.24	5.6	(4^-)	24.7	5.5
2450.3	(5)	3.10	6.5	$4^-,5^\pm,6^+$	2.8	6.5
2530.5		1.07	6.8		0.6	7.1
2625.7		1.07	6.9			
2626.7		2.94	6.5	$4^-,5^+$	4.7	6.2
2801.1		2.24	6.4			
2848.3		1.14	6.8		1.4	6.5
2877.1	$(5^-,6^+)$	7.55	5.8	(5^-)	8.3	5.8
2976.6	$(5^+,4^+)$	4.51	6.1	$4^-,5^+$	3.5	6.1

Table 8. Excitation energies, γ ray energies, relative intesities (I_{235keV}=100), and DCO ratios of the high spin states of ^{128}La produced by the ^{16}O+^{115}In reaction. Doublets are marked by asterisks.

$E_X(keV)$	$E_\gamma(keV)$	Intensity	DCO ratio
84.9	84.9	50.7(46)	0.73(17)
	48.4	3.9(2)	
151.3	114.0	4.8(5)	0.69(31)
	66.4*	45.4(41)	1.19(16)
255.8	170.9	2.0(1)	
	104.1	90.3(83)	1.04(6)
394.0	242.7	7.8(3)	0.79(22)
	138.2	94.1(88)	1.02(6)
629.1	373.3	21.0(4)	0.72(17)
	234.8	100.0(6)	1.14(7)
851.1	457.6	35.5(5)	0.76(15)
	222.0	77.6(5)	1.06(11)
1186.5	557.4	15.4(4)	0.63(17)
	334.8	54.5(5)	1.05(14)
1485.2	633.8	24.1(9)	0.61(20)
	298.7	20.5(5)	1.33(37)
1903.6	717.5	16.7(4)	
	418.4	15.9(4)	
2271.8	786.7	12.2(5)	
	368.2	9.1(3)	
2761.4	857.8	5.0(4)	
3194.6	922.8	4.0(3)	

Table 8. continued.

$E_X(keV)$	$E_\gamma(keV)$	Intensity	DCO ratio
70.3	70.3	31.3(28)	1.48(58)
	65.2*	20.5(19)	1.68(75)
151.9	146.1	1.6(1)	
	81.6	45.3(41)	1.07(14)
271.6	201.9	1.4(1)	0.50(25)
	119.7	58.6(54)	1.00(8)
445.4	293.5	5.1(2)	0.72(21)
	173.4	50.1(6)	1.00(9)
654.4	382.8	9.7(3)	0.52(16)
	209.0	44.7(4)	1.13(13)
915.0	469.6	10.5(3)	0.54(20)
	260.0	33.5(4)	1.09(21)
1205.3	550.6	14.7(3)	
	290.2	14.5(3)	0.97(29)
1543.8	628.8	14.9(4)	
	338.2	14.9(3)	
1906.4	700.8	26.8(4)	
	362.6	11.9(3)	
2313.3	769.5	8.4(3)	
	407.0	8.0(4)	
2737.7	831.1	10.8(4)	
	424.4	4.0(2)	
3197.8	884.5	16.1(4)	
	459.9	4.6(2)	
3652.4	914.7	8.1(3)	
	452.7	6.0(3)	

Table 9. The β_2 and γ of minmum points of calculation of the total routhian surface.

Configuration is p(-,-1/2) and n(-,-1/2)			Configuration is p(-,-1/2) and p(+,-1/2)		
ω	β_2	γ	ω	β_2	γ
0.060	0.274	1.0	0.060	0.281	0.5
0.120	0.271	1.4	0.120	0.281	0.9
0.180	0.269	1.2	0.180	0.281	1.2
0.300	0.268	-0.2	0.300	0.282	1.4
0.420	0.263	0.2	0.420	0.267	1.9
0.540	0.247	2.8	0.540	0.272	1.1

Figure captions

Figure 1.

Spectra of γ rays observed in the ^{35}Cl+^{92}Mo reaction at a bombarding energy of 135 MeV. In the singles spectrum, a prominent peak at 137 keV is due to the Coulomb excitation of the target. The spectrum denoted by "3p0n gate" was obtained by placing the gate on the $3p0n$ channel in a particle-γ coincidence measurement. A charged-particle multiplicity filter and a neutron detector were employed to generate the gates for channel selection. The photo peaks at 230, 421 and 577 keV correspond to the γ rays of the ground-state of ^{124}Ba produced in the ^{92}Mo(^{35}Cl,3p)^{124}Ba reaction. The spectrum in the lowest panel was processed by setting the gate on $1p1n$ and $2p1n$ channels. Most of the photo peaks can be ascribed to ^{124}La.

Figure 2.

Examples of coincidence spectra observed by the NORDBALL spectrometer, in order to construct the level scheme of ^{124}La using the ^{92}Mo(^{35}Cl, 2pn)^{124}La reaction at 150 MeV. The spectrum (A) is a sum of two spectra obtained by placing the gate on 450 keV γ ray and on the 803 keV γ ray the band 1(see Fig.3). Other spectra are produced in a similar manner to the spectrum (A). The gates are set on the 274, 425 and 594 keV γ rays of the band 1 in (B), the 261 keV γ ray of the band 3 in (C) and the 838, 914 and 976 keV γ rays of the band 2 in (D).

Figure 3.

Partial level scheme of ^{124}La constructed in the present work. Since the ground and low-lying states are not known, the excitation energies are not determined. The

energies given in the figure are measured from the lowest level.

Figure 4.

A singles spectrum of X rays and γ rays measured during off beam periods after the irradiation of ^{28}Si beam on a ^{103}Rh target.

Figure 5.

The decay curves of 68 and 104 keV γ rays and Lanthanum X ray.

Figure 6.

Low-lying excited states in ^{128}La constructed from the $\gamma - \gamma$ coincidence measurement after the β decay of ^{128}Ce.

Figure 7.

The decay curves of the 284, 479 and 643 keV γ rays of the ground-state band of ^{128}Ba.

Figure 8.

The level scheme of ^{128}Ba obtained by the β decay of ^{128}La.

Figure 9.

The ratios of yields measured at two correlation angles of 20° and 80° for the γ rays of ^{128}Ba populated by the β decay of ^{128}La. The angular correlation were measured by three HPGe detectors. The expression "gate" in each figure from (a) to (d) means that the γ ray with this energy is the second radiation in a cascade consisting of two successive γ transitions.

Figure 10.

Ratios of theoretical values of angular correlation function. The first radiation in a

cascade of two successive transitions are assumed to be a mixed multipole transition with mixing ratio δ. The numbers like "$5-4-2$" indicate the spin sequence of a cascade.

Figure 11.

Coincidence spectra obtained to construct the level scheme of ^{128}La (a) from ^{103}Rh(^{28}Si,2pn)^{128}La. (b) from ^{115}In(^{16}O,3n)^{128}La. The gates are placed on 222, 66 and 85 keV γ rays.(see also Fig. 14)

Figure 12.

Coincidence spectra obtained to construct the level scheme of ^{128}La from ^{115}In(^{16}O,3n)^{128}La. The gates are placed on 104, 138 and 114 keV γ rays.(see also Fig. 14)

Figure 13.

Coincidence spectra obtained to construct the level scheme of ^{128}La from ^{115}In(^{16}O,3n)^{128}La. The gates are placed on 120, 82 and 70 keV γ rays.(see also Fig. 14)

Figure 14.

Partial level scheme of ^{128}La established from γ-γ coincidence from ^{115}In(^{16}O,3n)^{128}La. The spin assignment are based on the investigation of β decays(see text).

Figure 15.

Coincidence spectra obtained to construct the level scheme of ^{128}La. The gates are placed on 138, 104 and 66 keV γ rays.(see also Fig. 14)

Figure 16.

Level schemes in the vicinity of the band head of the band 1 in ^{128}La. The level schemes (a) and (b) are reported by Nolan *et al.* and Godfrey *et al.* A new level scheme constructed in this work is presented as (c).

Figure 17.

DCO ratios for transitions in the bands 1 and 2 in ^{128}La.

Figure 18.

Experimental routhians e' as a function of rotational frequency $\hbar\omega$ for ^{124}La. Harris parameters are taken to be J_0=17 MeV$^{-1}\hbar^2$ and J_1=25.8 MeV$^{-3}\hbar^4$.

Figure 19.

Experimental spin alignments $i(\omega)$ as a function of rotational frequency $\hbar\omega$ for ^{124}La. Harris parameters are taken to be J_0=17 MeV$^{-1}\hbar^2$ and J_1=25.8 MeV$^{-3}\hbar^4$.

Figure 20.

Calculated quasiproton energies e' as a function of rotational frequency $\hbar\omega$ for ^{124}La. The paring gaps are assumed to be $\Delta p = 1.26$ MeV for proton and $\Delta n = 1.13$ MeV for neutron, respectively. The parameters of quadrupole deformation are ϵ_2 =0.26 and $\gamma = 0°$.

Figure 21.

Calculated quasineutron energies e' as a function of rotational frequency $\hbar\omega$ for ^{124}La. The same parameters as for quasiproton are used.

Figure 22.

Calculated quasineutron energies e' as a function of rotational frequency $\hbar\omega$ for ^{126}La. The same parameters as for quasiproton are used.

Figure 23.

A conceptual decay scheme for the β decays ^{128}Ce and ^{128}La.

Figure 24.

Experimental data of the signature splitting in odd-odd Ce and La isotopes. It should be noted that the experimental spin assignments are performed only three nuclei of ^{124}Cs, ^{126}Cs and ^{128}La.

Figure 25.

The experimental and calculated signature splittings of ^{128}La. New data obtained in the present work are marked by open circles. Diamond marks are the old data taken from ref. [18]. The theoretical values are the results of calculations by particle-rotor model, in which triaxial deformation and the residual interaction between valence proton and neutron are taken into account.

Figure 26.

The experimental and calculated signature splitting of odd-odd Cs and La isotopes. This figure is taken from ref. [13].

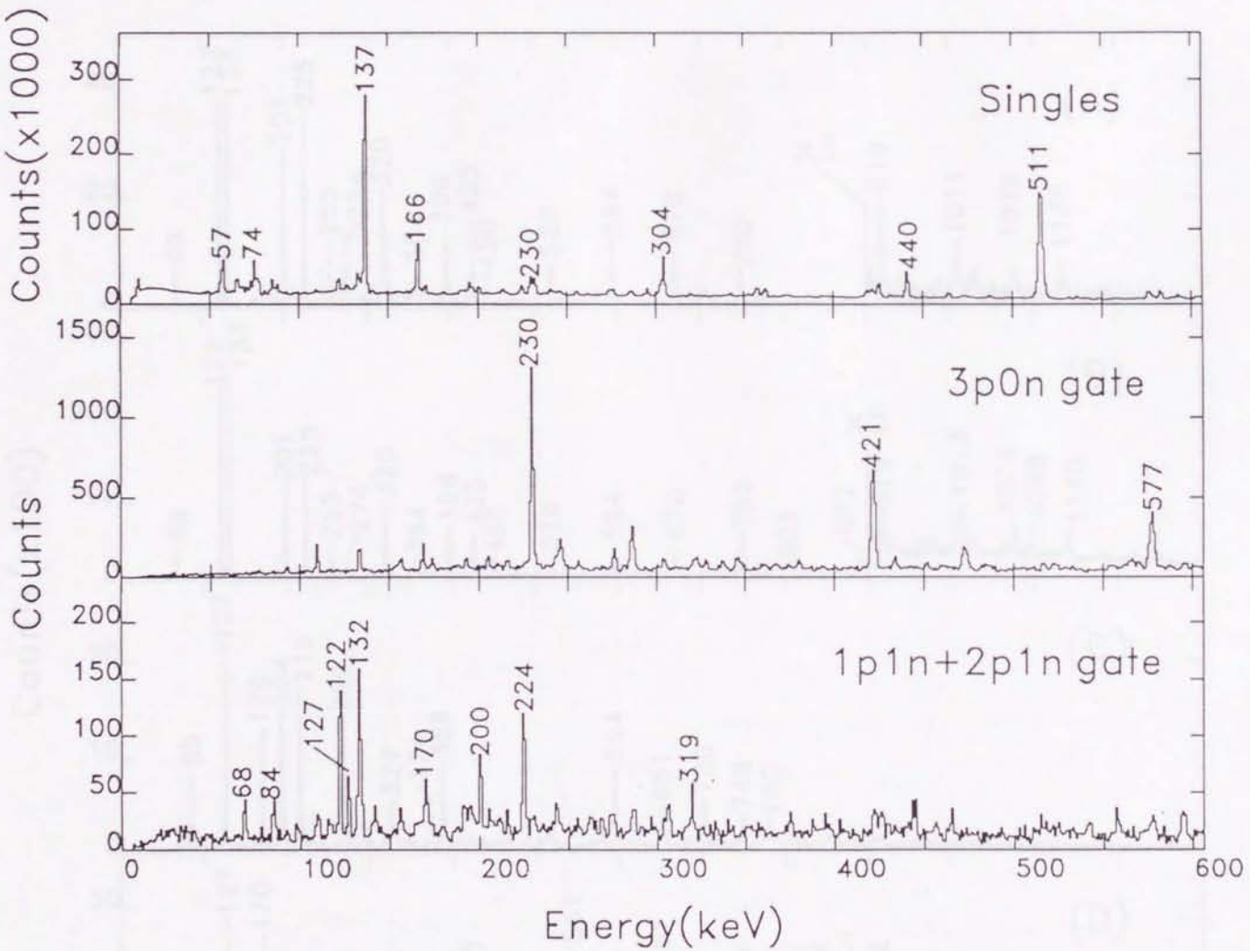
Counts(x1000)
Singles
57
74
137
166
230
304
440
511
Counts
3p0n gate
230
421
577
1p1n+2p1n gate
68
84
127
122
132
170
200
224
319
Energy(keV)

Fig.1

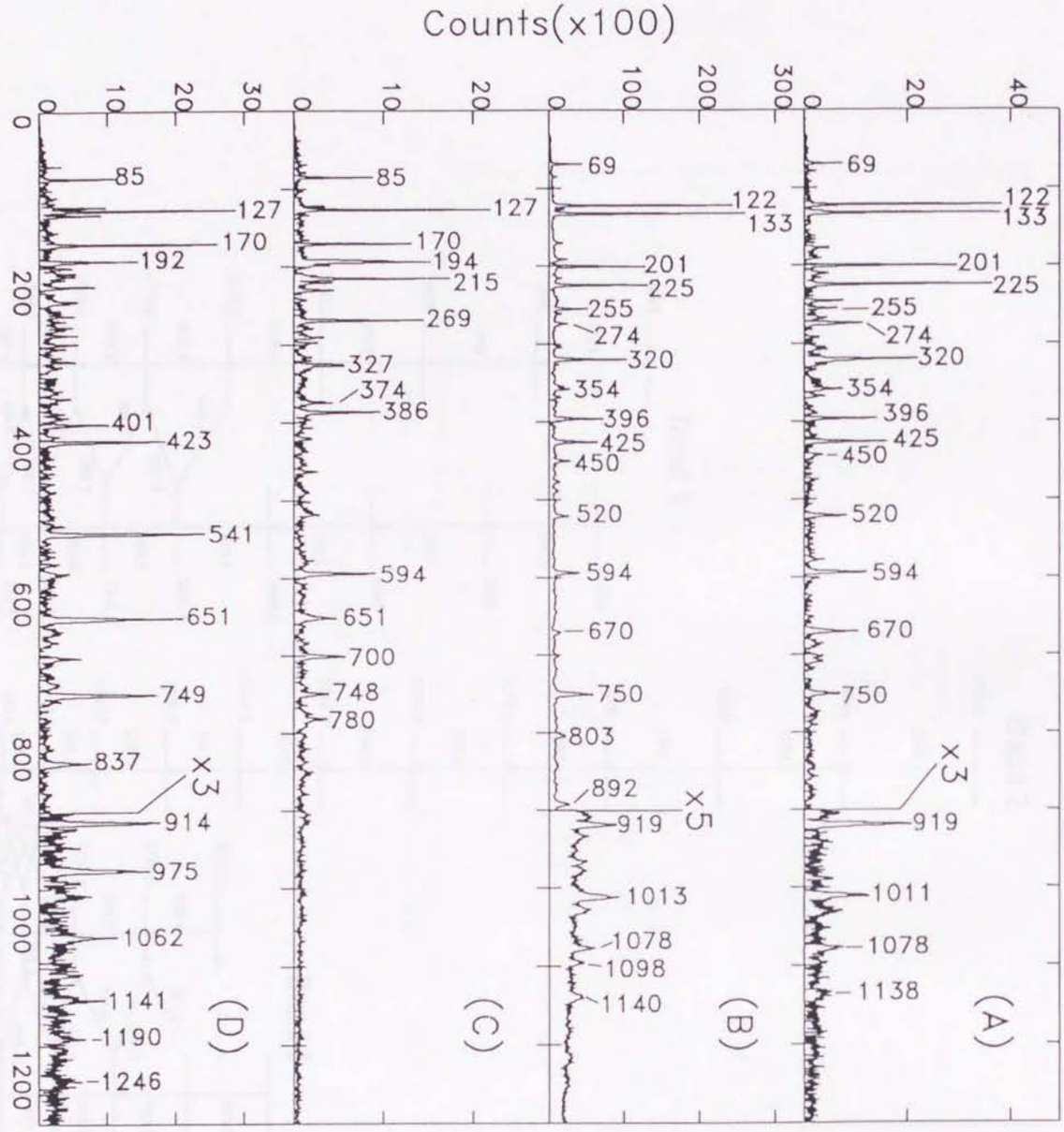
Counts(x100)
Energy(keV)
(A)
(B)
(C)
(D)
69
122
133
201
225
255
274
320
354
396
425
450
520
594
670
750
803
892
919
1011
1078
1138
1013
1098
1140
85
127
170
194
215
269
327
374
386
651
700
748
780
192
401
423
541
749
837
914
975
1062
1141
1190
1246
×3
×5

Fig.2

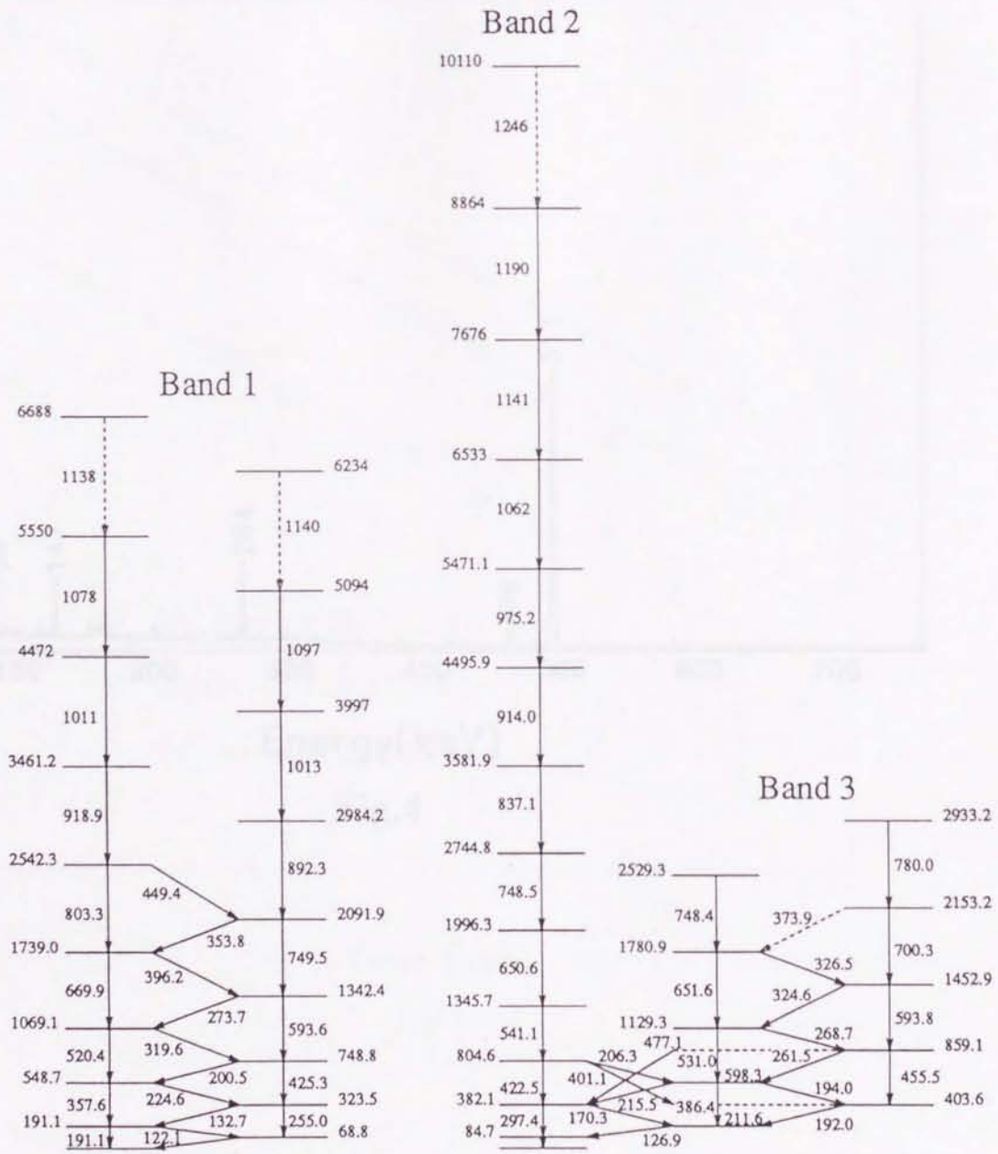
Band 1
6688
1138
5550
1078
4472
1011
3461.2
918.9
2542.3
803.3
1739.0
669.9
1069.1
520.4
548.7
357.6
191.1
191.1
122.1
449.4
353.8
396.2
273.7
319.6
200.5
224.6
132.7
6234
1140
5094
1097
3997
1013
2984.2
892.3
2091.9
749.5
1342.4
593.6
748.8
425.3
323.5
255.0
68.8
Band 2
10110
1246
8864
1190
7676
1141
6533
1062
5471.1
975.2
4495.9
914.0
3581.9
837.1
2744.8
748.5
1996.3
650.6
1345.7
541.1
804.6
422.5
382.1
297.4
84.7
Band 3
2529.3
748.4
1780.9
651.6
1129.3
477.1
531.0
598.3
386.4
211.6
206.3
401.1
215.5
170.3
126.9
2933.2
780.0
2153.2
373.9
700.3
1452.9
326.5
324.6
593.8
859.1
268.7
261.5
455.5
403.6
194.0
192.0

Fig.3

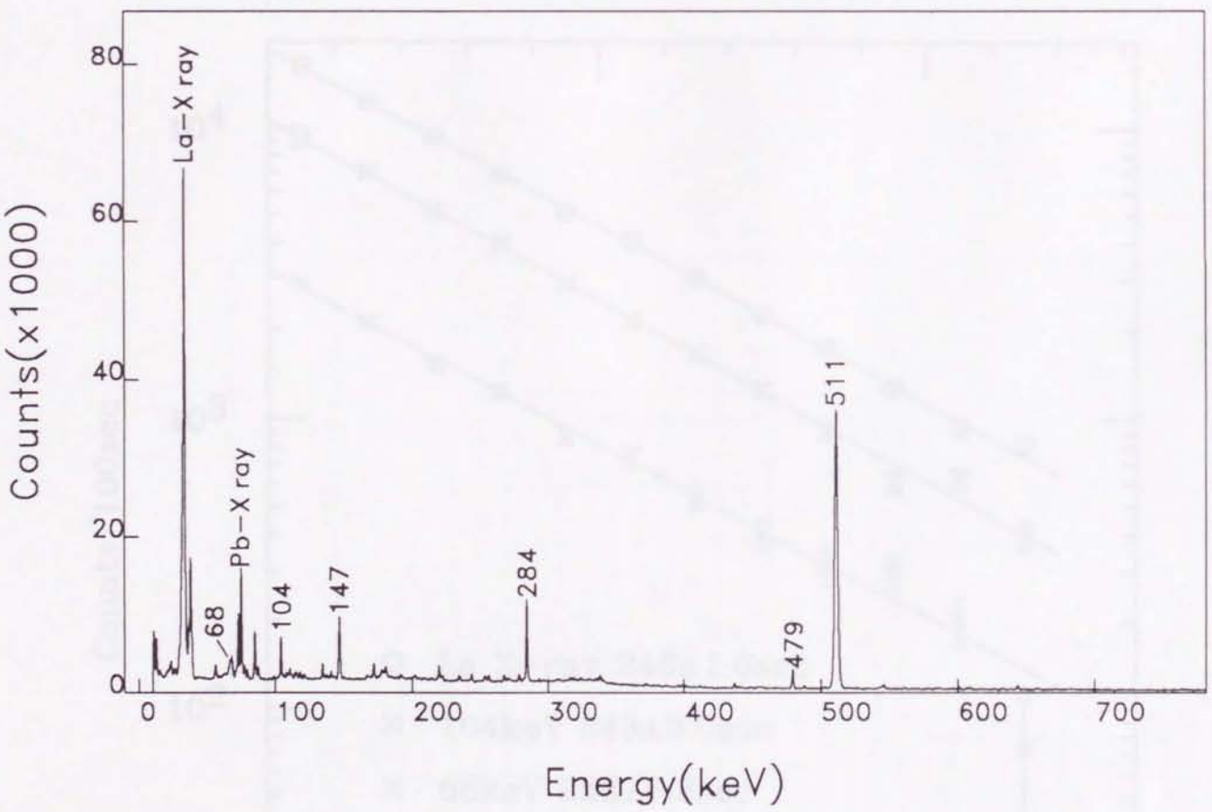
Counts(x1000)
80
60
40
20
0
La-X ray
Pb-X ray
68
104
147
284
479
511
0
100
200
300
400
500
600
700
Energy(keV)

Fig.4

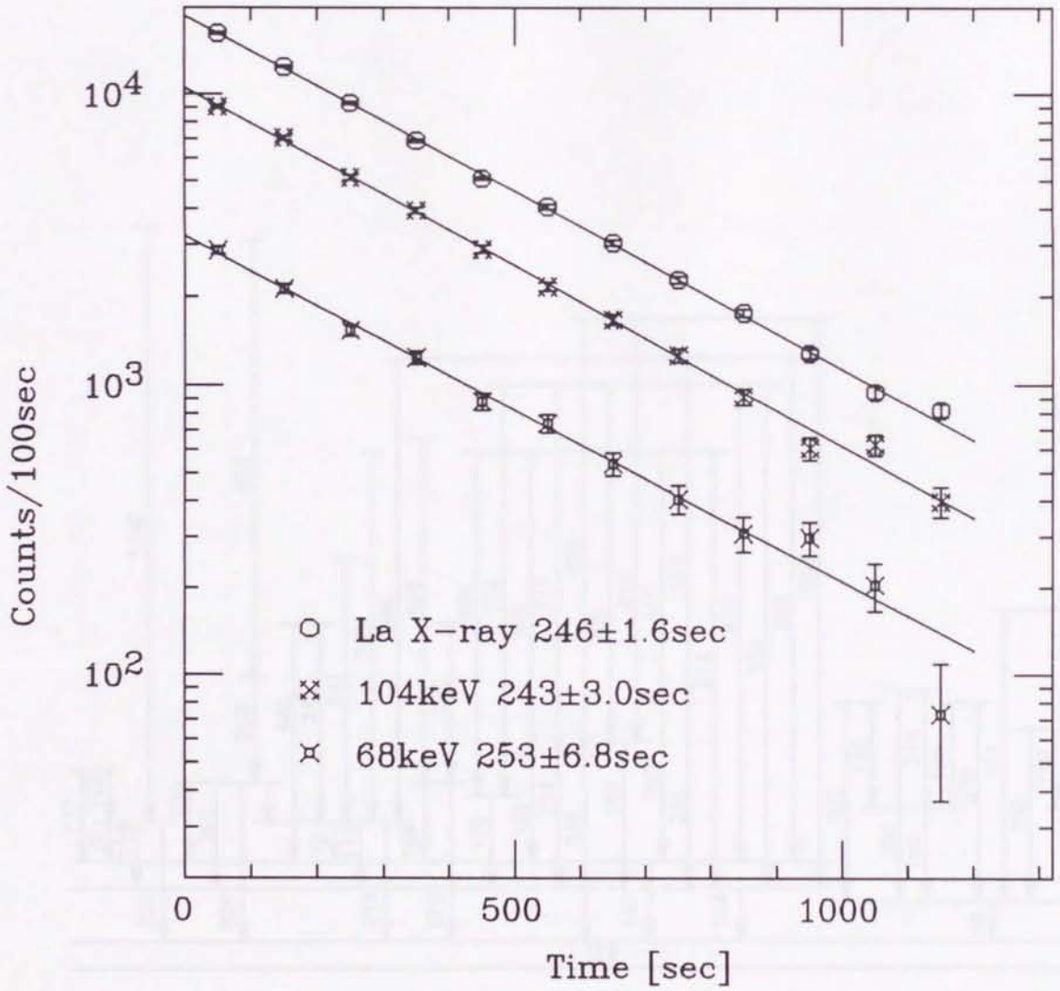
10^4
10^3
10^2
Counts/100sec
La X-ray 246±1.6sec
104keV 243±3.0sec
68keV 253±6.8sec
0
500
1000
Time [sec]

Fig.5

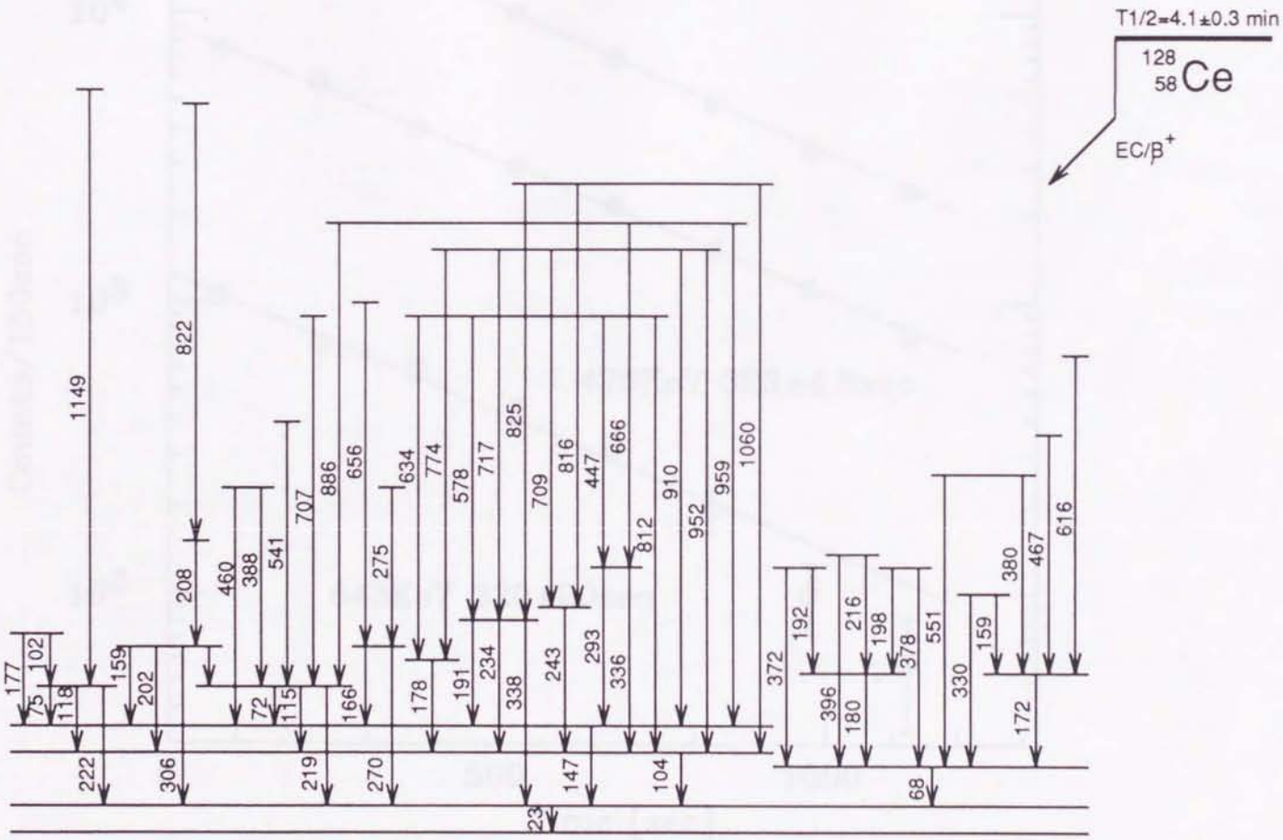

$^{128}_{57}La$

Fig.6

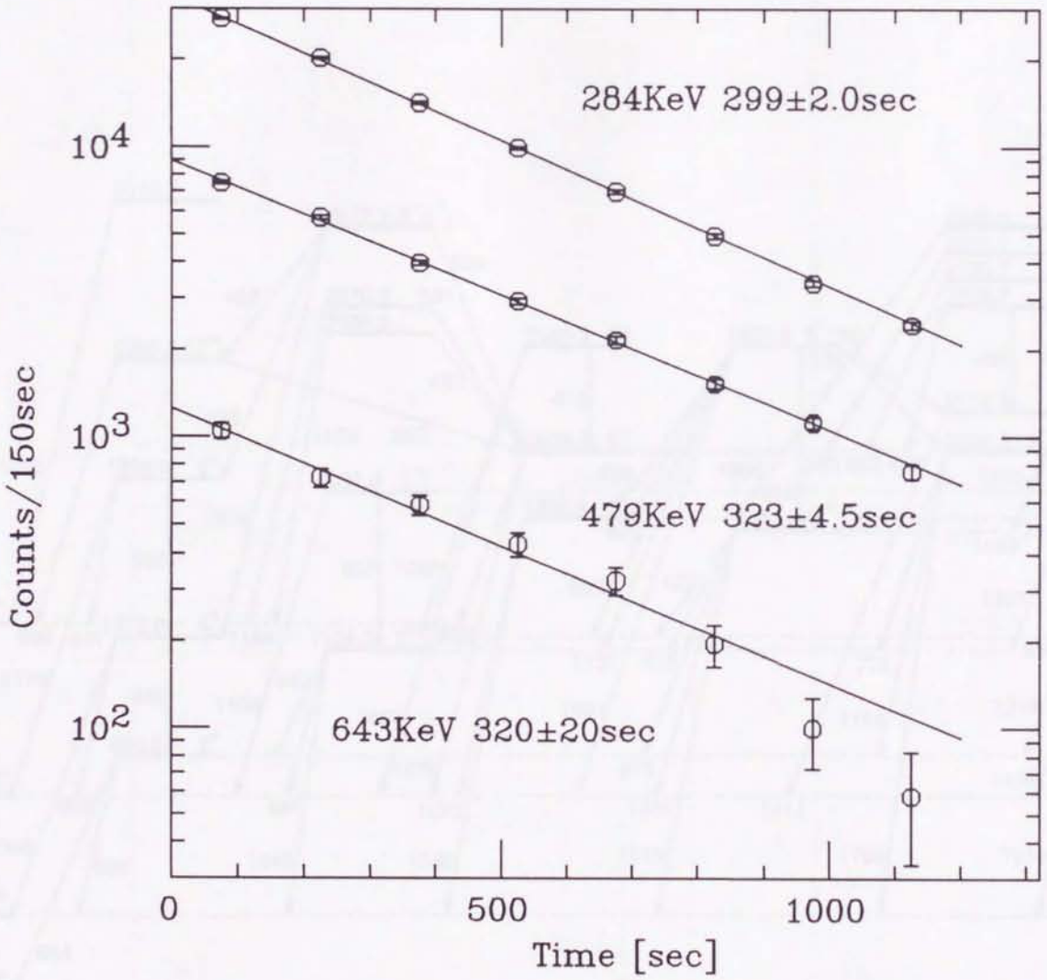
284KeV 299±2.0sec
479KeV 323±4.5sec
643KeV 320±20sec
Counts/150sec
10^4
10^3
10^2
0
500
1000
Time [sec]

Fig.7

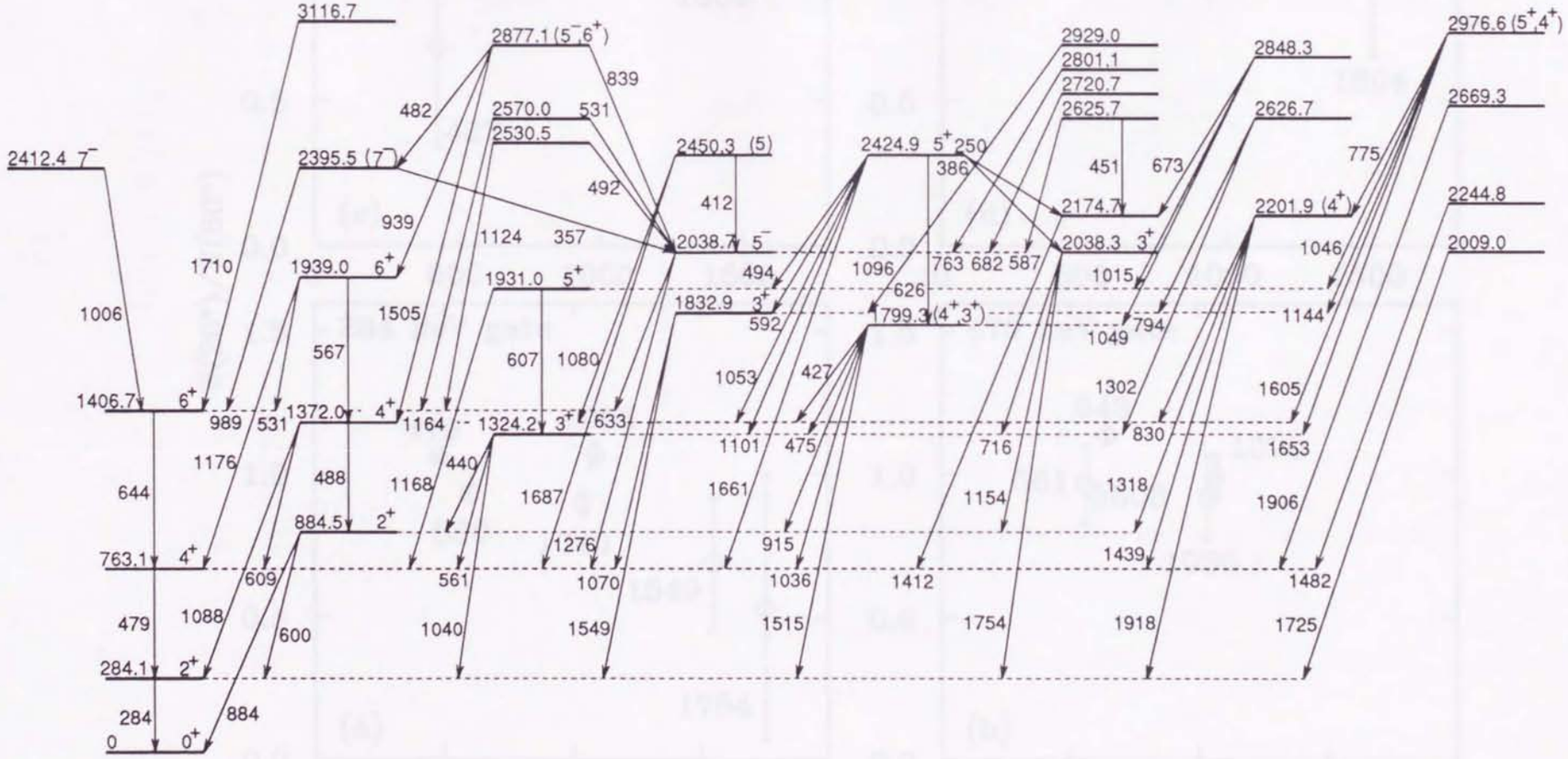
3116.7
2877.1 (5⁻,6⁺)
2570.0
2530.5
2450.3 (5)
2424.9 5⁺
2929.0
2801.1
2720.7
2625.7
2848.3
2626.7
2976.6 (5⁺,4⁺)
2669.3
2244.8
2009.0
2412.4 7⁻
2395.5 (7⁻)
2038.7 5⁻
2174.7
2038.3 3⁺
2201.9 (4⁺)
1939.0 6⁺
1931.0 5⁺
1832.9 3⁺
1799.3 (4⁺,3⁺)
1406.7 6⁺
1372.0 4⁺
1324.2 3⁺
884.5 2⁺
763.1 4⁺
284.1 2⁺
0 0⁺
1710
482
839
531
492
939
1124
357
412
386
250
451
673
775
1046
494
1096
763
682
587
1015
626
1144
1049
794
1006
1505
567
607
1080
592
1053
427
1302
1605
989
531
1164
633
1101
475
716
830
1653
1176
488
1168
440
1687
1661
1154
1318
1906
644
1276
915
1439
609
561
1070
1036
1412
1482
479
1088
600
1040
1549
1515
1754
1918
1725
284
884

Fig.8

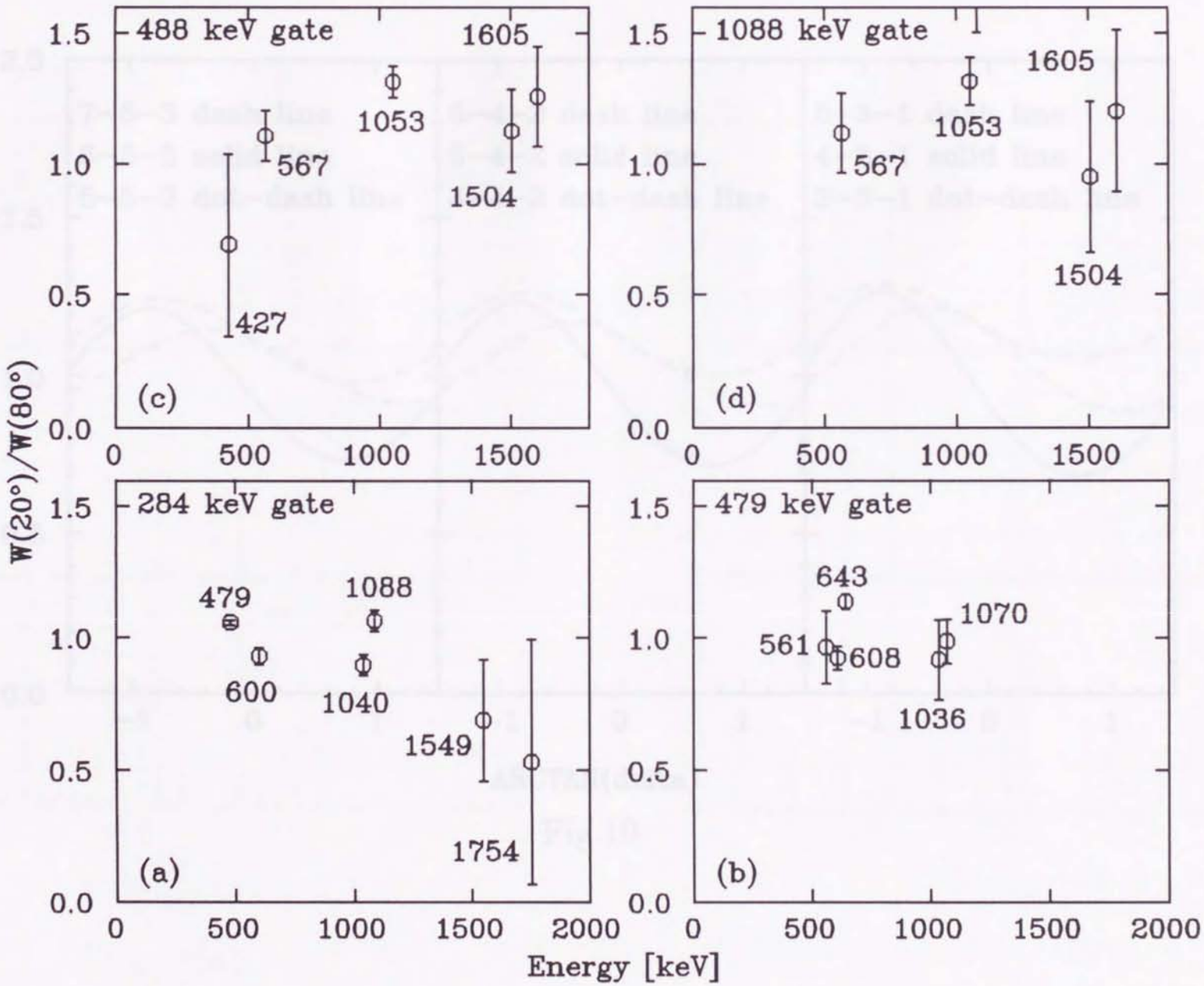
488 keV gate
1088 keV gate
284 keV gate
479 keV gate
(a)
(b)
(c)
(d)
W(20°)/W(80°)
Energy [keV]
427
567
1053
1504
1605
600
479
1088
1040
1549
1754
561
608
643
1070
1036

Fig.9

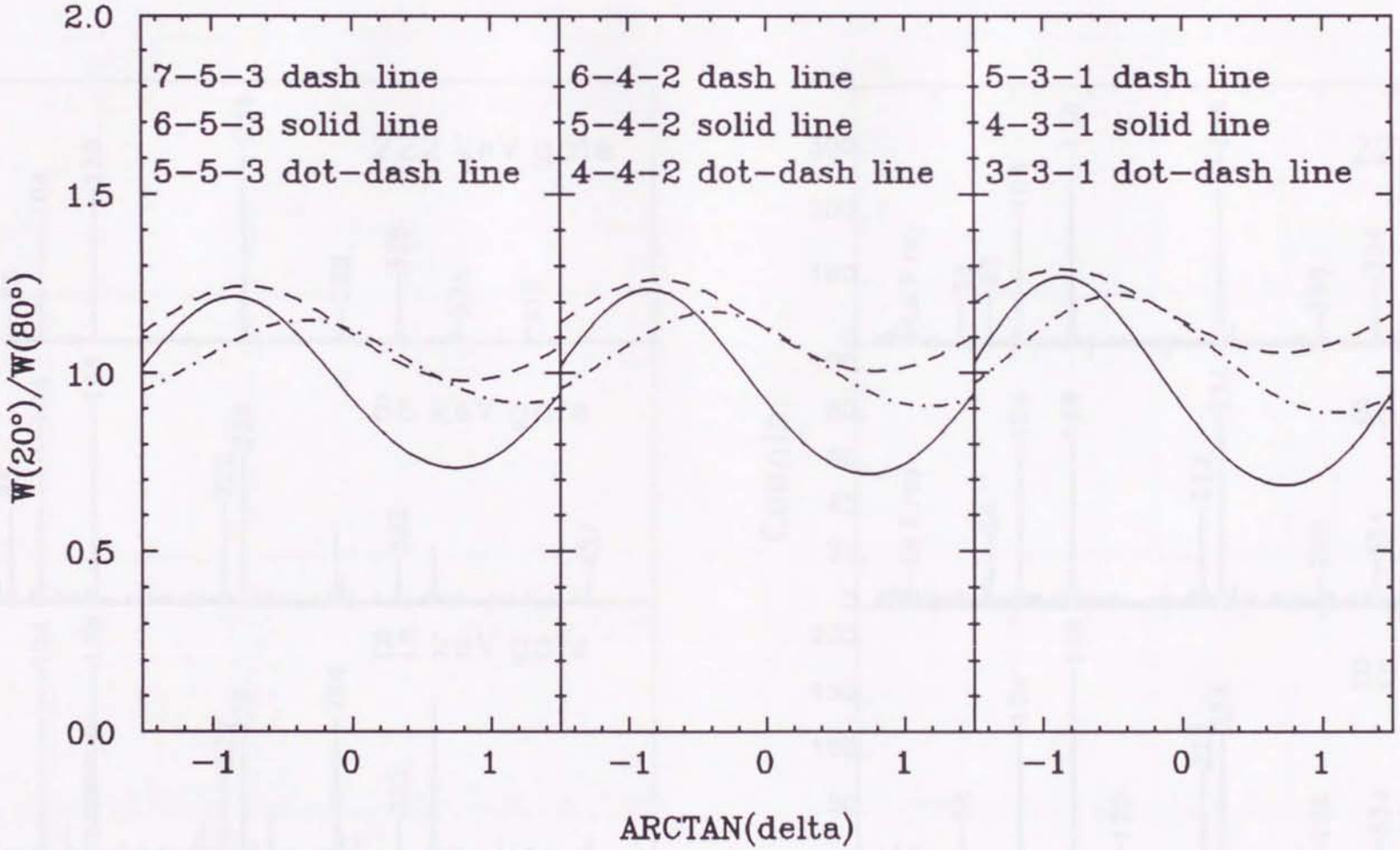
7−5−3 dash line
6−5−3 solid line
5−5−3 dot−dash line
6−4−2 dash line
5−4−2 solid line
4−4−2 dot−dash line
5−3−1 dash line
4−3−1 solid line
3−3−1 dot−dash line
W(20°)/W(80°)
2.0
1.5
1.0
0.5
0.0
−1
0
1
ARCTAN(delta)

Fig.10

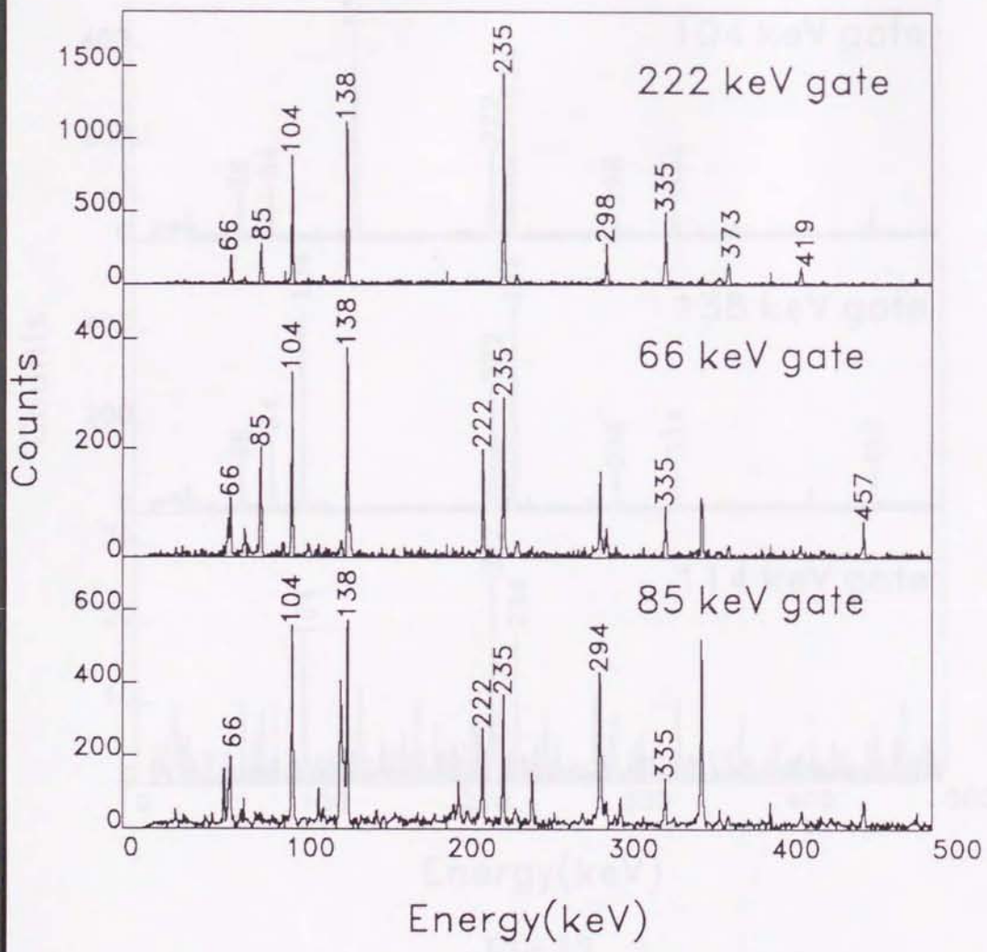

Fig.11(a)

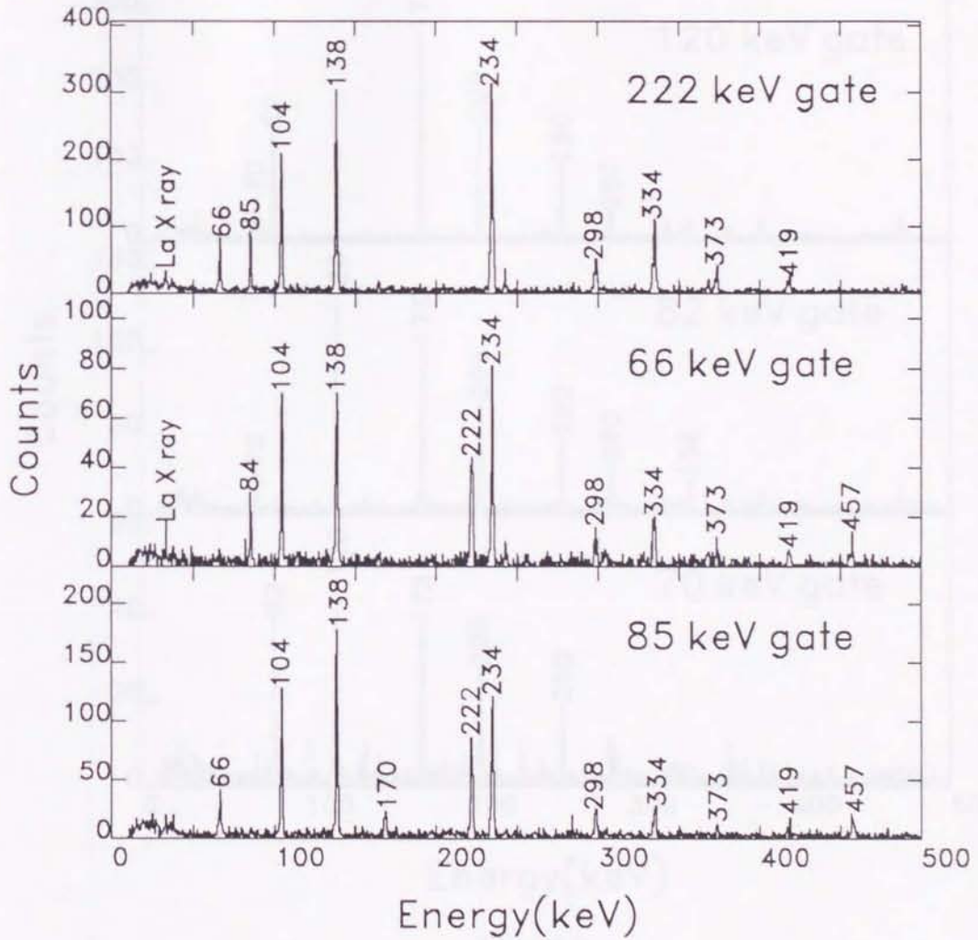

Fig.11(b)

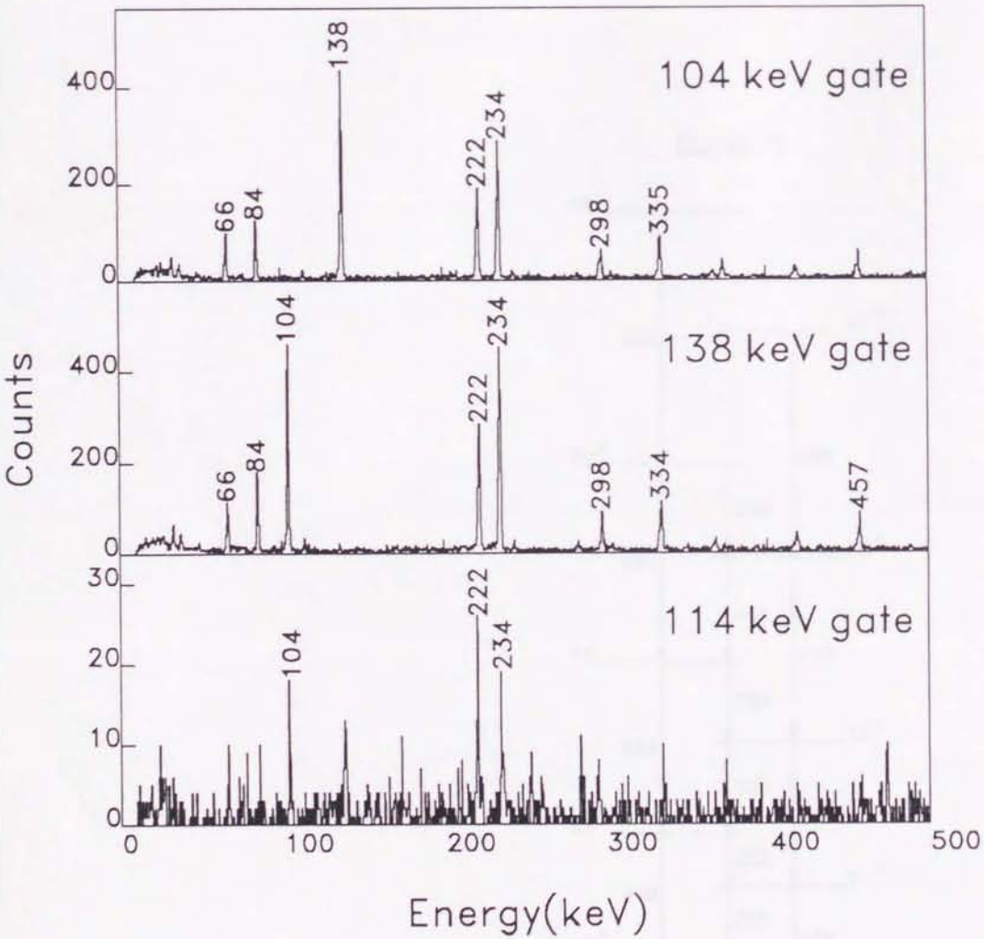
104 keV gate
138 keV gate
114 keV gate
Counts
Energy(keV)

Fig.12

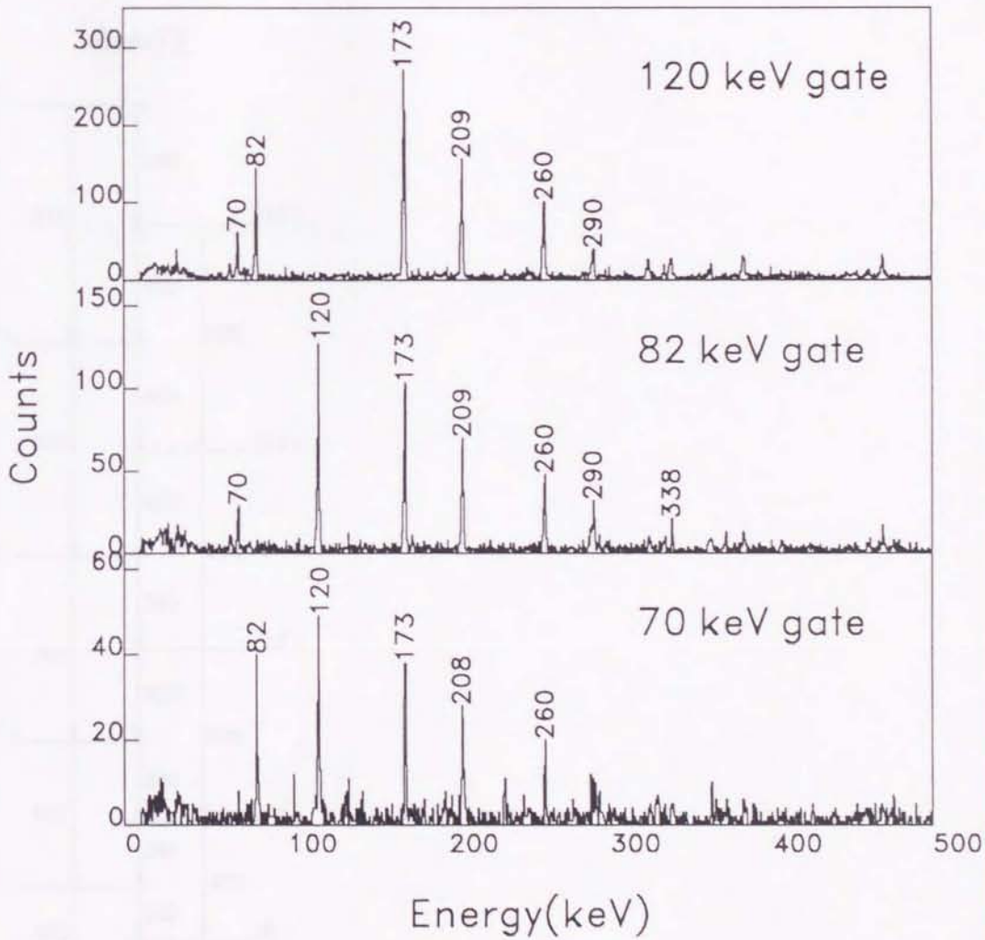
120 keV gate
82 keV gate
70 keV gate
Counts
Energy(keV)

Fig.13

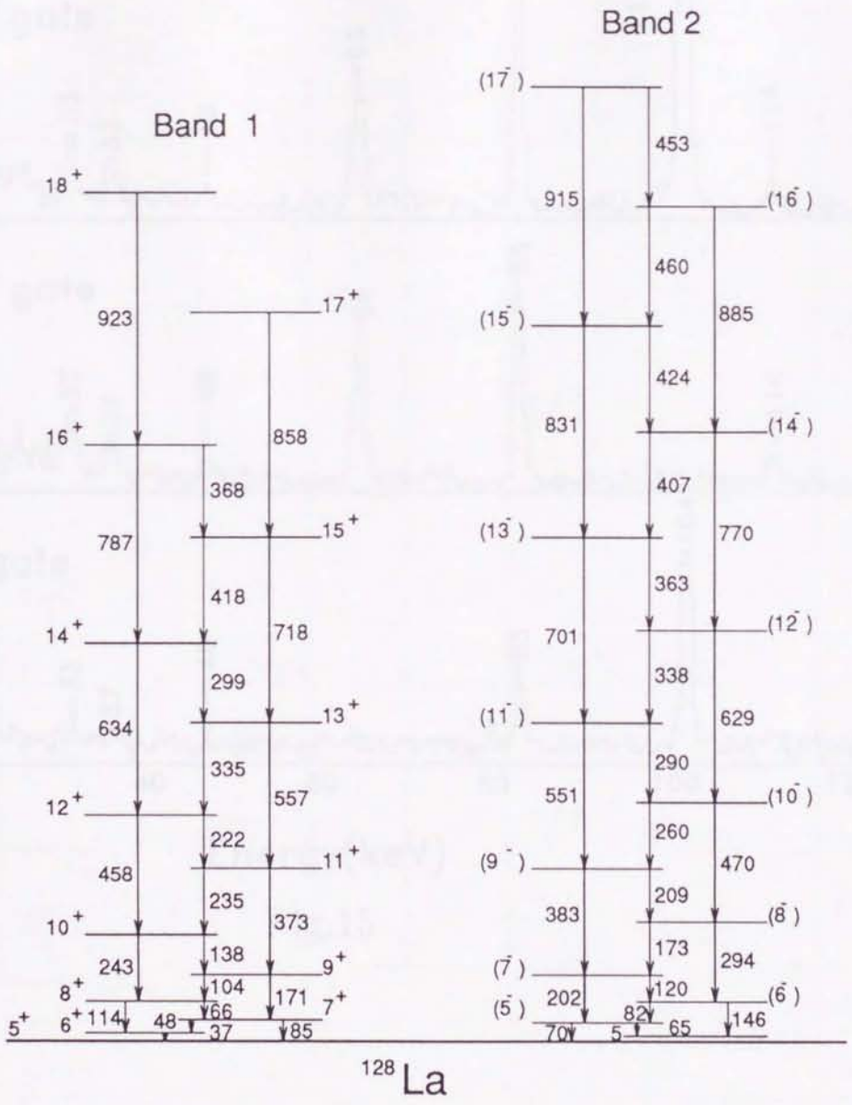
Band 1
Band 2
18+
17+
16+
15+
14+
13+
12+
11+
10+
9+
8+
7+
6+
5+
(17-)
(16-)
(15-)
(14-)
(13-)
(12-)
(11-)
(10-)
(9-)
(8-)
(7-)
(6-)
(5-)
923
858
368
787
418
718
299
634
335
557
222
458
235
373
138
243
104
171
114
48
66
37
85
453
915
460
885
424
831
407
770
363
701
338
629
290
551
260
470
209
383
173
294
202
120
82
146
70
5
65
128La

Fig.14

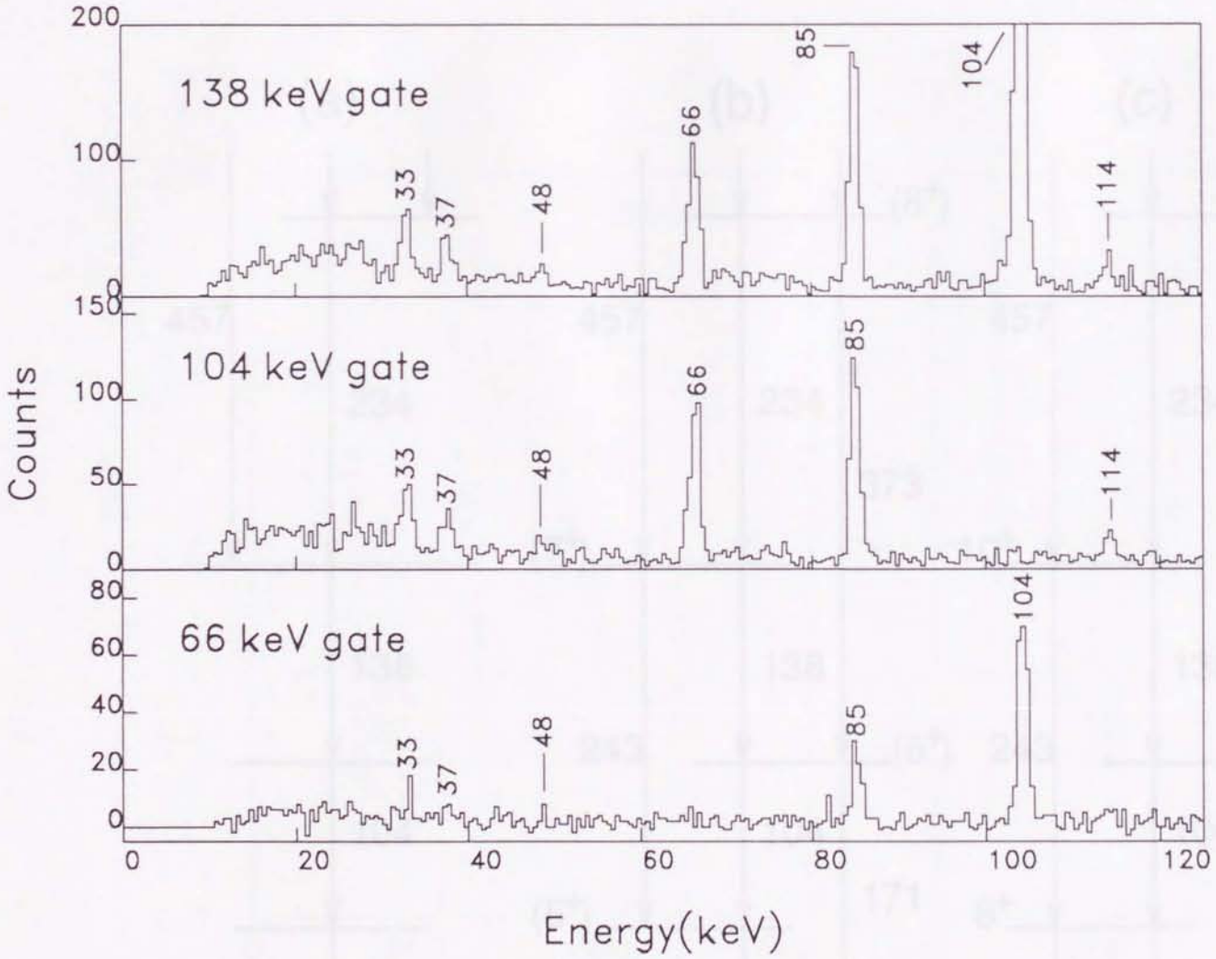
138 keV gate
104 keV gate
66 keV gate
Counts
Energy(keV)
33
37
48
66
85
104
114

Fig.15

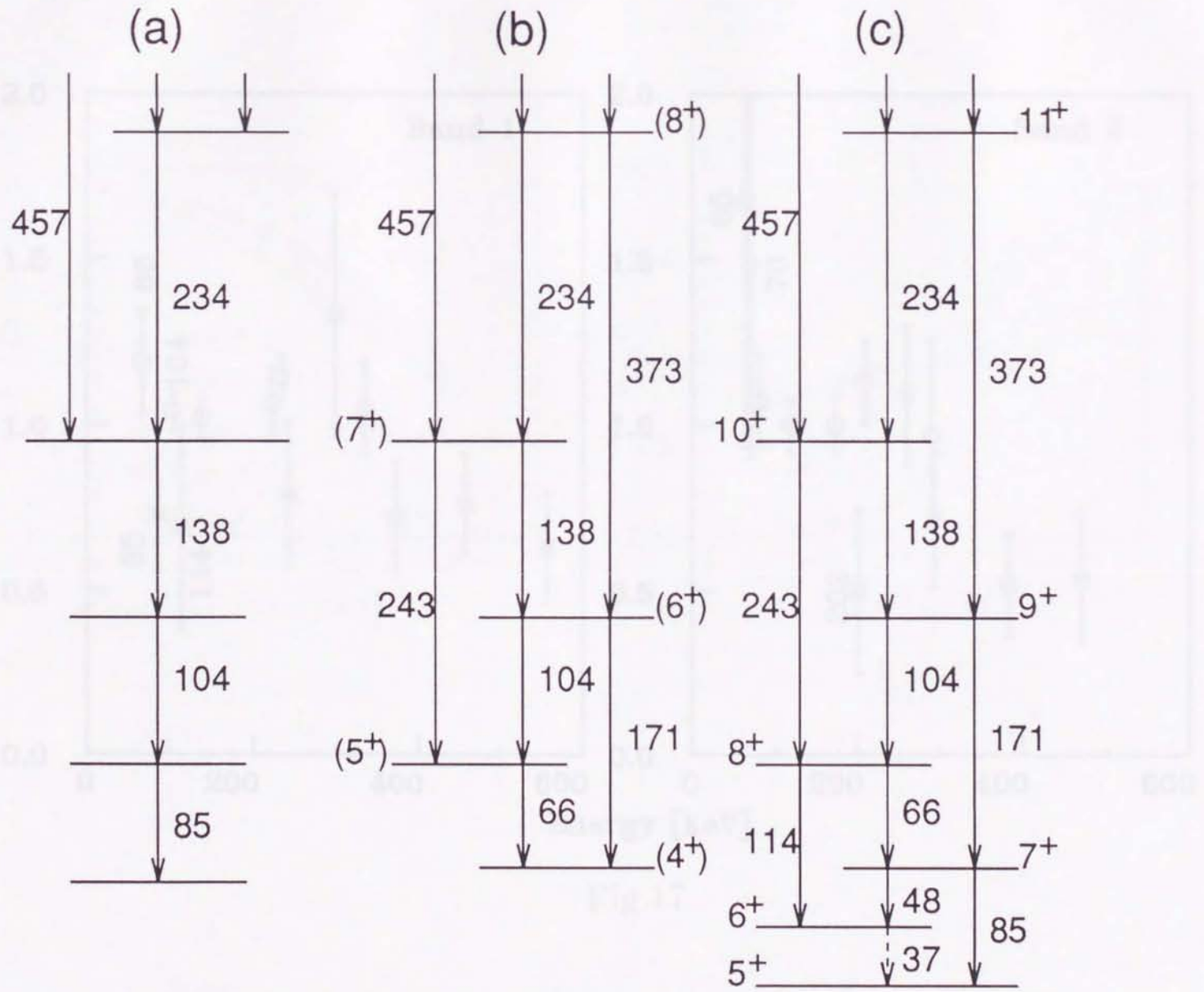

Fig.16

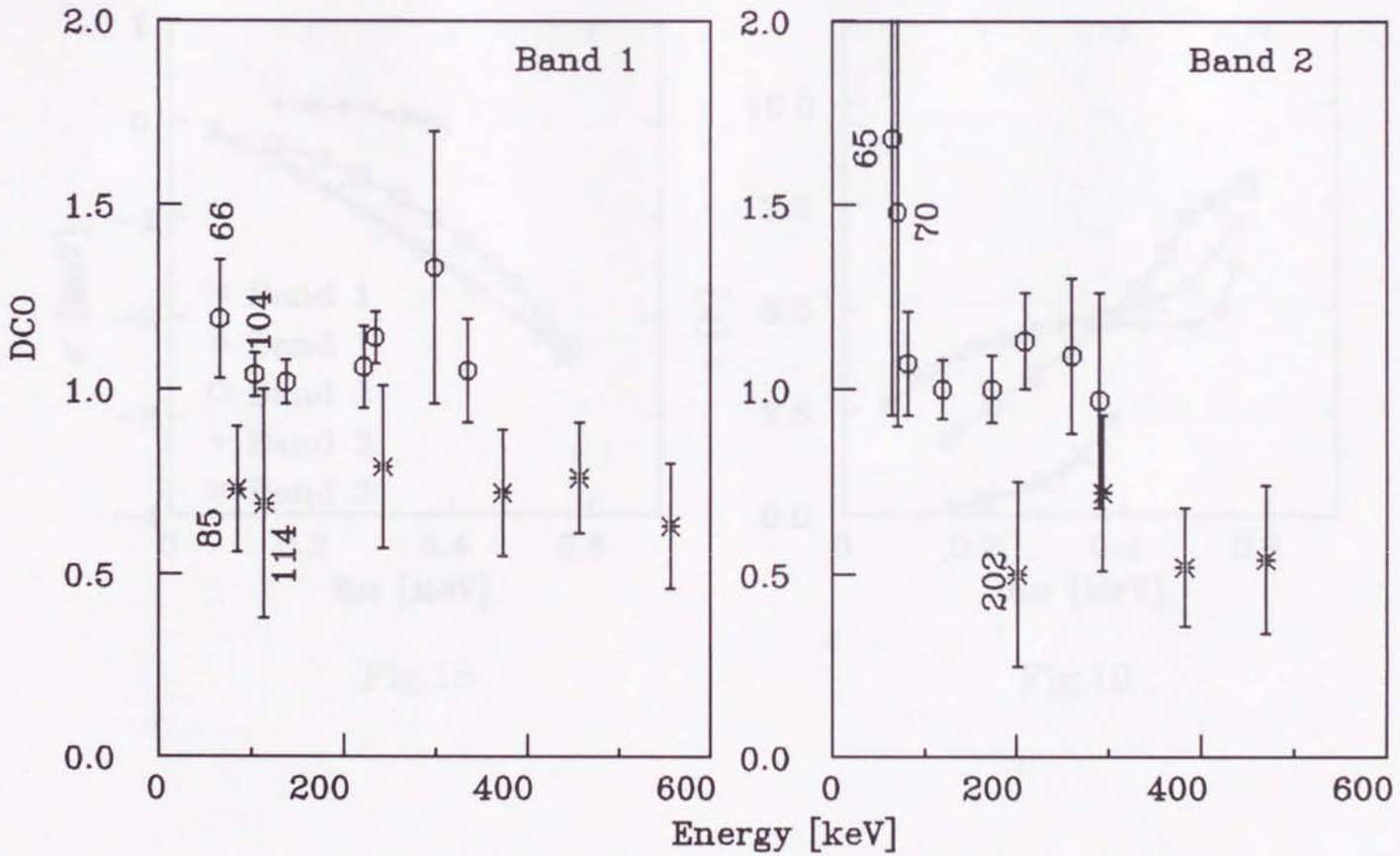
Band 1
Band 2
DCO
Energy [keV]
2.0
1.5
1.0
0.5
0.0
0
200
400
600
66
104
85
114
65
70
202

Fig.17

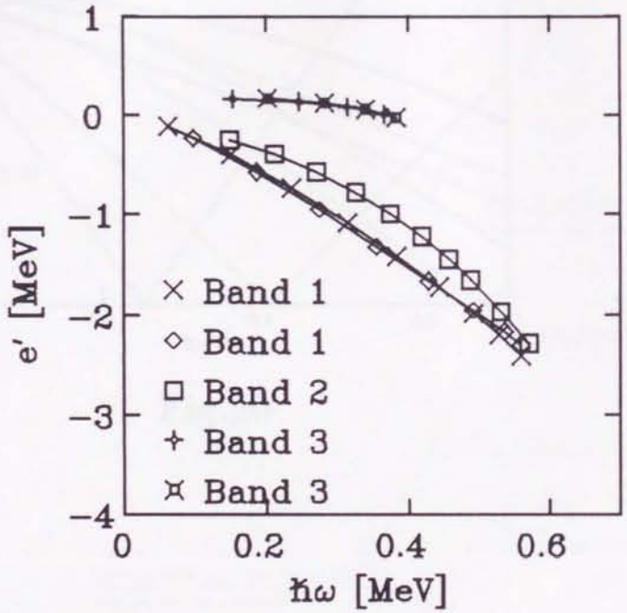
1
0
−1
−2
−3
−4
e' [MeV]
0
0.2
0.4
0.6
ħω [MeV]
Band 1
Band 1
Band 2
Band 3
Band 3

Fig.18

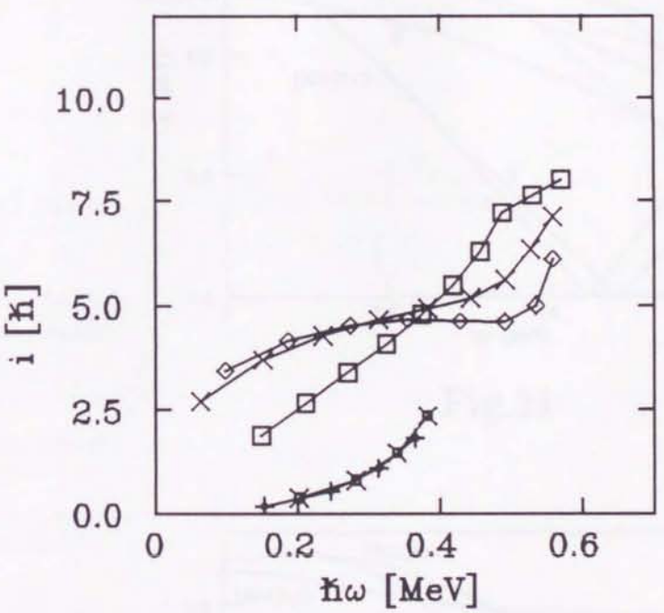
10.0
7.5
5.0
2.5
0.0
i [ħ]
0
0.2
0.4
0.6
ħω [MeV]

Fig.19

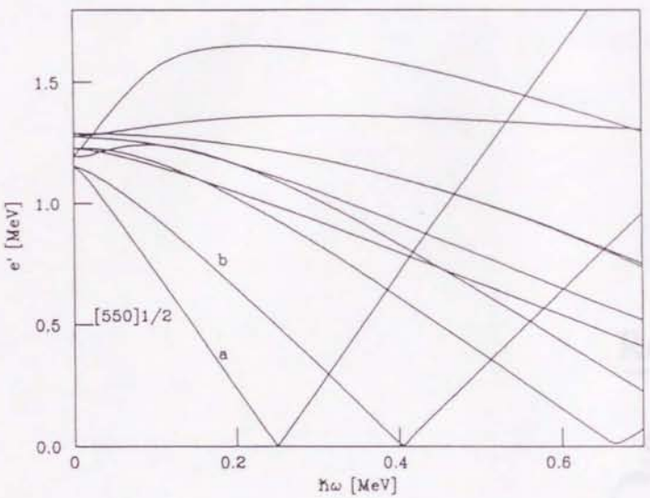

Fig.20

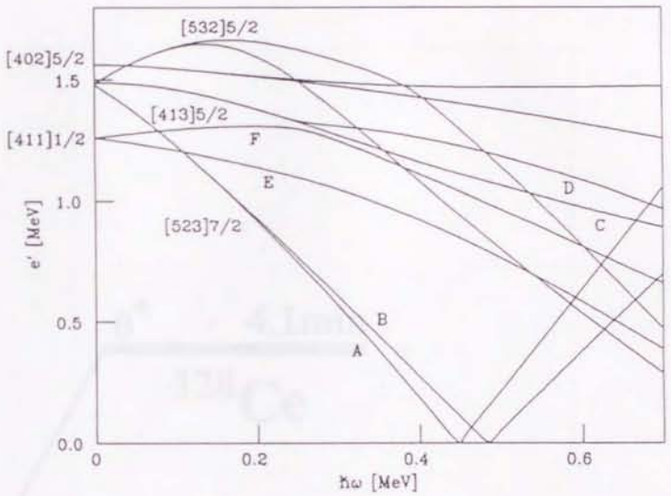

Fig.21

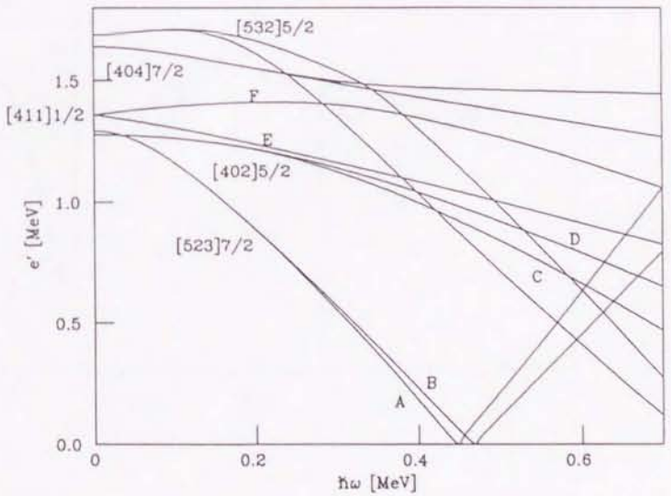

Fig.22

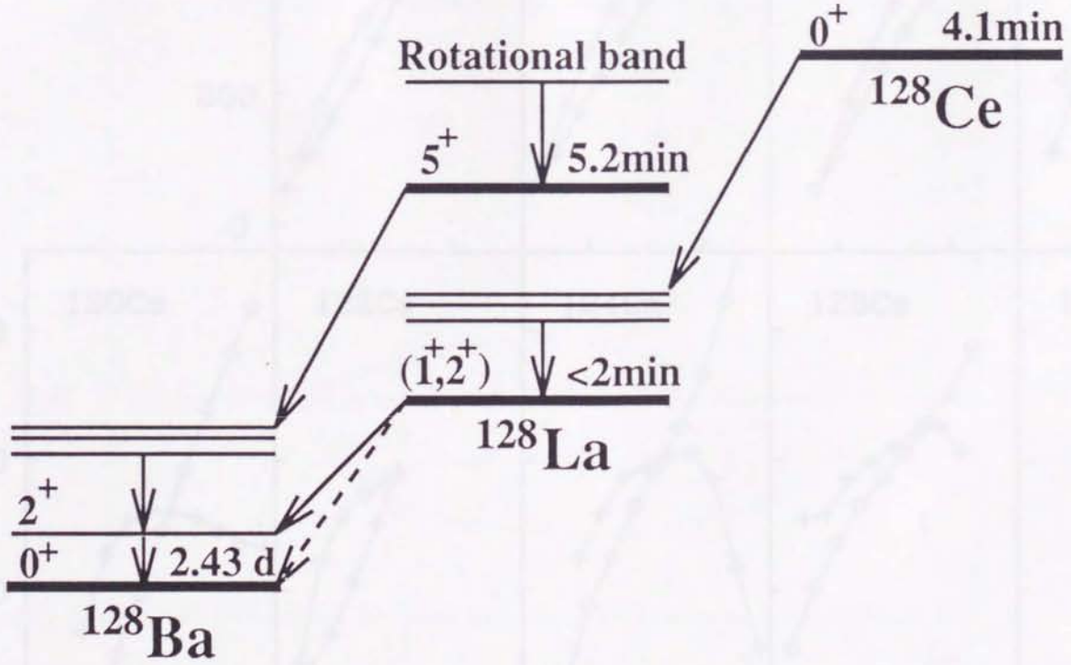
Rotational band
5+
5.2min
0+
4.1min
128Ce
(1+,2+)
<2min
128La
2+
0+
2.43 d
128Ba

Fig.23

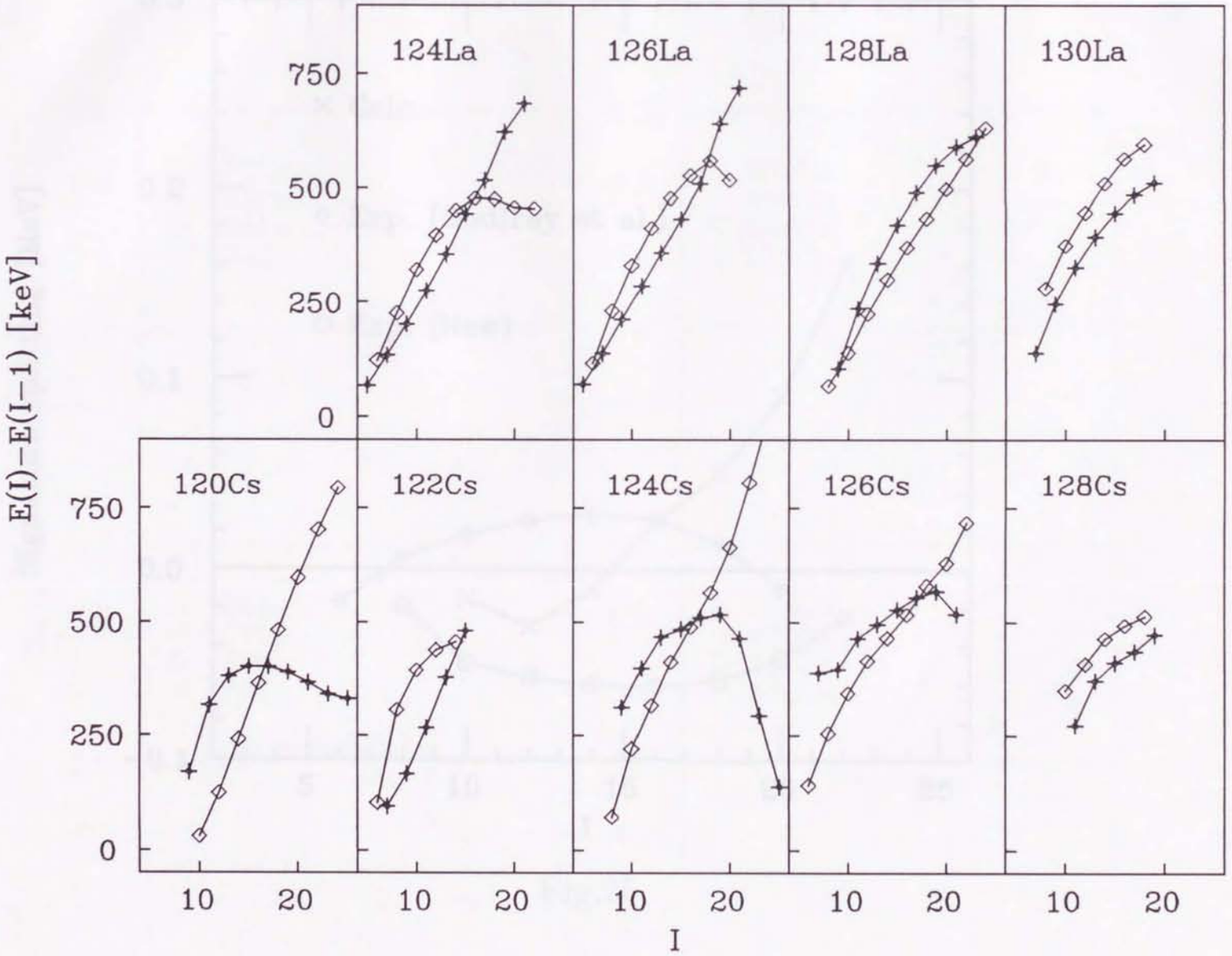
124La
126La
128La
130La
120Cs
122Cs
124Cs
126Cs
128Cs
E(I)−E(I−1) [keV]
750
500
250
0
10
20
I

Fig.24

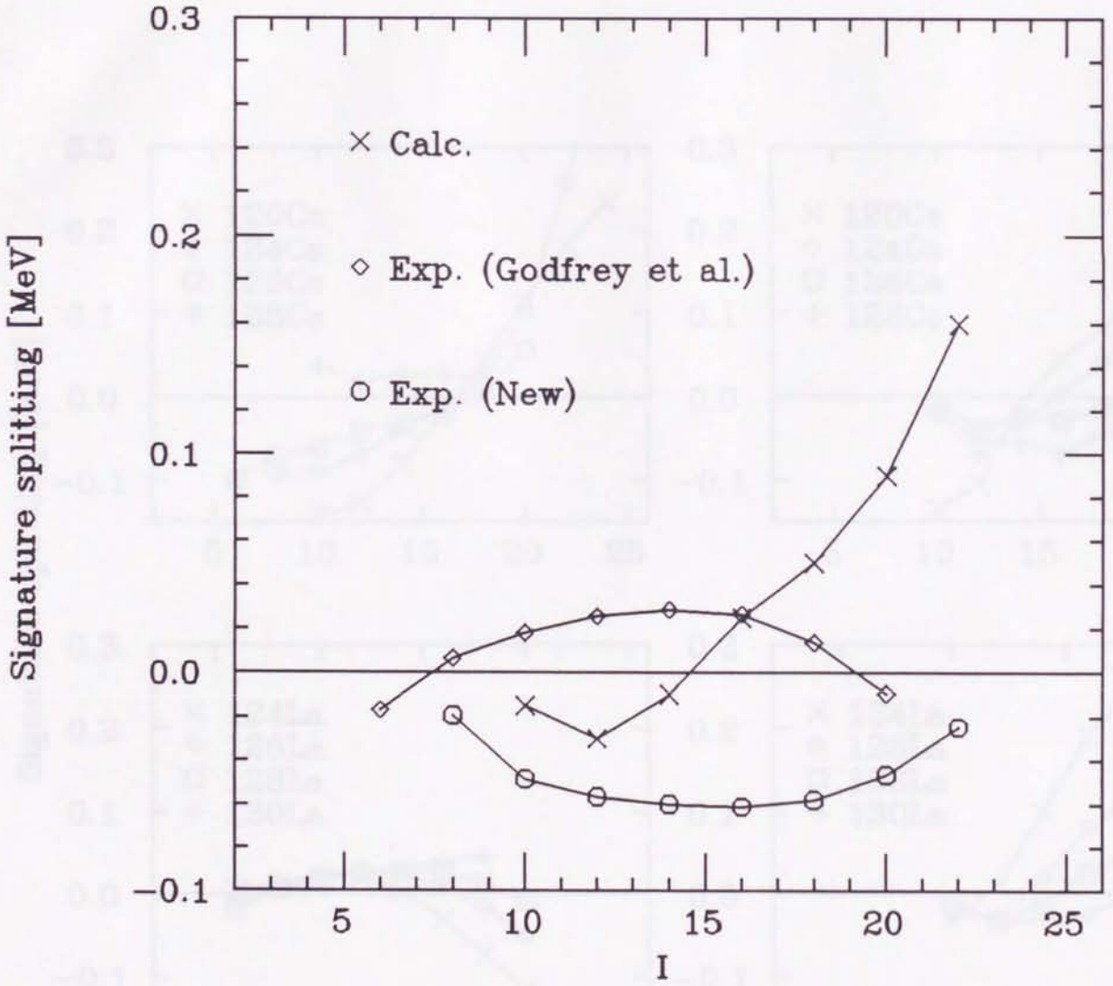
0.3
0.2
0.1
0.0
−0.1
5
10
15
20
25
I
Signature splitting [MeV]
× Calc.
◇ Exp. (Godfrey et al.)
○ Exp. (New)

Fig.25

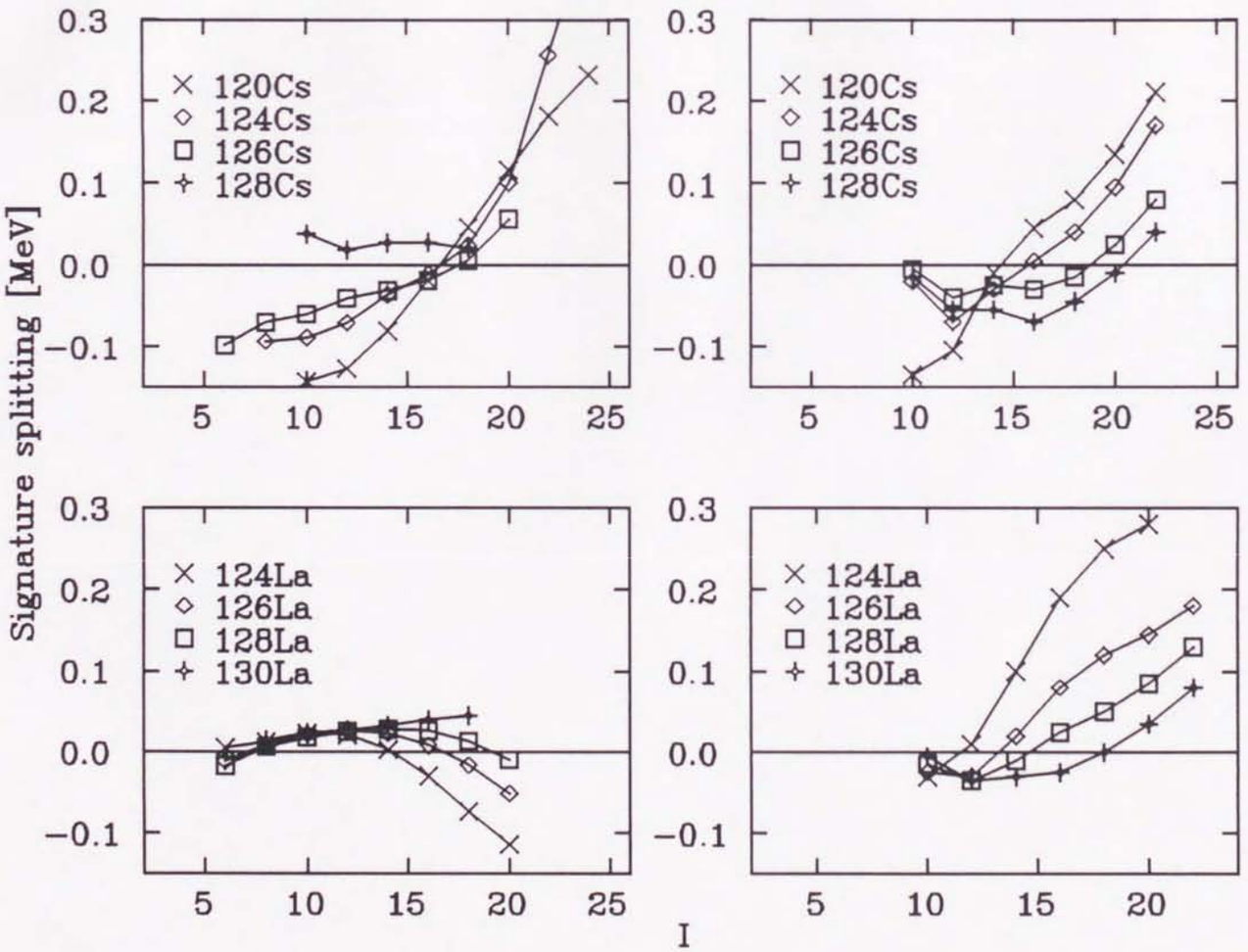
Signature splitting [MeV]
0.3
0.2
0.1
0.0
−0.1
5
10
15
20
25
120Cs
124Cs
126Cs
128Cs
124La
126La
128La
130La
I

Fig.26

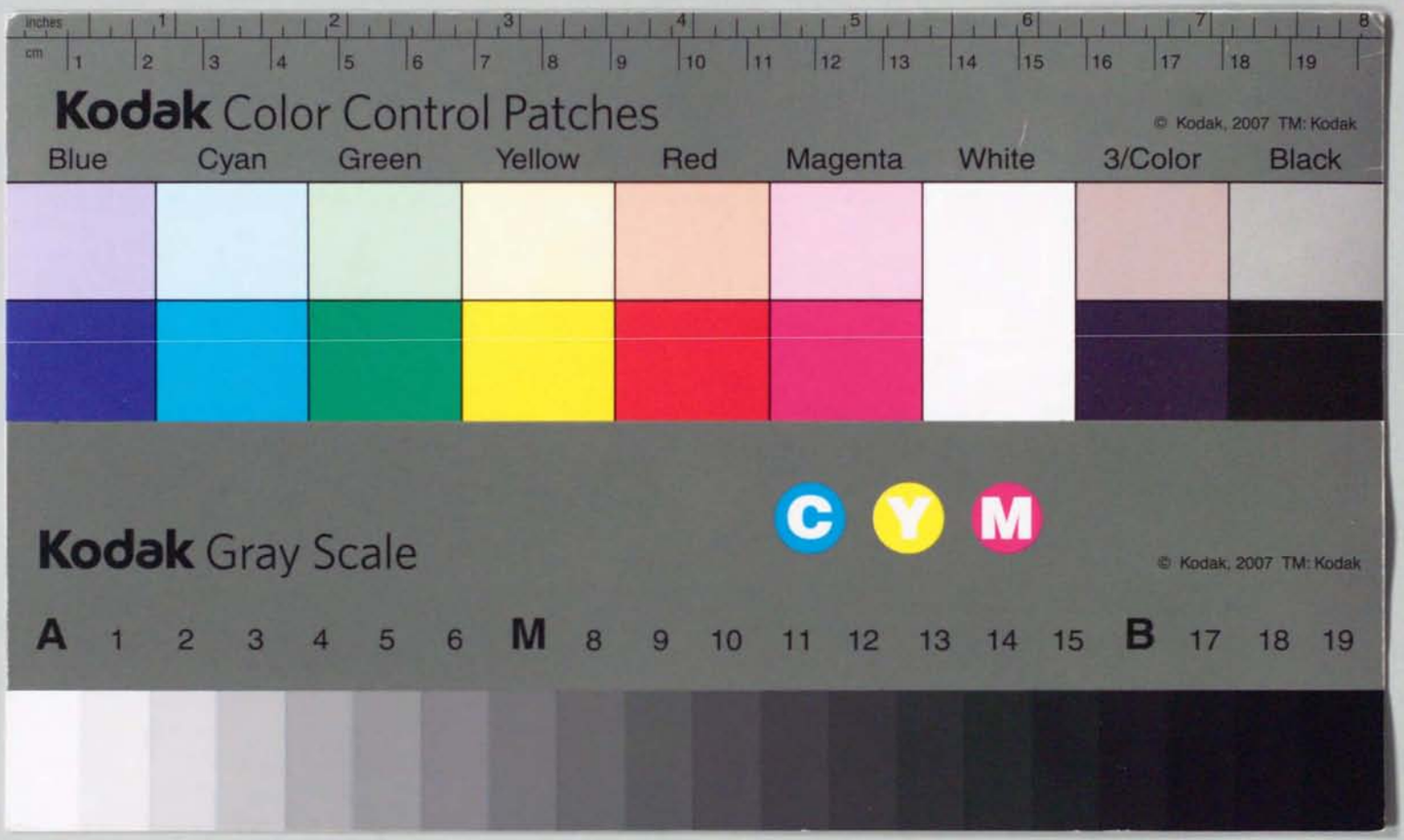
inches
cm
Kodak Color Control Patches
© Kodak, 2007 TM: Kodak
Blue
Cyan
Green
Yellow
Red
Magenta
White
3/Color
Black
Kodak Gray Scale
C
Y
M
© Kodak, 2007 TM: Kodak
A 1 2 3 4 5 6 M 8 9 10 11 12 13 14 15 B 17 18 19